VSC-TR-81-29

VFM DISCRIMINATION RESULTS FROM A TEN STATION NETWORK

J. M. Savino

C. B. Archambeau

J. F. Masso

SYSTEMS, SCIENCE AND SOFTWARE
P. O. Box 1620
La Jolla, California 92038

July 1980

TECHNICAL REPORT

Monitored by:

VELA Seismological Center
312 Montgomery Street
Alexandria, Virginia 22314

UNCLASSIFIED

SECURITY CLASSIFICATION OF THIS PAGE (When Data Entered)

REPORT DOCUMENTATION PAGE	READ INSTRUCTIONS BEFORE COMPLETING FORM
1. REPORT NUMBER: VSC-TR-81-29	2. GOVT ACCESSION NO.: AD-A112 093
3. RECIPIENT'S CATALOG NUMBER:	
4. TITLE (and Subtitle): VFM DISCRIMINATION RESULTS FROM A TEN STATION NETWORK	5. TYPE OF REPORT & PERIOD COVERED: Technical Report 10/1/79 - 9/30/80
	6. PERFORMING ORG. REPORT NUMBER: SSS-R-80-4566
7. AUTHOR(s): J. M. Savino, C. B. Archambeau, J. F. Masso	8. CONTRACT OR GRANT NUMBER(s): F08606-79-C-0008
9. PERFORMING ORGANIZATION NAME AND ADDRESS: Systems, Science and Software, P. O. Box 1620, La Jolla, California 92038	10. PROGRAM ELEMENT, PROJECT, TASK AREA & WORK UNIT NUMBERS: Program Code No. 6H189, ARPA Order No. 2551
11. CONTROLLING OFFICE NAME AND ADDRESS: VELA Seismological Center, 312 Montgomery Street, Alexandria, Virginia 22314	12. REPORT DATE: July 1980
	13. NUMBER OF PAGES: 111
14. MONITORING AGENCY NAME & ADDRESS(if different from Controlling Office)	15. SECURITY CLASS. (of this report): Unclassified
	15a. DECLASSIFICATION/DOWNGRADING SCHEDULE

16. DISTRIBUTION STATEMENT (of this Report)

Approved for Public Release, Distribution Unlimited.

17. DISTRIBUTION STATEMENT (of the abstract entered in Block 20, if different from Report)

18. SUPPLEMENTARY NOTES

19. KEY WORDS (Continue on reverse side if necessary and identify by block number)

Seismic Discrimination
Narrow Band Filtering
Earth Noise
Anelastic Attenuation

This report describes

20. ABSTRACT (Continue on reverse side if necessary and identify by block number)

In this report we describe the results of a discrimination experiment performed on a large number of Eurasian events. ~~Our~~ The objective ~~in this experiment~~ was to identify each of these events as either an earthquake or an underground explosion based on an analysis of short-period P waves recorded at a global network of seismograph stations. ~~In all, there were~~ ten seismograph stations were involved in ~~this~~ the experiment. (continued)

DD FORM 1 JAN 73 1473 EDITION OF 1 NOV 65 IS OBSOLETE

UNCLASSIFIED

SECURITY CLASSIFICATION OF THIS PAGE (When Data Ente

20. ABSTRACT (continued)

The discrimination results obtained from this experiment support the theoretical predictions of Archambeau, et al. (1964) and demonstrate that the variable frequency magnitude (VFM) approach provides very effective discrimination between Eurasian earthquakes and explosions recorded at both teleseismic and regional distances. One of the principal findings of this study is that the effectiveness of $m_b(f)$ type discrimination at each of the stations included in this experiment is largely controlled by the attenuation properties of the upper mantle beneath a particular station. For instance, $m_b(f)$ estimates from data recorded at a station overlying high Q upper mantle (as evidenced either from the location of the station in a shield region and/or a region characterized by large negative P-wave travel-time residuals) consistently yield a greater degree of separation of earthquakes and explosions than do $m_b(f)$ estimates from a station located over low Q upper mantle.

AFTAC Project Authorization No. VT/0712/B/PMP
ARPA Order No. 2551, Program Code No. 6H189
Effective Date of Contract: November 17, 1978
Contract Expiration Date: November 15, 1981
Amount of Contract: $1,816,437
Contract No. F08606-79-C-0008
Principal Investigator and Phone No.
Dr. J. Theodore Cherry, (714) 453-0060
Project Scientist and Phone No.
Mr. Brian W. Barker, (202) 325-7581

This research was supported by the Advanced Research Projects Agency of the Department of Defense and was monitored by AFTAC/VSC, Patrick Air Force Base, Florida 32925, under Contract No. F08606-79-C-0008.

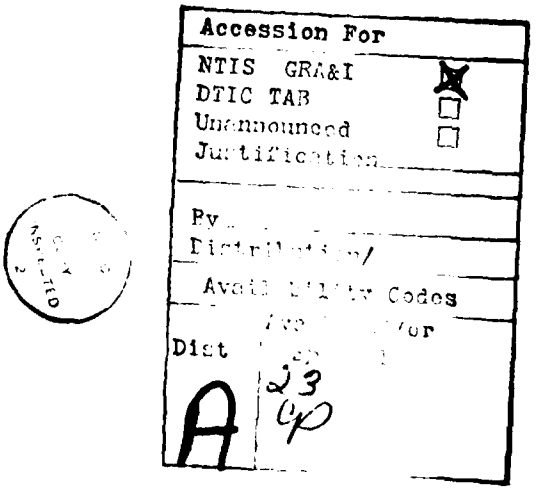

TABLE OF CONTENTS

LIST OF ILLUSTRATIONS

LIST OF ILLUSTRATIONS (continued)

LIST OF ILLUSTRATIONS (continued)

I. INTRODUCTION

In this report we describe the results of a discrimination experiment performed on a large number of Eurasian events. Our objective in this experiment was to identify each of these events as either an earthquake or an underground explosion based on an analysis of short-period P waves recorded at a global network of seismograph stations. In all, there were ten seismograph stations involved in this experiment. Results from related studies are presented in Savino, et al. (1979) and Savino, et al. (1980).

The discrimination technique that was used in this experiment is referred to as the variable frequency magnitude (VFM) technique. A fairly detailed formulation of the VFM approach and several examples of its application as an automated detection-discrimination technique will be discussed in later sections of this report. Briefly, the central feature of the VFM method is the use of a set, or "comb," of Gaussian shaped narrow band filters to decompose a digitial time series, consisting of signal plus noise, into a set of quasi-harmonic modulated signals. The Gaussian form of the filters ensures optimal time and frequency resolution within the constraints imposed by the sampling theorem or uncertainty principle (by contrast, purely harmonic components, or Fourier spectra, contain only frequency information). The filter center frequencies are selected to span the frequency range of the expected signal spectra. For each filter a time domain envelope function is constructed from the filtered and quadrature signals. The time of the maximum of a particular envelope function is the group or energy arrival time, t_g, of "signal" with a frequency near the filter center frequency. The amplitude of the envelope function at time, t_g, is the spectral amplitude, $A_g(f)$, of the signal energy arrival at the filter center frequency.

For identification of a signal as to the originating event type, the procedure is simply to compute the magnitude $m_b(f)$ ($\propto \log A_g(f)$) and construct $m_b(f)$ planes wherein event $m_b(f)$ values at a high frequency (e.g., > 2.0 Hz) are plotted versus $m_b(f)$ values at a lower frequency (e.g., 0.5 Hz). Observed signals can then be characterized by the location of their $m_b(f)$ values in these planes. It is predicted theoretically (Archambeau, et al., 1974) that ordinary earthquake signals fall in one particular area within such planes and that explosions (of all types) fall within a distinctly separate area.

The $m_b(f)$ results obtained from this experiment support the theoretical predictions of Archambeau, et al. (1974) and demonstrate that the VFM approach provides a very effective discriminant between Eurasian earthquakes and explosions recorded at both teleseismic and regional distances. One of the principal findings of this study, however, is that the effectiveness of $m_b(f)$ type discrimination at each of the stations included in this experiment is largely controlled by the attenuation properties of the upper mantle beneath a particular station. For instance, $m_b(f)$ estimates from data recorded at a station overlying high Q upper mantle (as evidenced either from the location of the station in a shield region and/or a region characterized by large negative P-wave travel-time residuals) consistently yield a greater degree of separation of earthquakes and explosions than do $m_b(f)$ estimates from a station located over low Q upper mantle. Based on this result, we devised a fairly simple station classification scheme (Savino, et al, 1979 and Savino, et al., 1980). Accordingly, stations were specified as being a Class I, II or III type depending upon discrimination performance and evidence of upper mantle attenuation properties – a Class I station providing the greatest separation of earthquake and explosion populations, a Class III station the least. In

terms of this classification scheme, the principal conclusions resulting from this experiment are the following:

- VFM discrimination can be achieved to $m_b \sim 4$ at Class I regional stations.
- VFM discrimination based on both regional and teleseismic stations is approximately 95 percent effective for all the events in this experiment.
- The VFM technique is an effective discriminant principally because of the enriched high frequency source spectra of explosions relative to earthquakes with the same spectral level near two seconds period.

The VFM discrimination procedure is embodied in the MARS (Multiple Arrival Recognition System) computer program. During the course of this discrimination experiment, and under support from both the Vela Seismological Center (VSC) and the U. S. Arms Control and Disarmament Agency (ACDA), an automated detection-discrimination algorithm based on the narrow band filtering technique was developed and added to MARS. The approach adopted in the formulation of the detection algorithm (Masso, et al., 1979) is one of pattern recognition. That is, based on the output from a comb of narrow band filters applied to a digital seismogram the algorithm searches for patterns in the signal and noise information as it is expressed in the t_g-f plane (the group arrival time versus frequency plane). In the case of a body wave, the pattern to be searched for is that of a (nearly) undispersed signal with spectral amplitudes significantly above background noise. Thus, in the t_g-f plane the algorithm searches for a straight line-up in time of envelope maxima over a band of frequencies. Included in the algorithm is a somewhat unique approach to the treatment of "noise" contamination of detected signals. All the event seismograms included in the discrimination experiment were processed with this automated version of MARS.

The organization of this report is as follows. In Section II we describe the narrow band filtering technique and the automated detection-discrimination algorithms that comprise the VFM technique used in this experiment.

In Section III we present the VFM discrimination results for each of the ten stations included in this phase of the experiment. A tabulation of all the VFM discrimination parameters is given in Appendix A for each station. Multistation estimates of event types (explosion or earthquake) based on the ten stations included in this phase of the experiment and a number of other stations are discussed in Savino, et al. (1980).

II. AUTOMATED DETECTION AND DISCRIMINATION

2.1 VFM DISCRIMINATION PROCEDURE

The variable frequency magnitude (VFM) discriminant, as originally proposed by Archambeau, et al. (1974) and subsequently developed and applied by Savino and Archambeau (1974), is the basic technique that was used to identify the Eurasian events included in this experiment. While the VFM approach is completely general in its application, that is, it can be applied to multicomponent long and short period data, the emphasis here is on short period vertical-component P-wave seismograms.

2.1.1 Narrow Band Filtering

The central feature of the VFM signal analysis approach is the use of narrow band frequency filters to break up or decompose a time series consisting of signal-plus-noise into a set of quasi-harmonic modulated "signals." This set of filtered signals, one for each filter center frequency, can then be used to determine the energy arrival time (the group time, t_g) and amplitude of the signal for each center frequency by analysis of the time modulation of the filter outputs.

Over the past several years, the VFM signal analysis procedure has undergone several stages of refinement. The automated procedure that was used during this experiment is embodied in a large versatile computer program referred to as the Multiple Arrival Recognition System (MARS). Figure 1 summarizes the flow of operations in the MARS program: Figure 1a provides a verbal outline; Figure 1b presents the key mathematical operations performed in this program. Although not exercised on the data set in this experiment, the polarization filtering techniques that have been implemented in MARS are included.

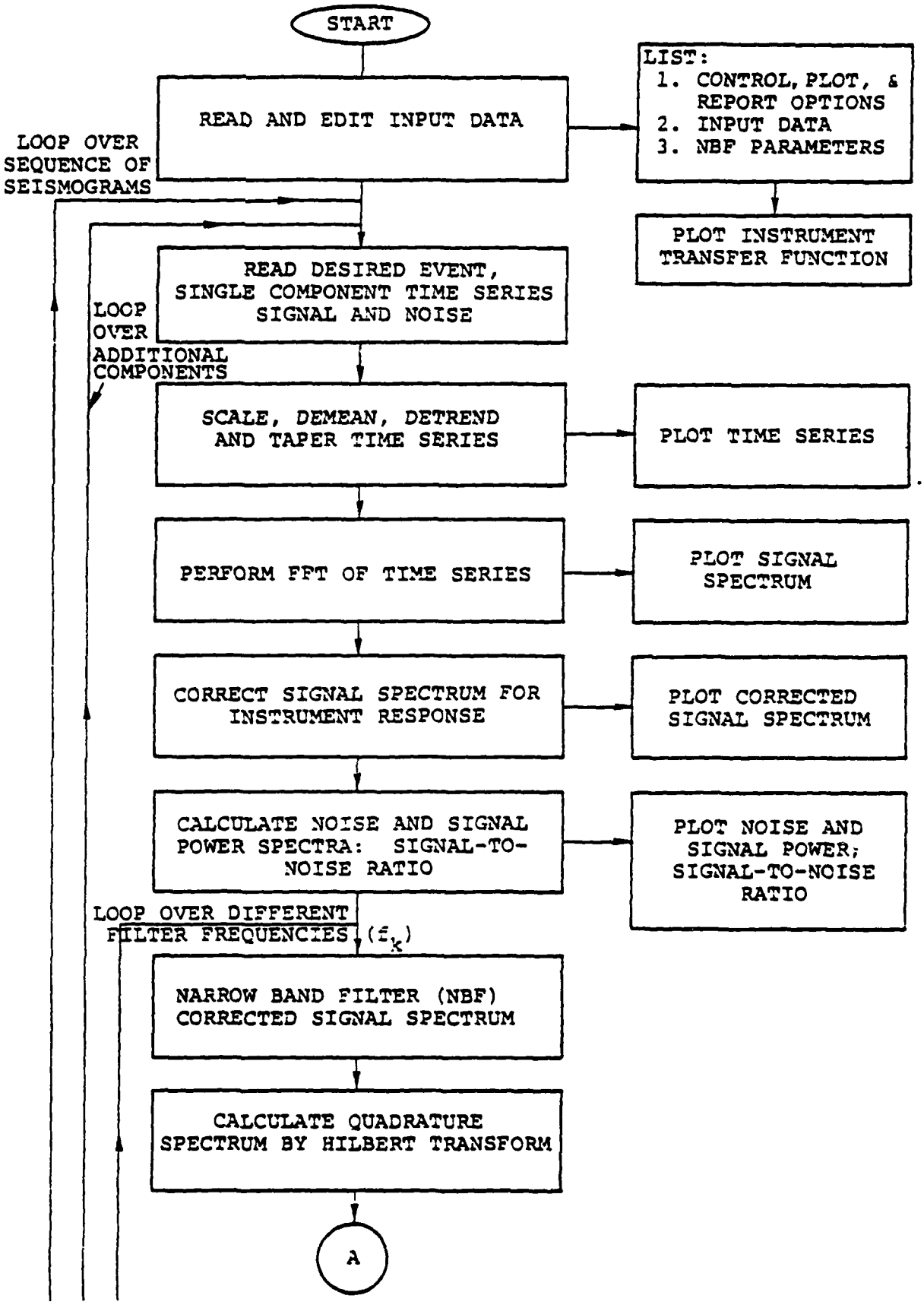

Figure 1a. MARS flowchart.

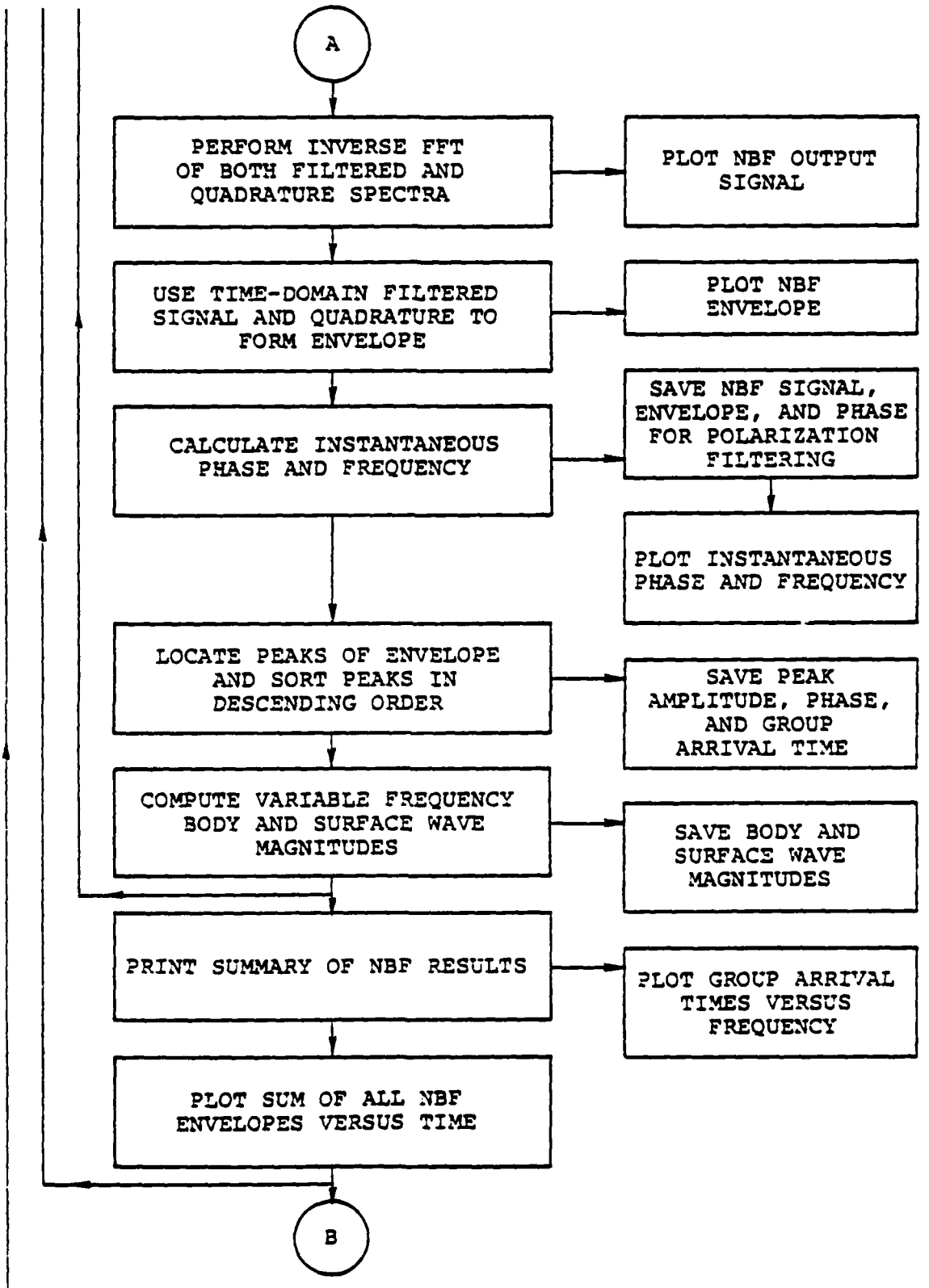

Figure 1a. (continued)

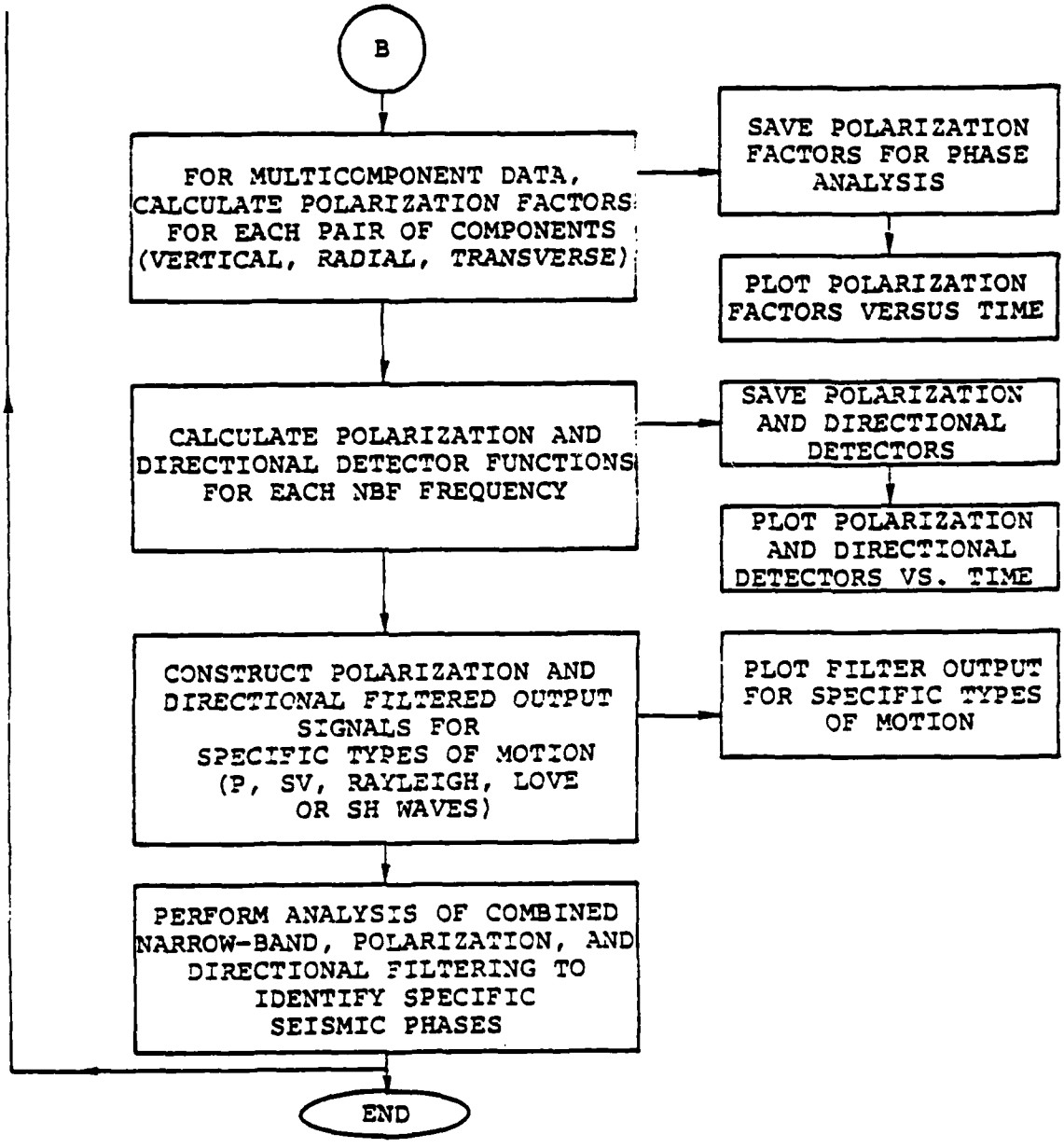

Figure 1a. (continued)

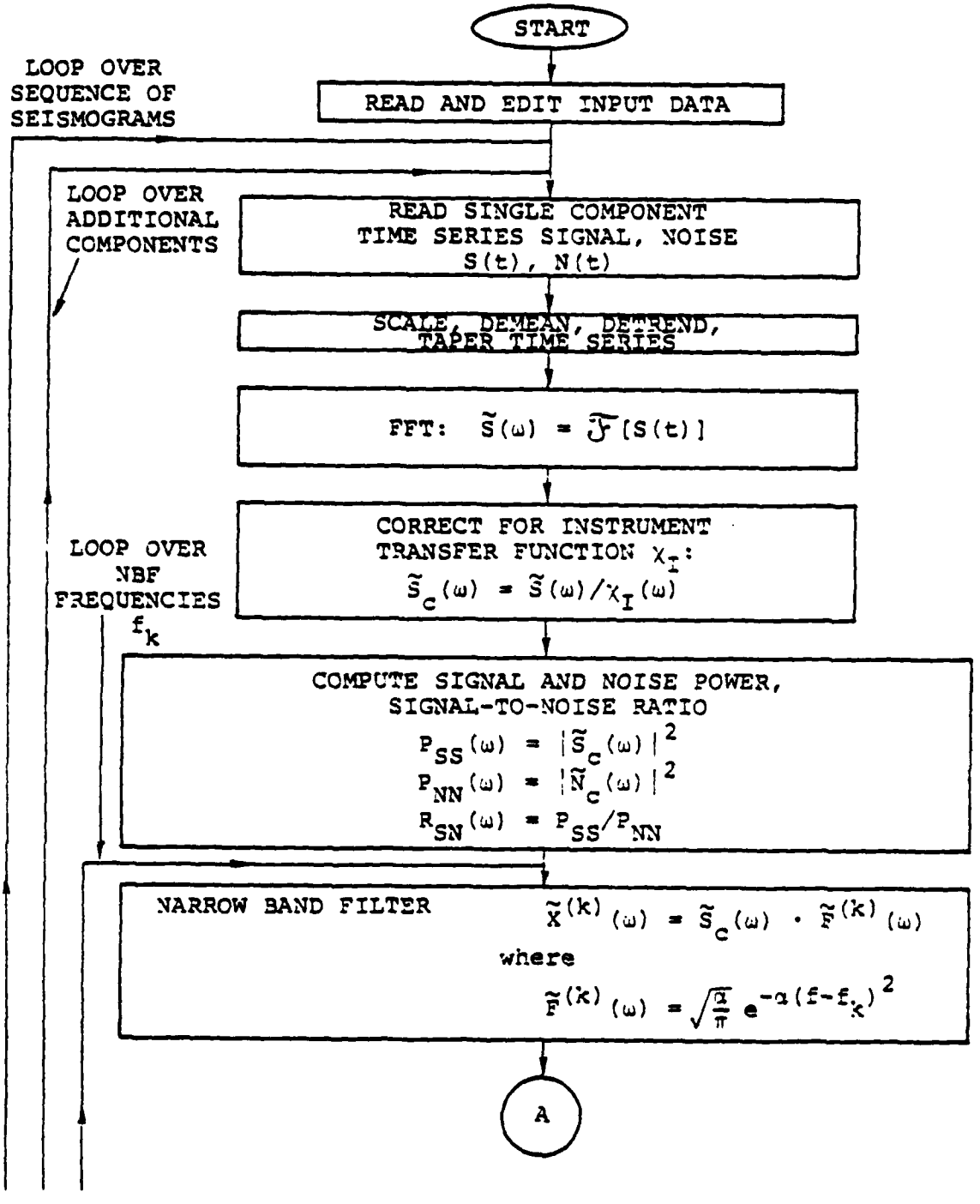

Figure 1b. Flowchart indicating principal mathematical operations in the MARS program.

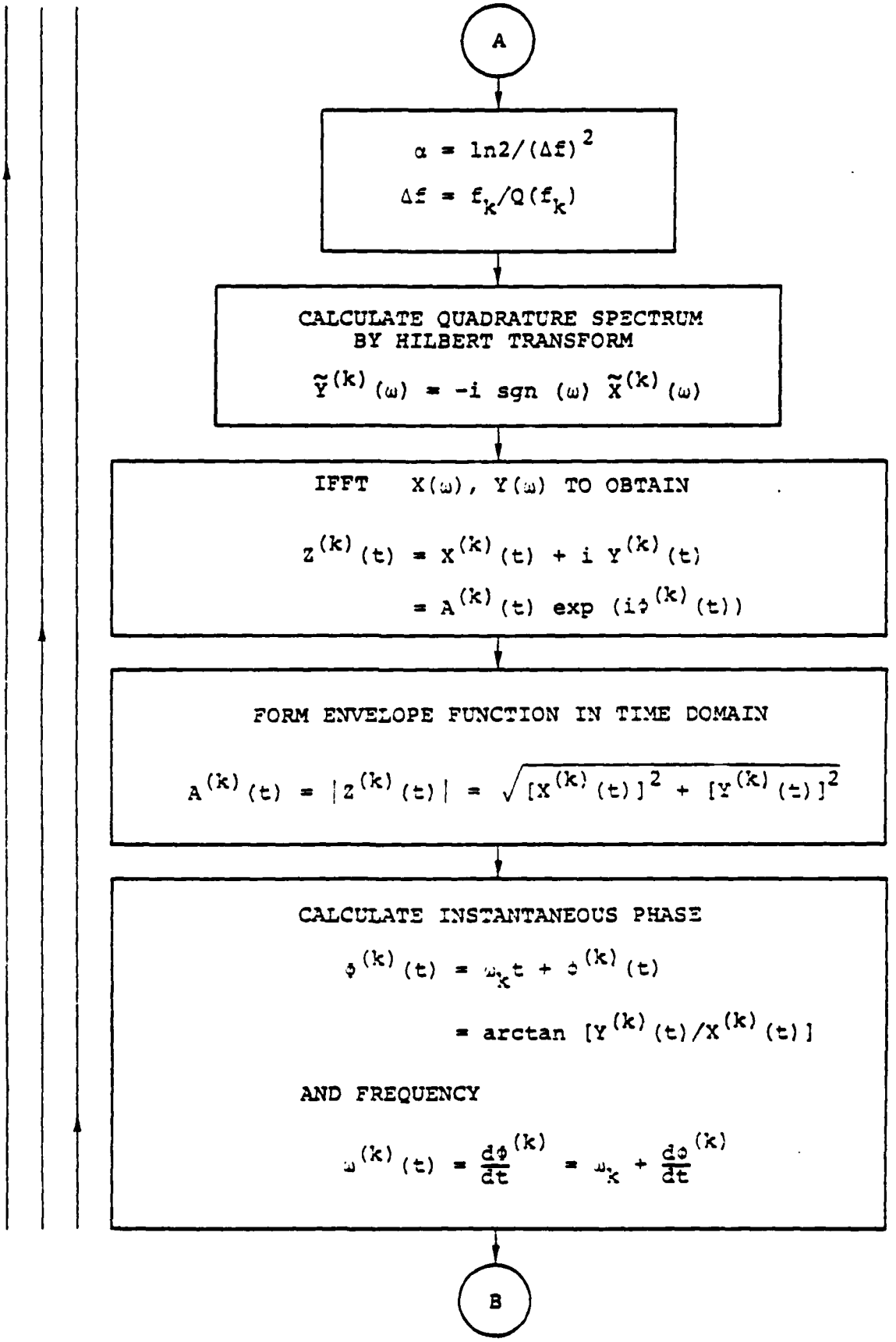

Figure 1b. (continued)

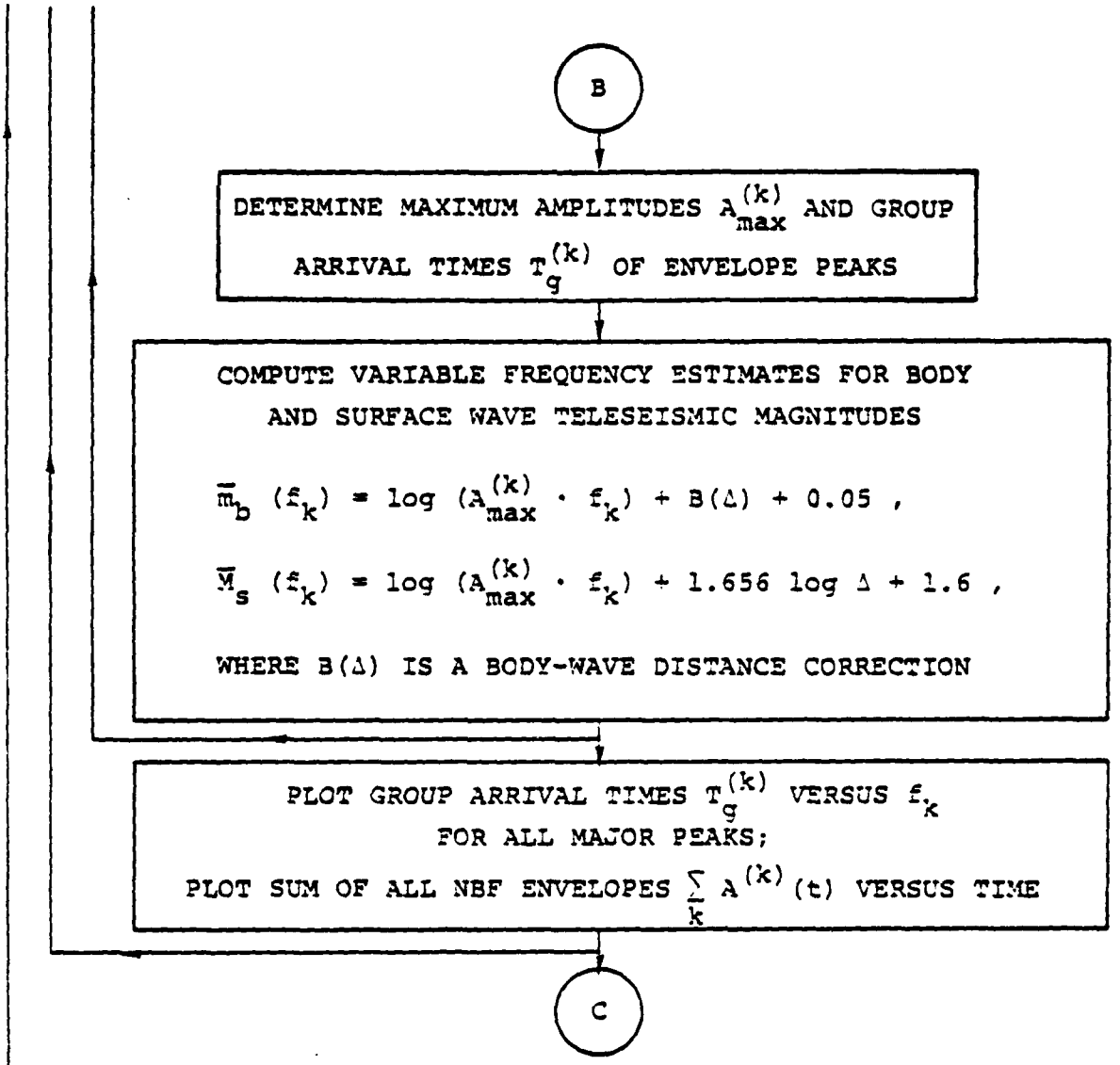

Figure 1b. (continued)

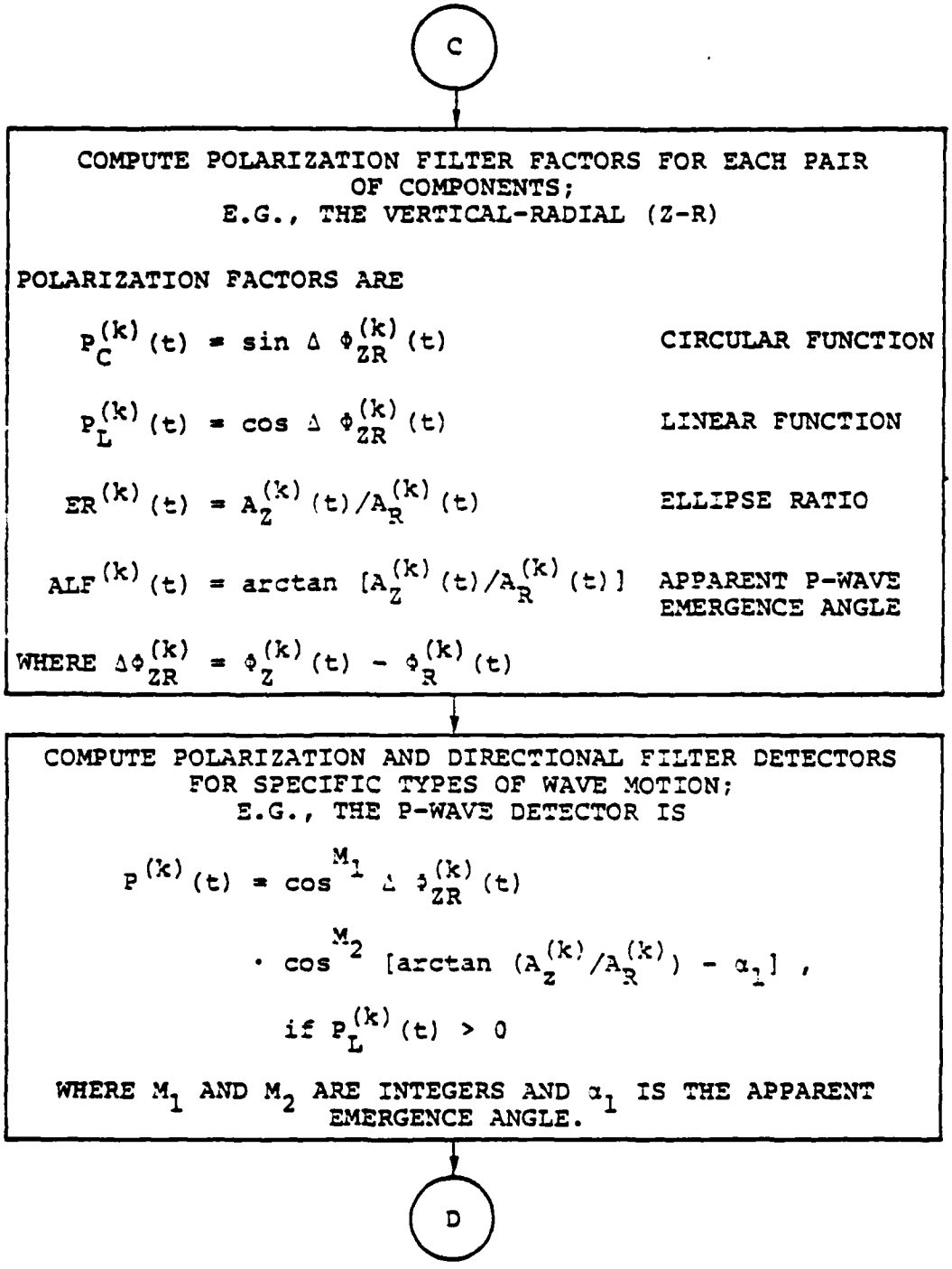

Figure 1b. (continued)

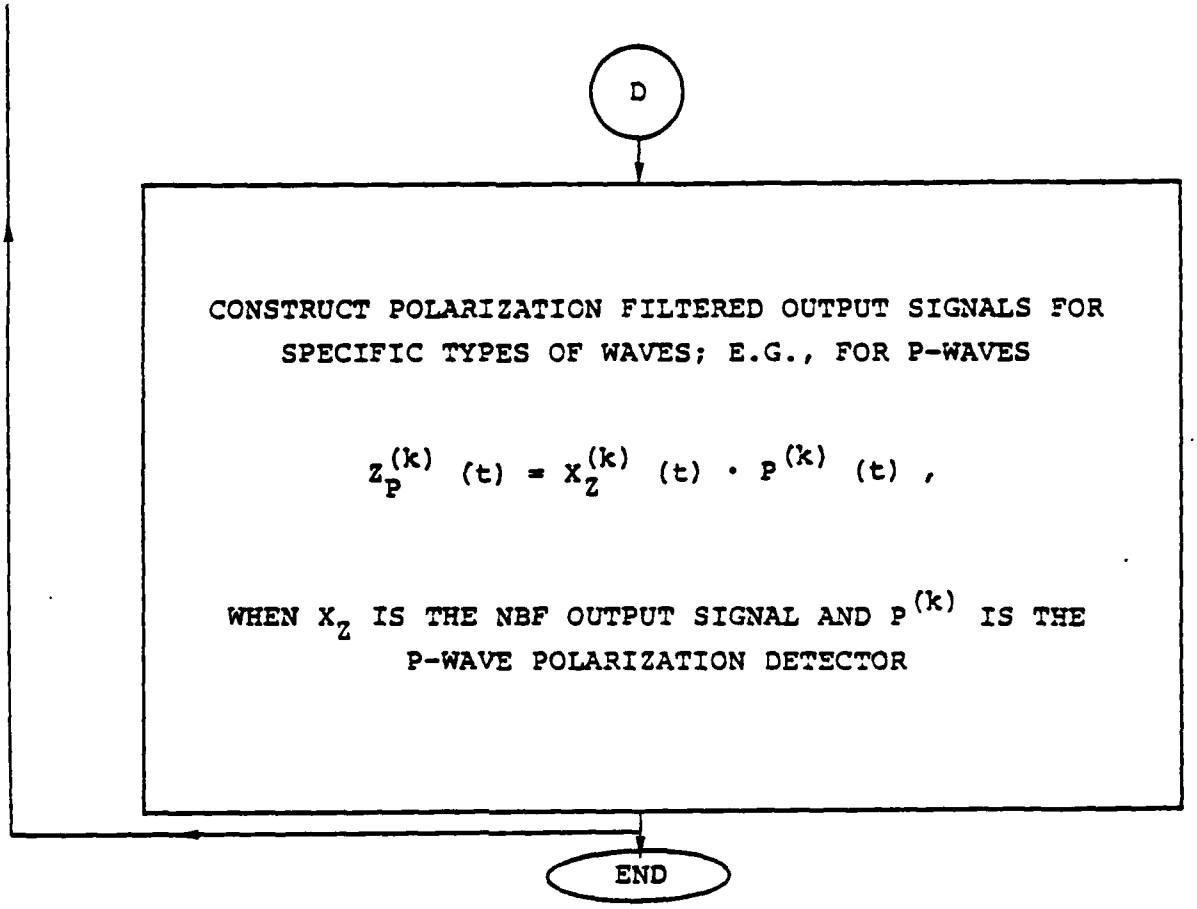

Figure 1b. (continued)

Seismic data are read into the program in the form of time series (Figures 1a and 1b) generally of about 500 to 2000 points in length. The data are then optionally detrended, demeaned and tapered. The program then selects the smallest power of two which is greater than the number of points input and performs a discrete Fourier transform using the Cooley-Tukey algorithm. The signal spectrum is corrected for the appropriate instrument response; i.e., the signal transform is divided by the instrument transfer function.

Referring to Figures 1a and 1b, the signal is next filtered in the frequency domain by multiplication by a narrow band Gaussian-shaped filter. This particular filter form is selected to satisfy two goals: (1) minimum width in the frequency domain, and (2) maximum ripple suppression in the time domain. As a consequence of the sampling theorem, or uncertainty principle, one cannot simultaneously satisfy these two goals to arbitrary precision. The filter employed was selected for its optimal time and frequency domain characteristics within this basic limitation. Once the signal has been narrow band filtered, the resulting complex spectrum is then inverse Fourier transformed into the time domain, to produce what will hereafter be referred to as the filtered signal.

The narrow band filtered signal will appear as a quasi-sinusoidal carrier wave contained within a smooth envelope. The next step in the program (Figures 1a and 1b) is to construct the envelope function by means of the Hilbert transform. In particular, a quadrature signal is formed by multiplying the transform of the filtered signal by $-i\ \mathrm{sgn}(\omega)$ and then inverting this to the time domain by an inverse transformation. The envelope function is then constructed by taking the square root of the sum of the squares of the filtered signal and its quadrature. The maximum of the envelope function

occurs at the time of arrival of energy at the center frequency of the filter and the amplitude of the maximum is proportional to the spectral amplitude of the filtered signal at the center frequency of the filter. The narrow band filtering procedure can be performed on a particular component seismogram at a number of different frequencies within some band of interest. Correlation of the resulting envelope functions indicates the arrival times of the various frequency components.

The instantaneous frequency and phase are computed from the filtered signal and its quadrature signal; both signals are stored for subsequent use in polarization filtering with additional components of ground motion when available.

The output of the narrow band filter processing is a table including the envelope peak amplitudes (A_k) and associated arrival times (t_g) for each center frequency (f_k). Generally there are many A_k, T_g pairs for each filter, depending on the complexity of the signal.

Let us look more closely at the narrow band filter. As given in Figure 1b, the functional form is

$$\tilde{F}^{(k)}(w) = \sqrt{\frac{\alpha}{\pi}}\, e^{-\alpha(f-f_k)^2} \qquad (1)$$

where

$$\alpha = \frac{\ell n\ 2}{2}\,\frac{Q^2}{f_k^2} \quad .$$

Viewed as a Gaussian probability distribution, this filter has standard deviation

$$\sigma_f = \frac{1}{\sqrt{\ell n 2}} \frac{f_k}{Q} \quad , \tag{2}$$

which means that 68.3 percent of the area under the filter is contained in the frequency band $f_k - \sigma_f \leq f_k \leq f_k + \sigma_f$.

It is easily shown that the time domain expression of the filter (Equation 1) is

$$F^{(k)}(t) = \frac{2\pi}{\alpha} \cos(2\pi f_k t)\, e^{-\frac{\pi^2 t^2}{\alpha}} \quad . \tag{3}$$

The Gaussian envelope function then has standard deviation

$$\sigma_T = \frac{\sqrt{\ell n 2}}{2\pi} \frac{Q}{f_k} \quad . \tag{4}$$

We see that the width of the narrow band filter is controlled by the parameter Q which appears in the definition of α. From Equations (2) and (4) it is clear that the narrower the filter in frequency, the wider in time and vice versa. For high Q we get an excellent estimate of the spectral amplitude for a broad time window; there will be few A_K, t_g pairs for each filter. For low Q the spectral estimate is less precise but the t_g are more accurate and there are generally many peaks for each filter.

A choice of a preferred Q was made by trial and error testing of different values on both synthetic and observed seismograms. For short period data sampled 20 times/second, we have adopted the following Q values for all the seismograms processed in this experiment:

$$Q = 12.5\, f_k, \qquad f_k \geq 0.70,$$

$$Q = 8.00, \qquad f_k < 0.70. \tag{5}$$

For $f_k \geq 0.70$ we compute from Equation (2) that

$$\sigma_f = 0.096 \text{ Hz}.$$

Thus, the width of the filter within one standard deviation is 0.192 Hz. For $f_k < 0.70$ Equation (2) gives $\sigma_f = 0.15\, f_k$ and the filter is narrower.

From Equation (4) we have for $f_k \geq 0.70$ that

$$\sigma_T = 1.66 \text{ seconds}.$$

The filter width is therefore approximately three seconds for these f_k, using standard deviation as the criterion, and somewhat wider at lower center frequencies.

Figure 2 shows the outputs of a suite of narrow band filters applied to two event seismograms, event 47 in Figure 2a and event 21 in Figure 2b. As shown later, event 47 is identified as a Kurile earthquake while event 21 is identified as a presumed explosion north of Lake Baikal. The original unfiltered seismograms are the topmost traces in each figure. The center frequencies of the narrow band filters range from 4.0 to 0.5 Hz. In terms of signal-to-noise ratio (S/N), the basic features of the VFM discriminant can be seen here. For instance, the presumed explosion signal in Figure 2b is quite evident over the frequency range 3.5 to 0.8 Hz. The earthquake signal (Figure 2a) does not persist above the ambient noise level at frequencies higher than 2.75 Hz, whereas it exhibits a higher S/N at 1.0 Hz and 0.8 Hz than the presumed explosion.

A final point to be noted from Figures 2a and 2b is the approximate time alignment of the maximum narrow band filter

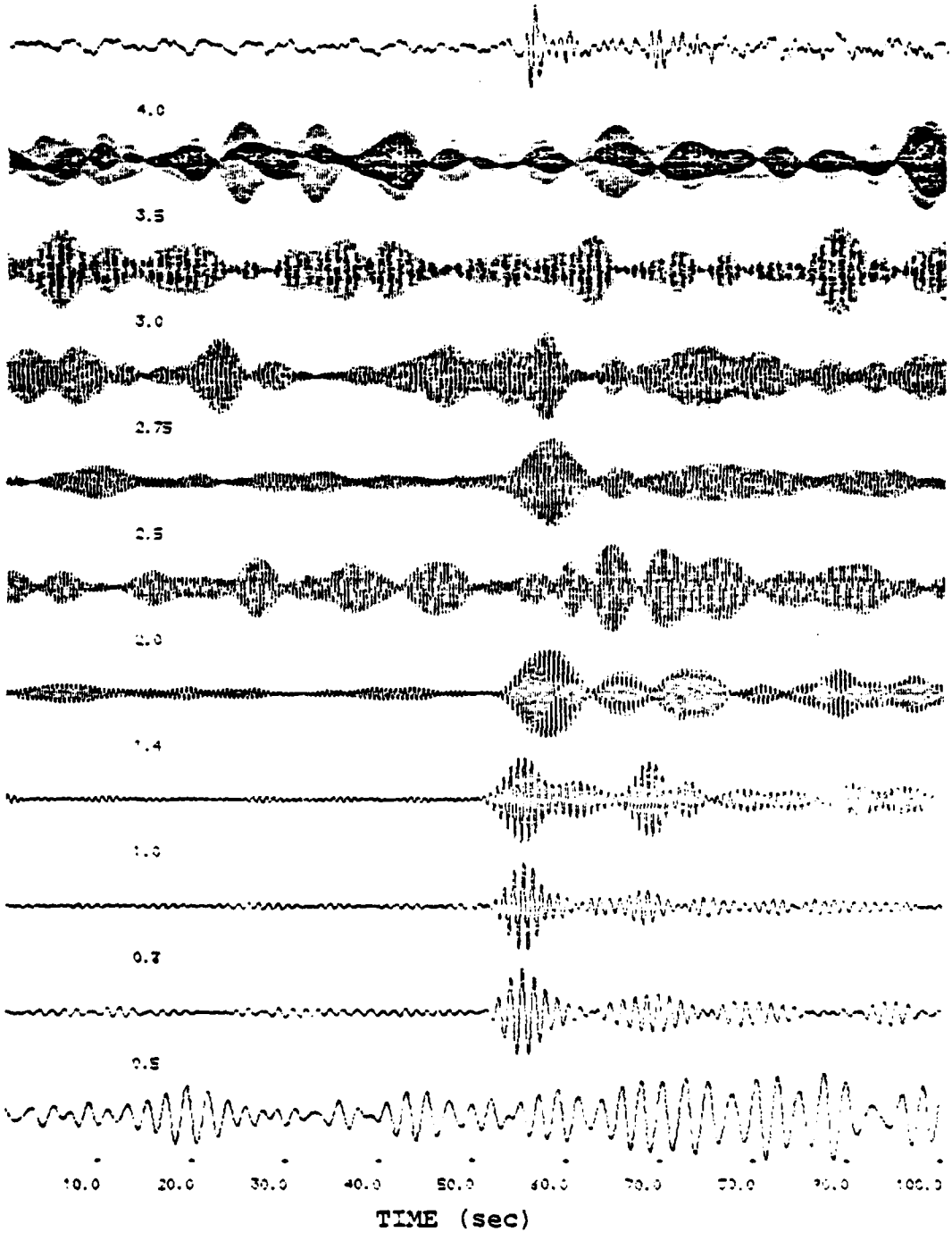

Figure 2a. Examples of the outputs of a suite of 4.0 to 0.5 Hz narrow band filters applied to a seismogram (shown at top of figure) from a Kuril earthquake recorded at a station at teleseismic distances.

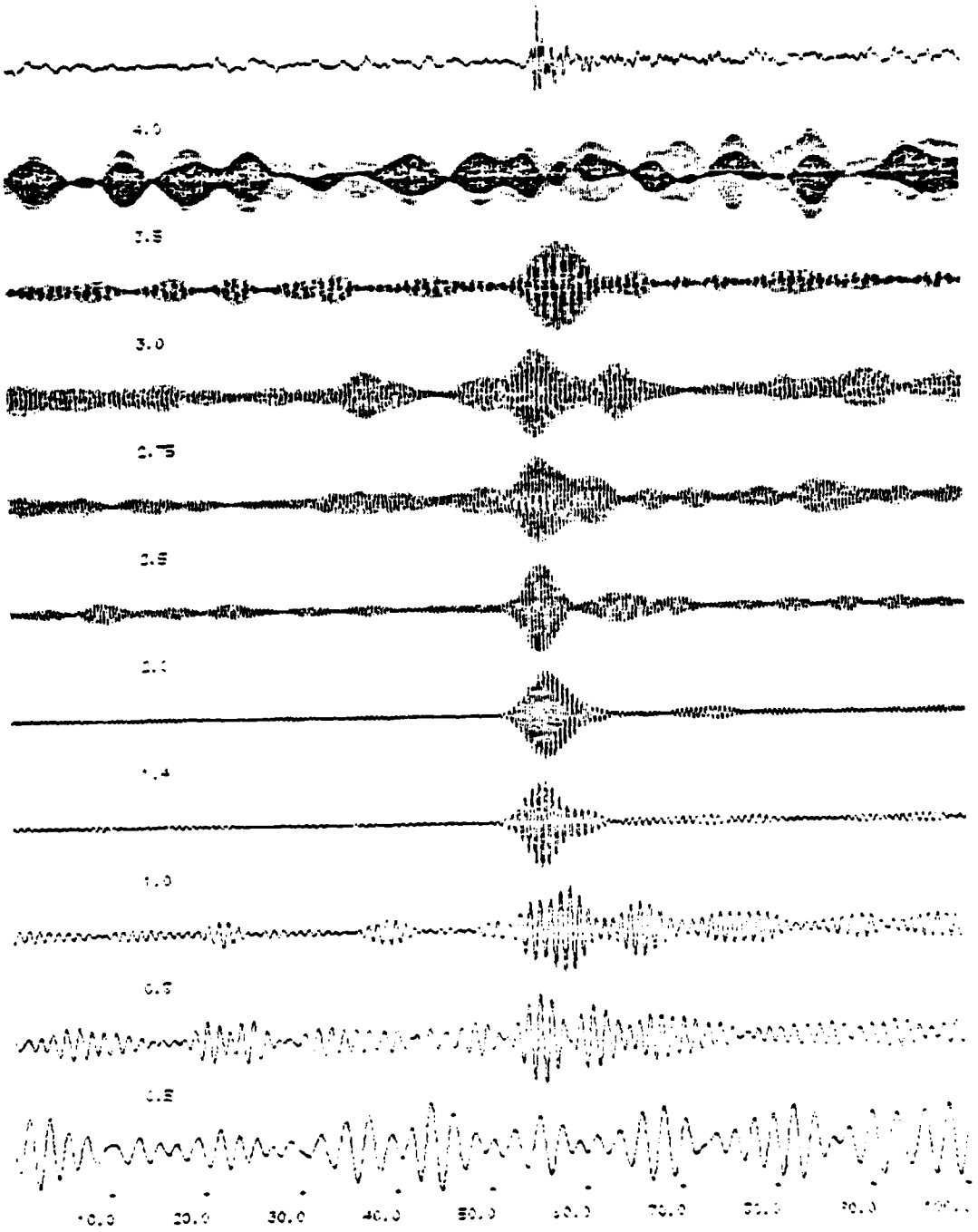

Figure 2b. Examples of the outputs of a suite of narrow band filters applied to a seismogram (top of figure) of a presumed explosion recorded at the same station as in Figure 2a.

amplitudes, with high S/N, corresponding to the signal arrival. This observation forms the basis for the automated detection-discrimination algorithm described in the following subsection of this report.

2.1.2 The Automated Detection Algorithm

The decomposition of a signal wave train into quasi-harmonic signals by the application of phaseless Gaussian-shaped narrow band filters provides the means of determining arrival time, amplitude and phase, all as functions of frequency. This is the basic signal information that can be used to detect a given type of signal in terms of its dispersion characteristics and to obtain its spectrum as well as its time and amplitude relationship with respect to other signals present in a complex wave train.

The basic approach used in the MARS program is to identify patterns from the signal and noise information as it is expressed in the t_g-f plane (the group arrival time, t_g, versus frequency plane). The pattern to be searched for in the t_g-f plane corresponds, in the case of a body wave, to a (nearly) undispersed signal, with spectral amplitude significantly above background in a frequency range corresponding to some fraction of the total band. This frequency band will be in a range where the signal power is expected to be highest relative to noise. (This means we make use of the matched filtering concept, in the sense that we know roughly what spectral content we expect for the signal. This concept is also used when we look for undispersed signals or signals of known dispersion characteristics.) Thus, in the t_g-f plane we search for a straight, horizontal line-up of envelope maxima in a selected frequency band, using the largest maxima as the beginning point in such a pattern recognition procedure. This implicitly uses a threshold detection criteria in a

detection band, since by starting with the largest envelope maxima we are essentially requiring that the signal power be above the background level in at least a part of the detection band.

Basically, then, by looking in this t_g-f-A_g-ϕ_g space, we apply criteria based on properties of the expected signal, namely its expected dispersion and spectral content, in order to recognize a signal pattern and thereby to detect the signal. An example of how this is accomplished is shown in Figure 3. In this figure we plot the times (t_g) of the envelope maxima from narrow band filter outputs, with of the order of N = 20 filters used so that the signal frequency content is sampled at about 20 points, f_n. With each envelope maxima point in the plane, there is also an associated (spectral) amplitude $A_g(f_n)$, instantaneous phase $\phi_g(f_n)$ and an instantaneous frequency $(d\phi/dt)_{t_g}$. Thus the t_g-f plot corresponds to a multidimensional display of spectral content and energy arrival time for a given segment of a time series. Normally either 1024 or 2048 points are used for time segments, and for the short period seismic data in the discrimination data base this corresponded to a 50 to 100 second segment which was processed in each pass. For on-line continuous processing, overlapping time segments would be used.

A sub-band within the entire frequency range covered by the set of filters is shown in Figure 3 and is used as a "detection band," that is a frequency band within which a signal pattern (straight horizontal line locus of envelope maxima in the case of an undispersed body wave) is sought. This band, from f_L^* to f_H^*, is selected externally, based on the expected signal frequency character. The largest envelope maxima within this band are flagged (denoted by [X] in the figure) and used to compute a mean "signal" arrival time (i.e., group time) $\bar{t}_g$ for the maximum power arriving in this frequency range. An acceptance window in time, for which

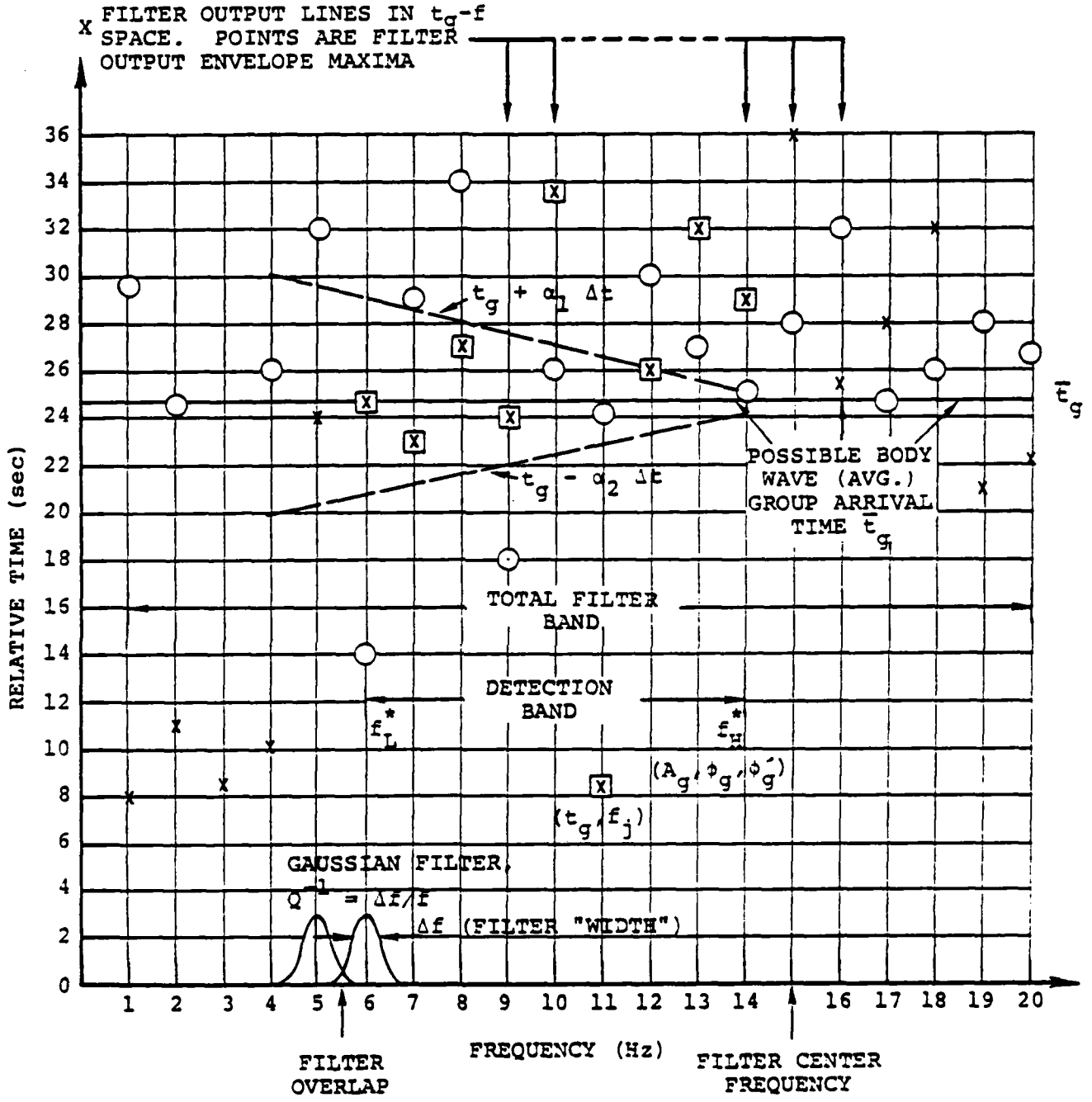

Figure 3. Typical t_g-f plane representation of a time series segment (0 to 36 sec) when the signal-to-noise ratio is low. Only the largest envelope maxima (X) and second largest maxima (○) are shown. Other, numerous, smaller envelope maxima are normally scattered throughout the t_g-f plane, but for this illustration they have been omitted. Each filter "output line" normally displays about ten such peaks.

maxima can actually be associated with an undispersed signal, is constructed using the relation: $t_w^{\pm} = \bar{t}_g \pm t_\sigma^{\pm} \pm \alpha\Delta t$; where Δt is the time uncertainty associated with the envelope maximum time t_g for a filter output at center frequency f and half power band width Δf. In particular, $\Delta t \Delta f \geq 1/4\pi$ is the theoretical uncertainty relation and since $\Delta f/f = Q^{-1}$, then $\Delta t \geq 1/4\pi(Q/f)$. Further we use $t_\sigma^{\pm}$ to denote the standard deviation in the time data used to compute t_g and make use of it to define the acceptance time window about $\bar{t}_g$ as well. Hence, taking an appropriately chosen constant α near unity, then two time window boundary lines can be defined to give the time window; that is: $\bar{t}_g + t_\sigma^{+} + (\alpha/4\pi)(Q/f)$ and $\bar{t}_g - t_\sigma^{-} - (\alpha/4\pi)(Q/f)$. All of the largest maxima within such a window are then taken as acceptable undispersed "signal" group arrivals and those outside are rejected.

The largest maxima within the initially defined window are now used to recompute a new group arrival time, $\bar{\bar{t}}_g$, and signal acceptance window. Finally, using all those filter peaks that lie within the $\bar{\bar{t}}_g$ acceptance window and exceed the ambient noise level, we define a final group arrival time, $\bar{\bar{\bar{t}}}_g$.

The $\bar{\bar{\bar{t}}}_g$ estimate corresponds to the arrival time of maximum signal energy. For purposes of multiple phase detection and event locations we added an algorithm to MARS that gives estimates of phase arrival times. This is accomplished by flagging the earliest filter peaks (envelope maxima) that occur within the final signal acceptance window. There must be a minimum number of such peaks, typically three, all of which exceed the mean noise level at the corresponding frequencies by at least one standard deviation.

Figures 4 through 7 are a sequence of examples of the application of the automated detection and first arrival algorithms to seismograms for two of the events in the discrimination data base; events 47 and 81. The events are

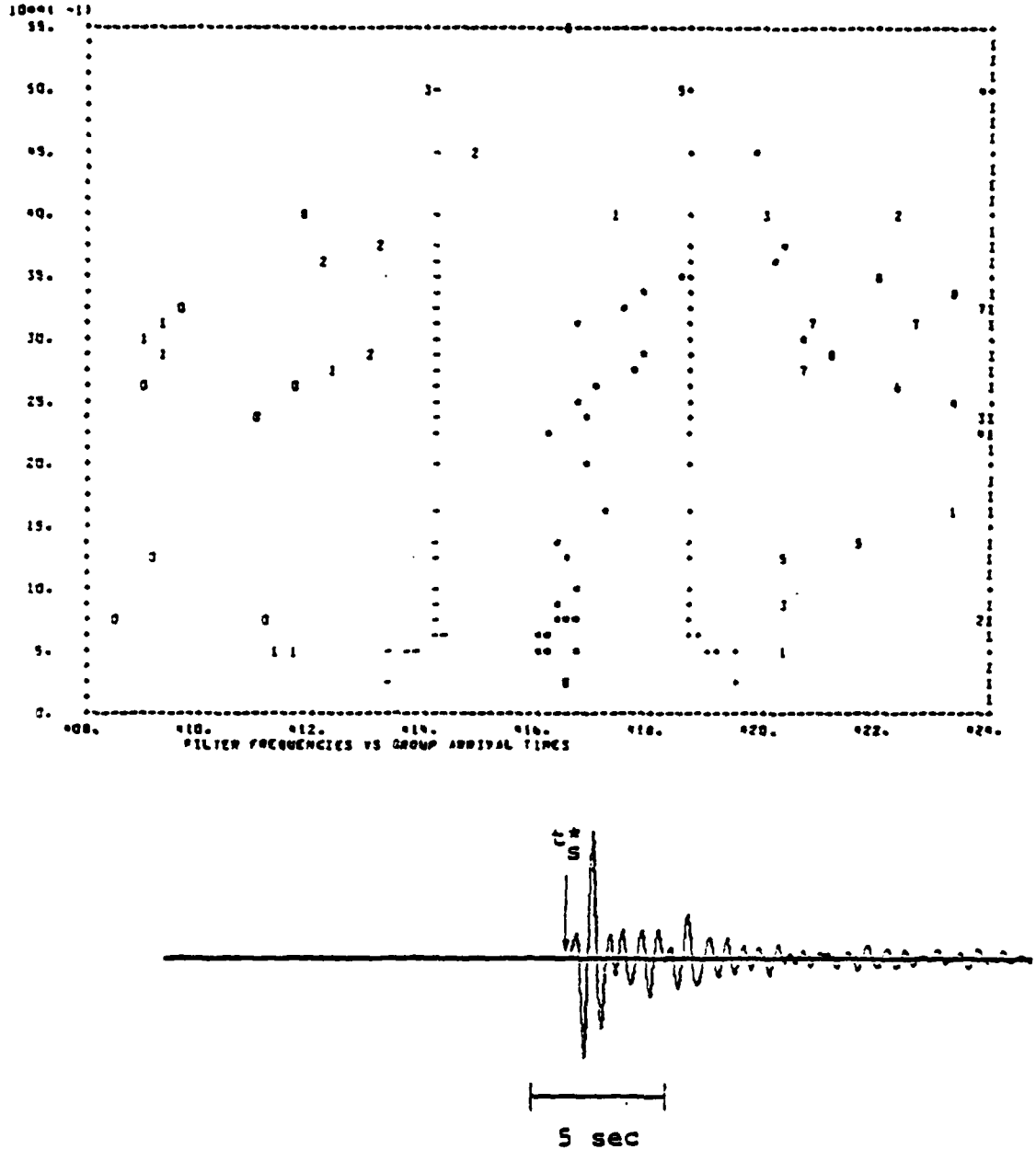

Figure 4. Bottom is a seismogram written at the Seismic Research Observatory (SRO) in Chiang Mai, Thailand (CHTO) from a presumed explosion in eastern Kazakhstan. The top is the f_c versus t_g plot for this seismogram.

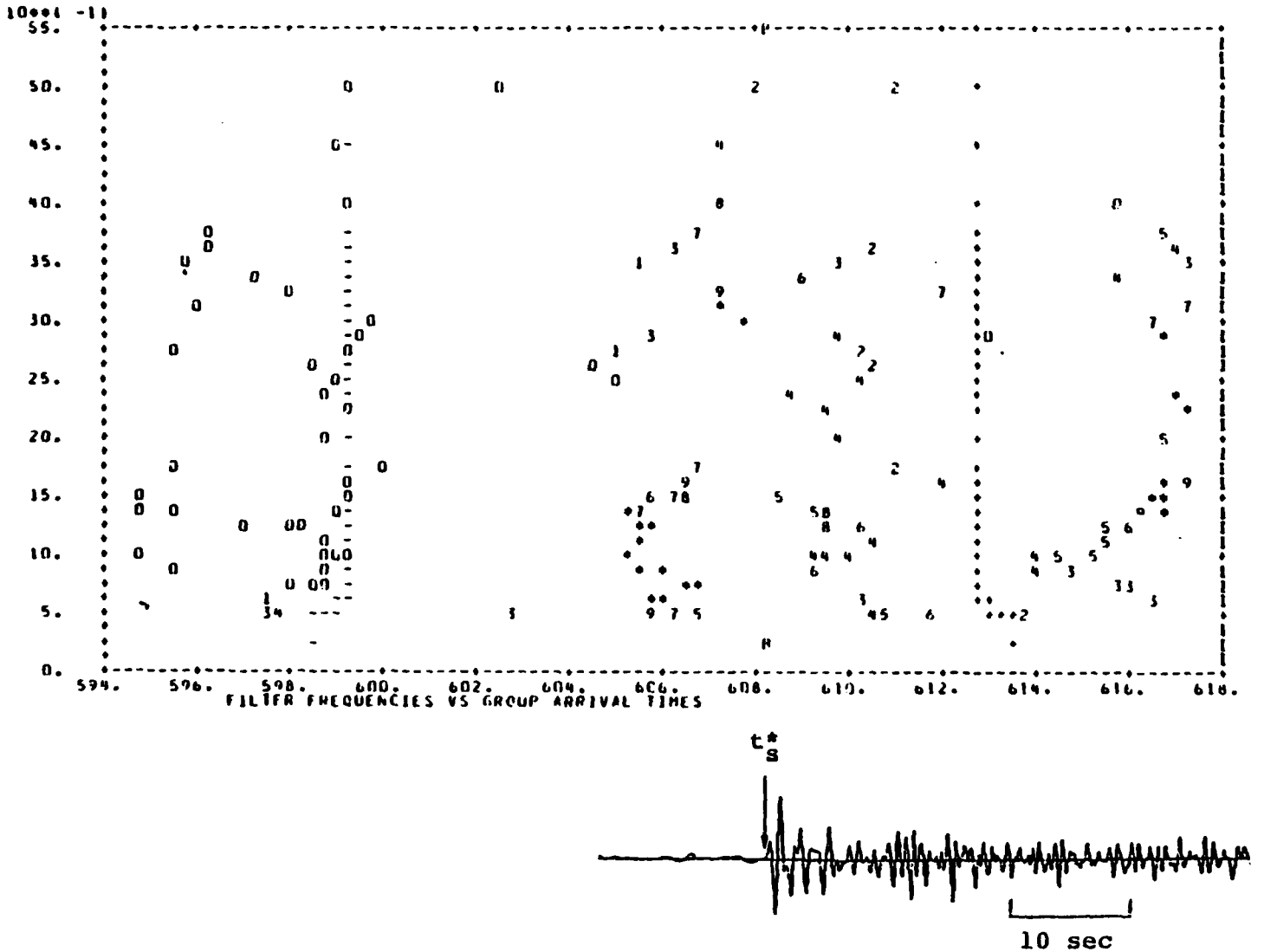

Figure 5. Seismogram (bottom) written at Tatalina, Alaska, for the same presumed explosion as in Figure 4.

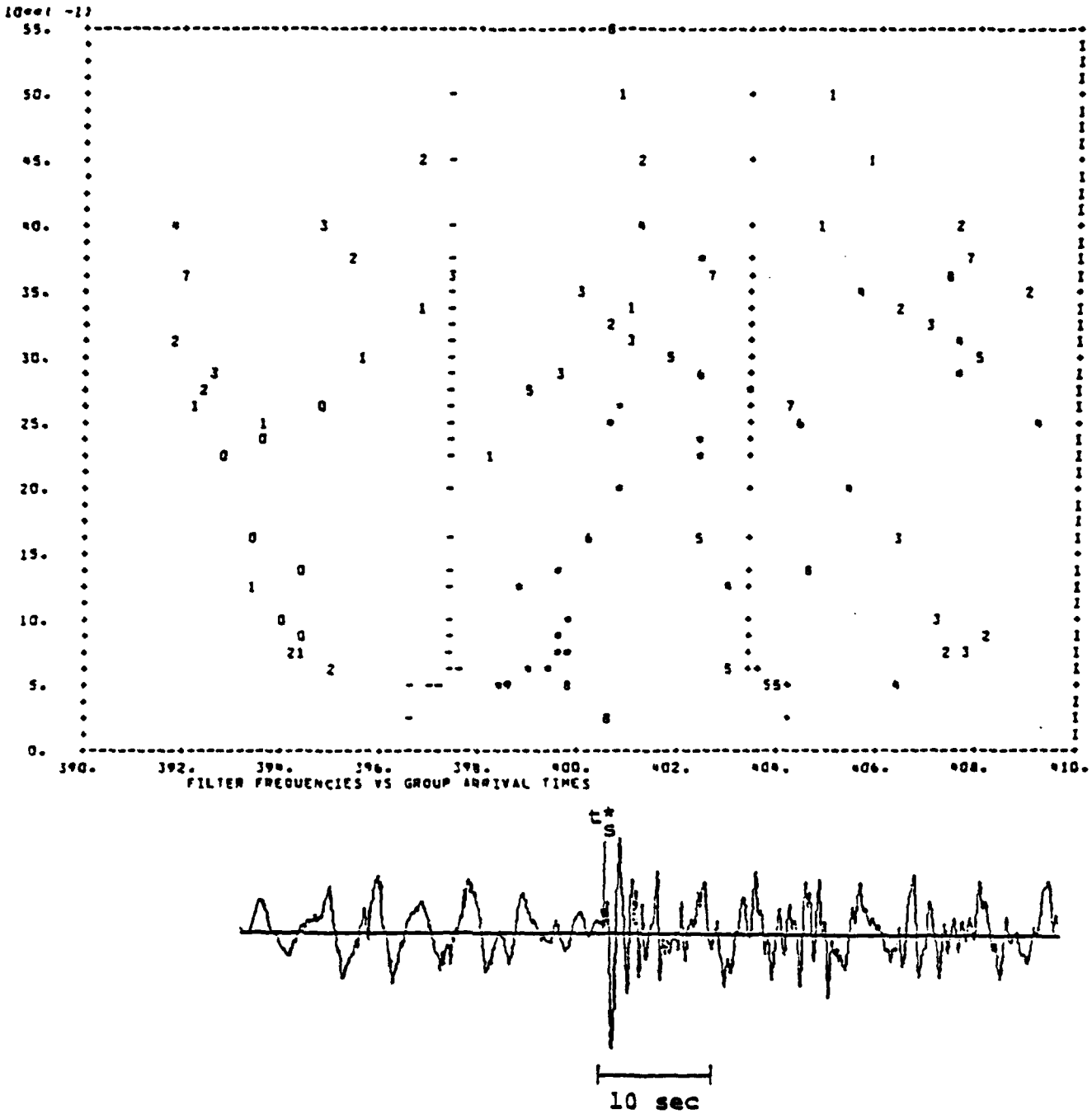

Figure 6. Bottom portion is a seismogram recorded at a station in Bluff, Alaska, from an event in the Kurils. The top half is a plot of filter center frequency versus group arrival time (sec). The t_s^* with arrow attached shows where the automated detection and first arrival algorithms picked the signal arrival time.

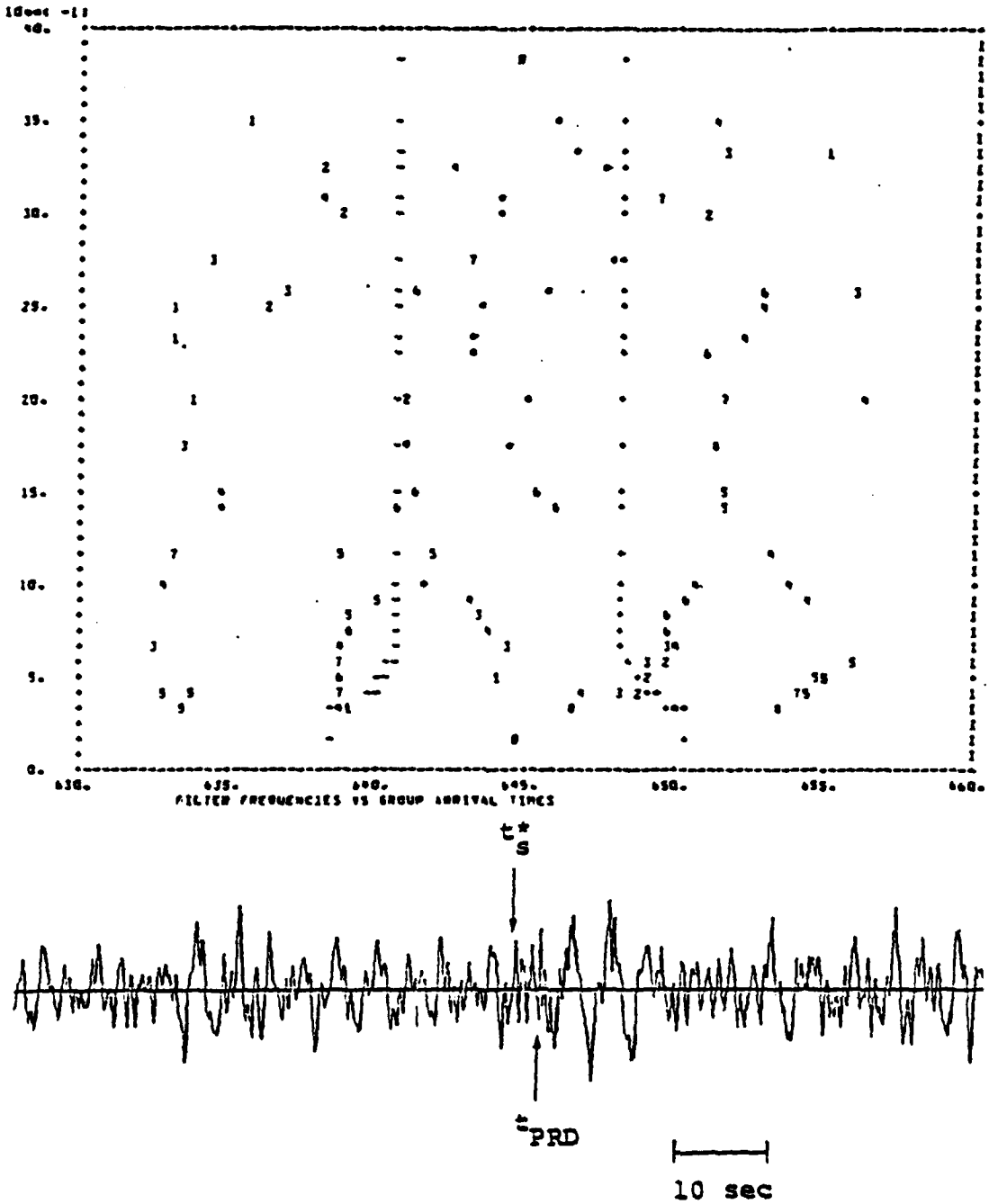

Figure 7. Bottom portion is a seismogram recorded at NORSAR for the same Kuril earthquake shown in Figure 6. The top portion of this figure is the f_c versus t_g plot determined for this time series by MARS.

shown in the order of decreasing signal-to-noise ratio. The bottom portions of these figures show the seismograms that were processed with MARS. In each case, the recordings are short-period vertical component seismograms. The corresponding digital time series were 100 seconds in duration with at least 50 seconds of background noise preceding the signal arrival.

The top portions of Figures 4 through 7 are the final t_g-f_c planes that are arrived at after iterating on the filter peaks as described above. The group arrival time, measured from the event origin time, is plotted along the abscissa and filter center frequency along the ordinate in each of these figures. The relative amplitudes of the filter envelope maxima are represented by the numbers 0 to 9 where, for instance, a 7 corresponds to an envelope peak that is between 70 and 80 percent of the largest envelope peak, designated by an (*), at the same frequency. The + and -'s define the signal acceptance window and give a measure of the uncertainty in time resolution due to scatter (in time) of the envelope peaks and the inherent limitation associated with the narrow band filtering procedure.

For most of the event seismograms (Figures 4, 5 and 6) the signal-to-noise ratio (S/N) is sufficiently high so that it is obvious from an examination of the figures that the arrival times picked by the algorithm correspond to those that an analyst would pick. Figure 7, however, is an entirely different matter and the close agreement between t_s^* and the predicted arrival time (t_{PRD}, based on the known event location, origin time and Herrin (1968) travel-time tables) is indicative of the power of the narrow band filter approach to signal detection.

An example of the multiple phase recognition capabilities of the automated detection algorithm implemented in MARS is shown in Figure 8. The bottom portion of this figure is a short-period vertical component seismogram written at the

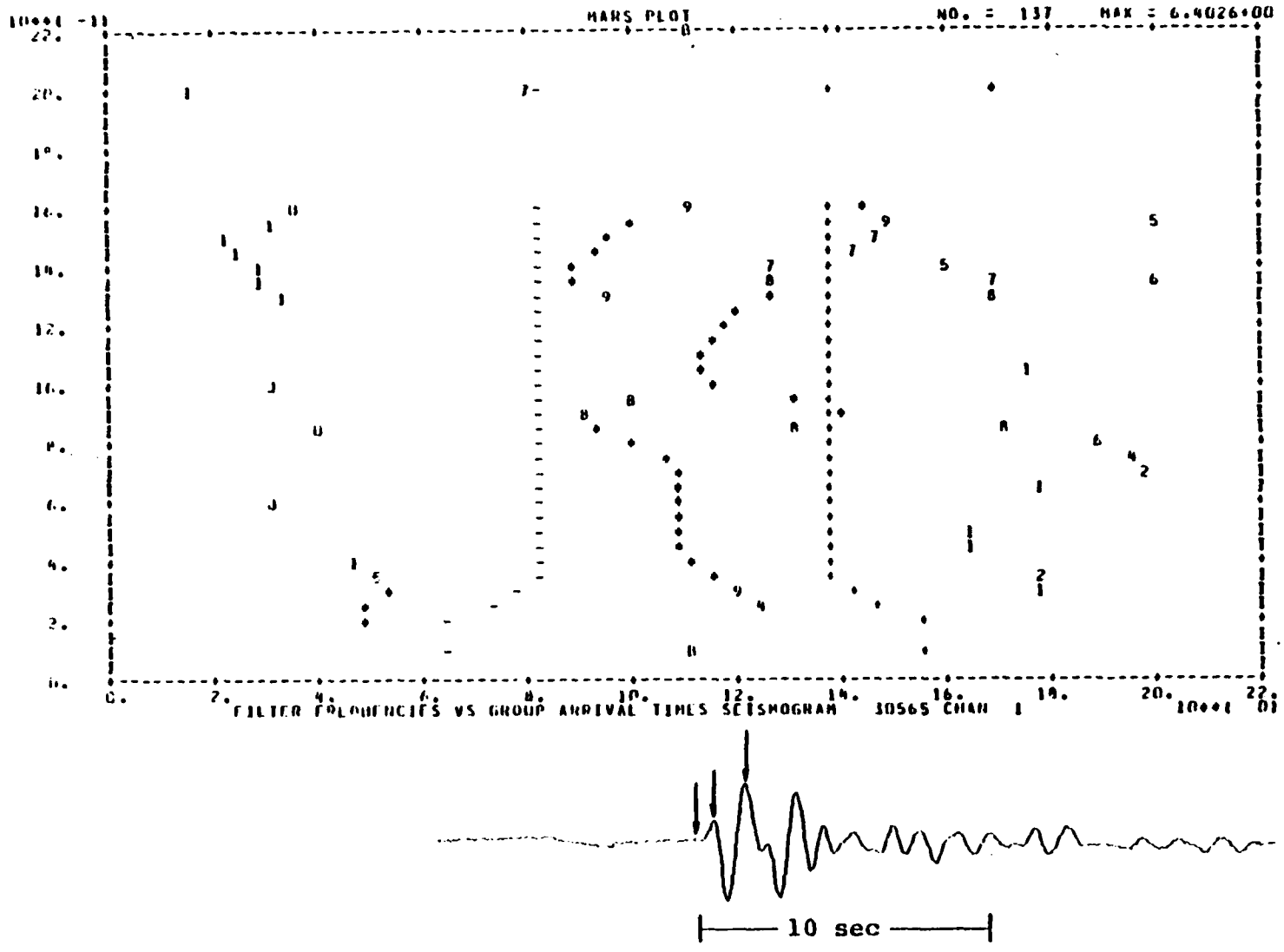

Figure 8. Example of timing of multiple phase arrivals by MARS. The seismogram at the bottom is for the NTS event, Camembert, written at Houlton, Maine. The top is the t_g-f plot for a series of narrow band filters.

station in Houlton, Maine (HNME) for the NTS explosion Camembert. The three arrows point to the arrival times of three separate phases picked by MARS. The phase arrival times are based on the t_g-f plot shown in the top-half of this figure.

Table 1 compares the lag times picked by MARS for Camembert and Mast with those used in synthetic seismogram calculations for these particular events. The synthetic seismograms, which matched the observed very closely (Bache, 1978) required the superposition of three separate phases corresponding to the direct P-wave, a second phase with a delay appropriate for pP and a third phase that could be either associated with spallation or tectonic stress release. Whatever the correct explanation for the later arrivals here, the remarkable agreement between the observed and calculated lag times implies that we are well on our way toward developing an automatic multiple phase identification technique.

Once a final signal acceptance window has been defined (e.g., the + and -'s in the t_g-f planes in Figures 4 through 8), the next step is to obtain estimates of the signal amplitudes at the different frequencies for subsequent magnitude calculations. To do this a combined amplitude-time scoring scheme is applied to each of the filter peaks that occur within the signal acceptance window. The time scoring is done with respect to the $\bar{\bar{t}}_g$ estimate indicated, for example, by the B's at the top and bottom of each of the t_g-f signal acceptance windows in Figures 4 through 8. The amplitude scoring is straightforward with the largest filter peak receiving a normalized amplitude score of one. At a particular frequency the highest total score will be awarded the largest peak that occurs at time $\bar{\bar{t}}_g$. With the signal amplitudes defined over the frequency band of interest in this experiment (i.e., 0.4 Hz to 5.0 Hz for the 20 samples/sec data and 0.3 to 3.5 Hz for the 10 samples/sec data), we turn to the discrimination algorithm.

TABLE 1

COMPARISON OF PHASE LAG TIMES

	$P_2 - P_1$ (sec)	$P_3 - P_1$ (sec)
MAST		
Synthetic	0.67	1.35
Observed (MARS)	0.69	1.25
CAMEMBERT		
Synthetic	0.64	1.92
Observed (MARS)	0.64	1.93

2.1.3 The Discrimination Algorithm

The results of one of our earliest (Savino and Archambeau, 1974) applications of the variable frequency magnitude, or $m_b(f)$, discriminant to seismic events are shown in Figure 9. The data shown are only two of the frequency dependent magnitudes that characterize the events, but for the teleseismic distances (Δ = 60 to 90°) and the type of receiver (LASA - full array beam) the two frequency dependent magnitudes at 0.45 and 2.25 Hz provide the best separation of the explosion-earthquake populations in the $m_b(f)$ parameter space.

An important point about the results in Figure 9 concerns the influence of background seismic noise on the event populations. Some of the scatter in both the earthquake and explosion populations is due to noise. This, of course, is relatively more important for events of small magnitude, since the signal power is low relative to the noise power. An additional effect is mixing of the populations at the very low magnitudes.

In view of the desirability of estimating noise properties and then correcting for noise contamination, the signal analysis program, as originally written, obtained noise spectral estimates and used these to obtain estimates of the signal spectral magnitudes. (In the original case, the average noise spectral amplitude at the appropriate frequency was subtracted from the signal spectral amplitude.) The nature of the noise has been investigated for each of the events making up the event set shown in Figure 9 using the signal analysis program, and it was found that noise time series, when viewed in an $m_b(f)$ plane such as that in Figure 9, occupies the same region as do the small magnitude earthquakes. This means that when the noise contaminates a small explosion signal, the result will be such as to make the explosion appear to be more earthquake-like and, for low signal-to-noise ratios, to actually move the

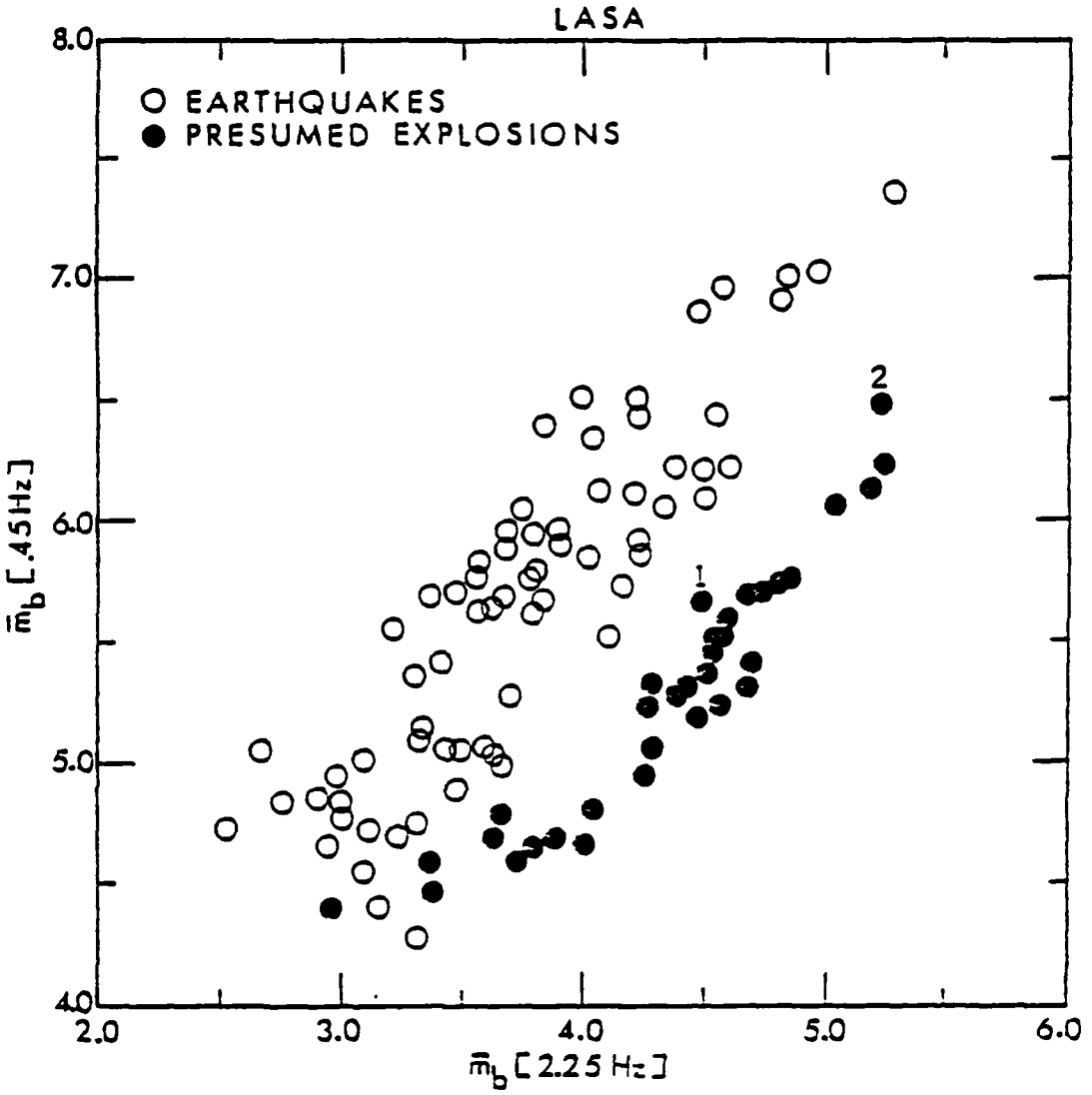

Figure 9. Spectral magnitudes, $m_b(f)$, computed at 0.45 Hz and 2.25 Hz. The presumed explosions numbered 1 and 2 occurred at Novaya Zemlya, all the other explosions occurred in eastern Kazakhstan.

explosion point into, or very near, the earthquake population. Further, the noise contamination will move the earthquake points, but always within the earthquake population and not outside of it.

This is illustrated in Figure 10a where a number of the small events observed at LASA and shown in Figure 9 have been detected at a Norway array and processed and plotted in the $m_b(f)$ plane for f = 0.6 Hz and f = 5.0 Hz. Again, in this plane, we observe convergence of the populations. The arrows on the smallest explosion data points indicate the direction in which a noise correction will move these points in this magnitude plane. Figure 10b shows the effect of the noise correction applied to <u>all</u> the events, including earthquakes as well as explosions. (In this figure only the log of the amplitude is plotted, the m_b plot would be identical except for a scale change.) It is evident that the explosion population is now well separated from the earthquake population. The arrows on the two small explosions, both with regular m_b magnitudes somewhat less than 4.0, indicate that it is likely that the estimate of the noise contamination is lower than that actually present and that the true event points are still lower in the direction indicated.

While the application of a noise "correction" to the data in Figure 10 was observed to improve discrimination, the form of this correction, namely the subtraction of an average noise level, was known to produce a biased (high) estimate of the probable noise level occurring during the signal window and also did not properly account for the phase of the noise relative to that of the signal. Thus, a more consistent and logical algorithm for estimating the influence of seismic noise on a transient signal was formulated and implemented in MARS.

In principle, the noise correction, as now applied, consists of a deterministic component and a statistical component.

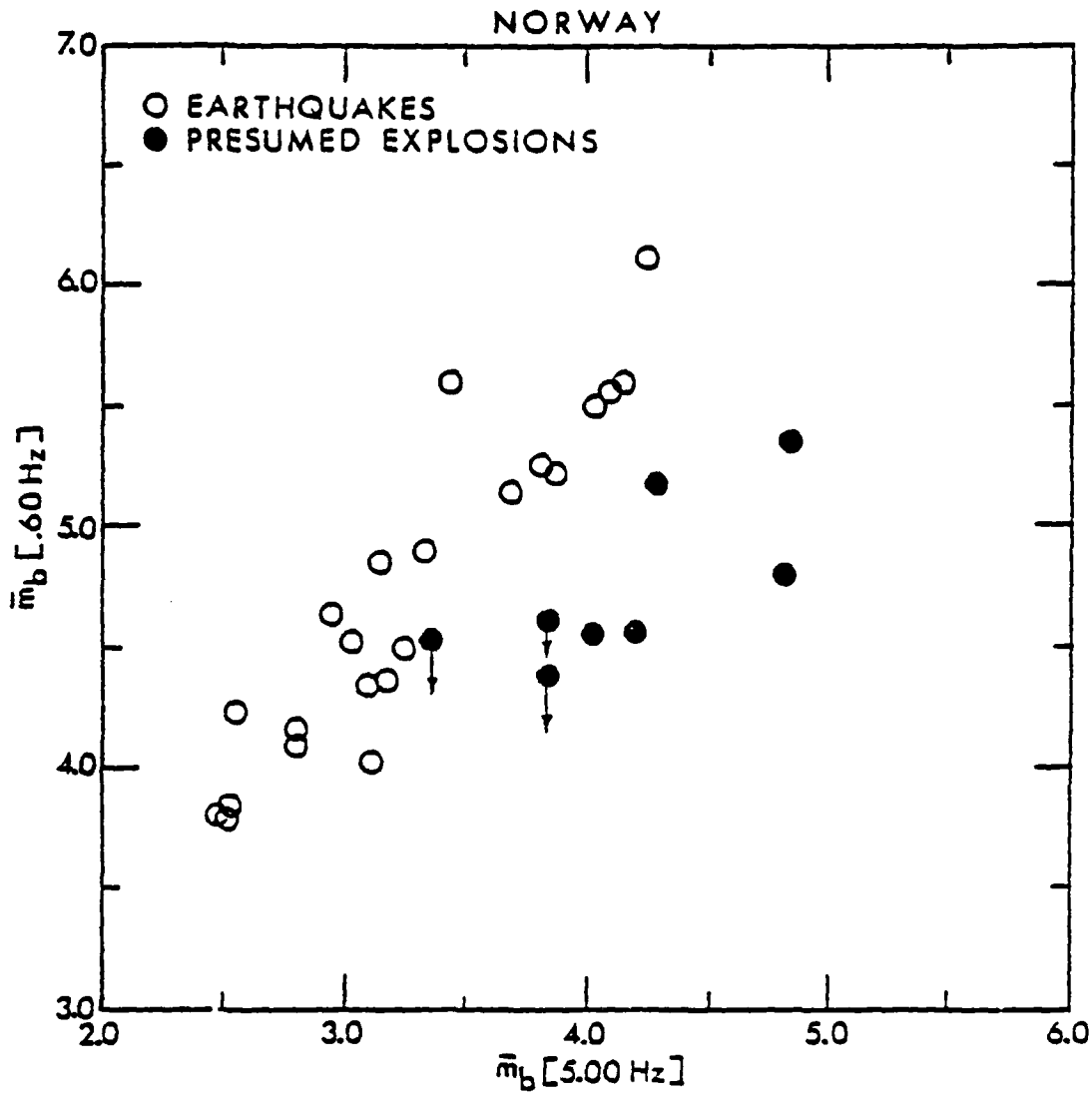

Figure 10a. Spectral magnitude estimates at f_c = 0.6 Hz and f_c = 5.0 Hz for an event population recorded at the Oyer array in Norway.

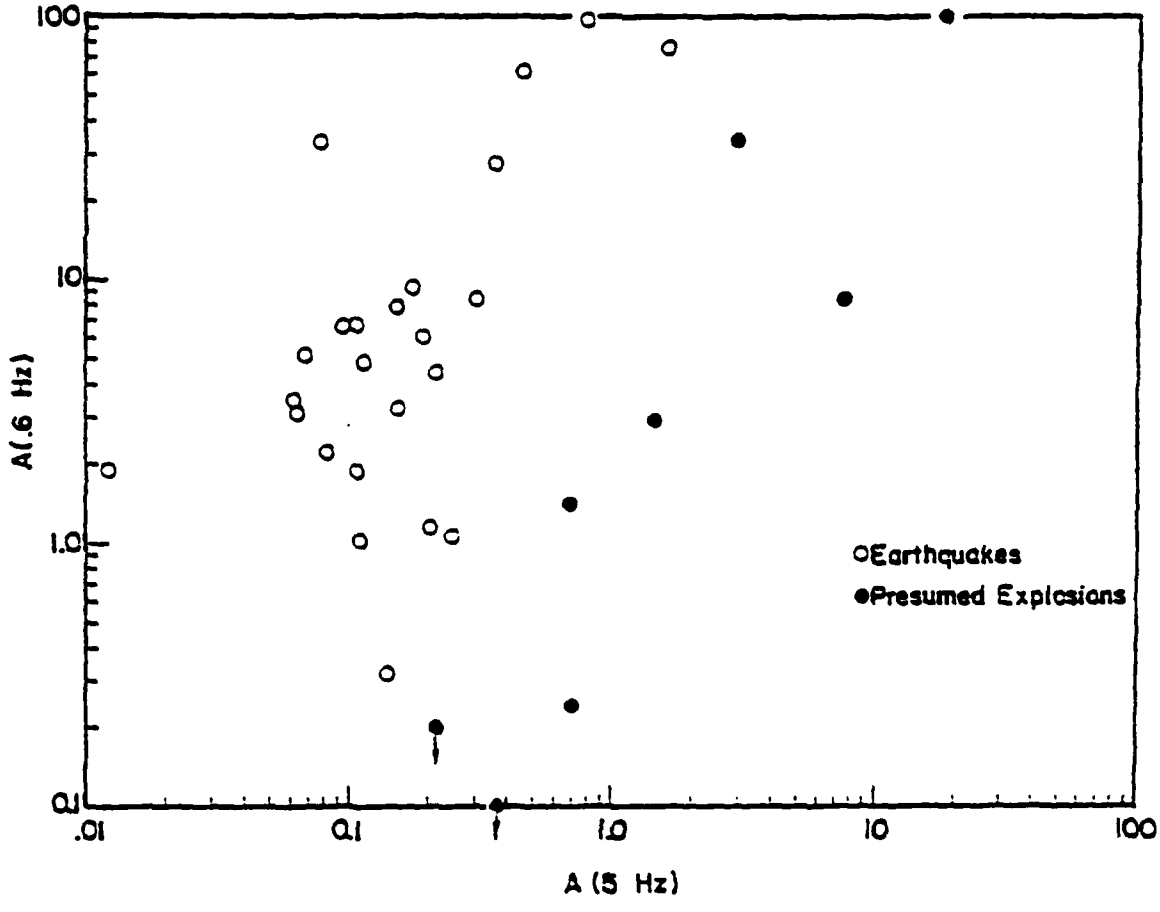

Figure 10b. Maximum filter amplitudes with noise correction for the same event population plotted in Figure 10a.

The deterministic component is based on a superposed pulse model for the noise, where noise is defined as all energy or group arrivals not identified with the particular signal being considered. Given this definition, the "noise" can be made up of what would ordinarily be considered signal (e.g., the coda of the first arrival P-wave), as well as normal background seismic noise. The particular form of the correction that treats this "local seismic noise" is termed deterministic because the effects of both the amplitude and instantaneous phase of the "noise" on the signal can be calculated, at least to first order.

As described earlier, the output of the narrow band filtering process consists of maxima of envelope functions as a function time. The deterministic noise correction is formulated as follows. Let $A_g^*(f)$ be the measured envelope amplitude associated with a signal of interest, and $t_g^*(f)$ be the energy, or group, arrival time. In addition, let $\{A_n(f)\}$ be a set of noise peaks with group times $\{t_g^N(f)\}$ such that, either: $t_g^* - \delta t \leq t_g^N(f) \leq t_g^* - \Delta t$, or $t_g^* + \Delta t \leq t_g^N(f) \leq t_g^* + \delta t$; where:

$$\delta t = \frac{10 \ \ell n 2}{\Delta\omega}; \quad t = \frac{1}{2\Delta\omega}$$

and suppose that there are M such noise peaks. Here $\Delta\omega$ is the half power band width of the Gaussian filters that are used in MARS.

We compute the "local noise corrected signal amplitude," $A_g^{**}(f)$, from:

$$A_g^{**}(f) = \left[\left\{ A_g^* \cos \Psi_p^*(t_g^*) - \sum_{m=1}^{M} A_N^{(m)} \exp \left[\frac{-\Delta\omega^2}{4\beta} (t_g^* - t_g^m)^2 \right] \cdot \cos \Psi_p^{(m)}(t_g^*) \right\}^2 + \left\{ A_g^* \sin \Psi_p^*(t_g^*) - \sum_{m=1}^{M} A_N^{(m)} \exp \left[\frac{-\Delta\omega^2}{4\beta} (t_g^* - t_g^{(m)})^2 \right] \sin \Psi_p^{(m)}(t_g^*) \right\}^2 \right]^{1/2}$$

where:

$$\beta = \frac{\ln 2}{2}$$

$\Psi_p^*(t_g^*)$ ≡ Instantaneous phase of the signal at the envelope peak time (group time) $t_g^*(f)$.

$A_g^*(t_g^*)$ ≡ Amplitude of the envelope at the peak in the envelope function, occurring at $t_g^*(f)$.

$\Psi_p^{(m)}(t_g^m)$ ≡ Instantaneous phase of the m^{th} "noise" pulse at the envelope peak time (group time), $t_g^m(f)$.

$\Psi_p^{(m)}(t_g^*) = \omega_o(t_g^* - t_g^m) + \Psi_p^{(m)}(t_g^m)$ = the noise phase at t_g^*, the <u>signal</u> group time.

$A_N^{(m)}(f)$ = Amplitude at the envelope peak for the m^{th} noise pulse (occurring at the time $t_g^m(f)$).

Here:

$$\delta A_N = \sum_{m=1}^{M} A_N^{(m)} \exp\left[\frac{-\Delta\omega^2}{4\beta}\,(t_g^* - t_g^m)^2\right]$$

$$\cos \psi_p^{(m)}(t_g^*)$$

is the deterministic noise correction for the signal with group time t_g^*, while

$$\delta A_N = -\sum_{m=1}^{M} A_N^{(m)} \exp\left[\frac{-\Delta\omega^2}{4\beta}\,(t_g^* - t_g^m)^2\right]$$

$$\sin \psi_p^{(m)}(t_g^*)$$

is the quadrature component corresponding to δA_N. We then compute both of these and evaluate the (deterministic) noise correction $|\delta A_N|$ as:

$$|\delta A_N| = [\{\delta A_N\}^2 + \{\delta \hat{A}_N\}^2]^{1/2}$$

and save for later use in describing the noise population in the $m_b(f)$ plane. This correction, while deterministic, is only to first order.

Associated with $A_g^{**}(f)$ will be an uncertainty due to the impossibility of resolving and correcting for noise peaks within the range $\Delta t = 1/2\Delta\omega$ on either side of the signal group time (t_g^*), at a frequency f. In addition, we will want to include in the uncertainty attached to the estimate A_g^{**}, the

impossibility of making an exact deterministic correction for noise contamination from the "local" noise pulses. This uncertainty will be $\pm \Delta A_N$, with ΔA_N given by:

$$\Delta A_N = \left(\frac{Q}{\omega}\right) \left(\frac{L}{T_o}\right) \bar{A}_N(f) = \frac{1}{\Delta\omega} \left(\frac{L}{T_o}\right) \bar{A}_N$$

where

T_o = Total (standard) time window being processed (typically above 100 sec).

L = Number of <u>noise</u> peaks in T_o. (Use the previously analyzed time window where all noise peaks have been identified.)

$\bar{A}_N(f)$ = Mean of the envelope amplitudes at the noise peaks in the window T_o, i.e.,

$$\bar{A}_N(f) = \sum_{\ell=1}^{L} A_N^{(\ell)}(f)/L \quad .$$

(Note that $L \propto \Delta\omega\, T_o$ as $\Delta\omega \to 0$, so that $\Delta A_N \to \bar{A}_N$ as $\Delta\omega \to 0$. Further, $\delta A_N \to 0$ as $\Delta\omega \to 0$ by definition of the time interval for the δA_N correction. Therefore as $\Delta\omega \to 0$, and the filter Q become infinite, we get the usual noise correction of a Fourier spectrum.) Thus the signal spectral amplitude will be described by $A_g^*(f) \pm \Delta A_N(f)$.

The final step in this formulation is the computation of the noise corrected instantaneous phase. This is given by:

$$\Psi_p^{**}(t_g^*(f)) = + \tan^{-1}\left[\frac{\hat{y}^* - \delta\hat{A}_N}{y^* - \delta A_N}\right]$$

where δA_N and $\delta\hat{A}_N$ are as defined above while

$$y^* \equiv A_g^* \cos \Psi_p^*(t_g^*)$$

$$\hat{y}^* \equiv + A_g^* \sin \Psi_p^*(t_g^*)$$

where $\hat{y}^*$ is the quadrature signal.

The application of the noise correction derived above is based on a magnitude relationship similar to the one originally proposed by Gutenberg and Richter (1956):

$$m_b(f) = \log_{10} [Af] + b$$

where b is the distance correction factor. Using this relationship we compute $m_b(f)$ values for the signal of interest from $A_g^*(f)$, $A_g^{**}(f)$, $A_g^{**}(f) + \Delta A_N$ and $A_g^{**}(f) - \Delta A_N$. The $m_b(f)$ are computed at frequencies corresponding to the center frequencies of the entire set of narrow band filters being used (i.e., typically 40 filters covering the band 0.4 to 5 Hz). For discrimination purposes, however, two sub-bands are defined: a low frequency set $\{f_L\}$ and a high frequency set $\{f_H\}$. The high and low frequency bands are defined in Table 2. In order to obtain more stable magnitude estimates than those based on individual filter center frequencies, fitted values at a single fixed high (f_H) and a fixed low (f_L) frequency are used. For the high frequency band, the least squares polynomial of degree two which best approximates the weighted set of $\log_{10} A_g^{**}(f)$ values over the band $\{f_H\}$ is first computed. The weight factors $w_k(f)$ which measure the

TABLE 2

HIGH AND LOW FREQUENCY BANDS

$\{f_H\}$	$\{f_L\}$	Sampling Rate	Number of Filters
5.0 - 2.0	1.4 - 0.40	20	40†
3.5 - 2.0	1.4 - 0.30	10	40††

† Twenty samples/second stations

†† NORSAR and LASA

signal information content or quality of the signal information at the frequency f_k are given by

$$w_k(f) = [A_g^*(f)/\bar{A}_N(f)]^2 \quad .$$

The fitted value at the single high fixed frequency f_H is then determined and used to derive a magnitude estimate. A similar procedure is applied to derive the low frequency estimate. The magnitude relationship is given by

$$m_b(F) = \log_{10} [A(F) \cdot F] + b \quad ,$$

where F is the single fixed frequency f_H or f_L and A(F) is the fitted value computed from the weighted least-squares polynomial defined above for the set of noise corrected amplitudes $A_g^{**}(f)$.

Finally, the uncertainty in the magnitudes at f_L and f_H due to the uncertainty in the noise correction is also computed. These are given by:

$$\Delta m_b^+(F) = \log_{10} [(A(F) + \Delta A_N) \cdot F] + b - m_b(F),$$

$$\Delta m_b^-(F) = \log_{10} [(A(F) - \Delta A_N) \cdot F] + b - m_b(F),$$

where A(F) is the fitted value for the noise corrected amplitude A_g^{**} at frequency F, ΔA_N is the noise uncertainty at F, and F = f_H or f_L. Note that $\Delta m_b^+ \neq -\Delta m_b^-$ in general, and that none of the Δm_b values obtained for the two sets of discrimination frequencies will be equal in general. We get from this then four distinct Δm_b values.

The results of applying the newly formulated noise correction to event $m_b(f)$ data are summarized in Figures 11a and 11b. Figure 11a shows the behavior of typical event (uncorrected for noise) and noise populations in the $m_b(f)$ plane. This figure is a generalization of earlier results previously reported (Savino, et al., 1975; Rodi, et al., 1978). Figure 11b demonstrates the manner in which the earthquake and explosion populations are expected to separate when the deterministic and statistical noise corrections, together with the uncertainty inherent in both these corrections, are applied. The enhanced separation of populations is especially significant in the low $m_b(f)$ range where noise plays an important role. This is the procedure that was routinely used in the discrimination experiment for the computation of the variable frequency magnitudes.

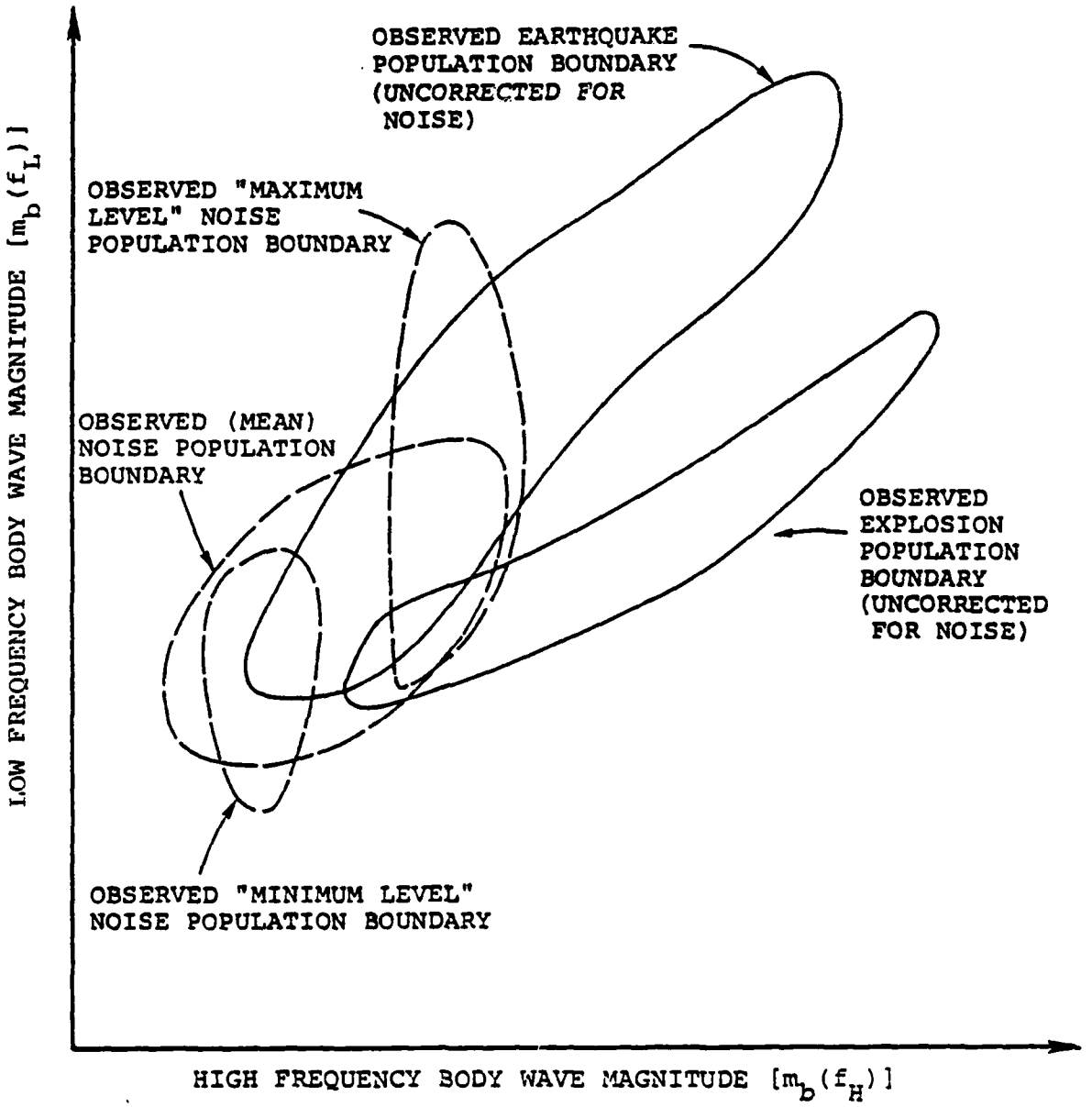

Figure 11a. Typical event distributions in the $m_b(f)$ plane for event data that is not corrected for noise contamination. Noise pulses, when viewed in this space appear roughly as shown and affect explosion event $m_b(f_L)$ values most strongly, causing population overlap at low magnitudes. The population boundaries for noise and events are somewhat source and receiver dependent due to earth structure variations.

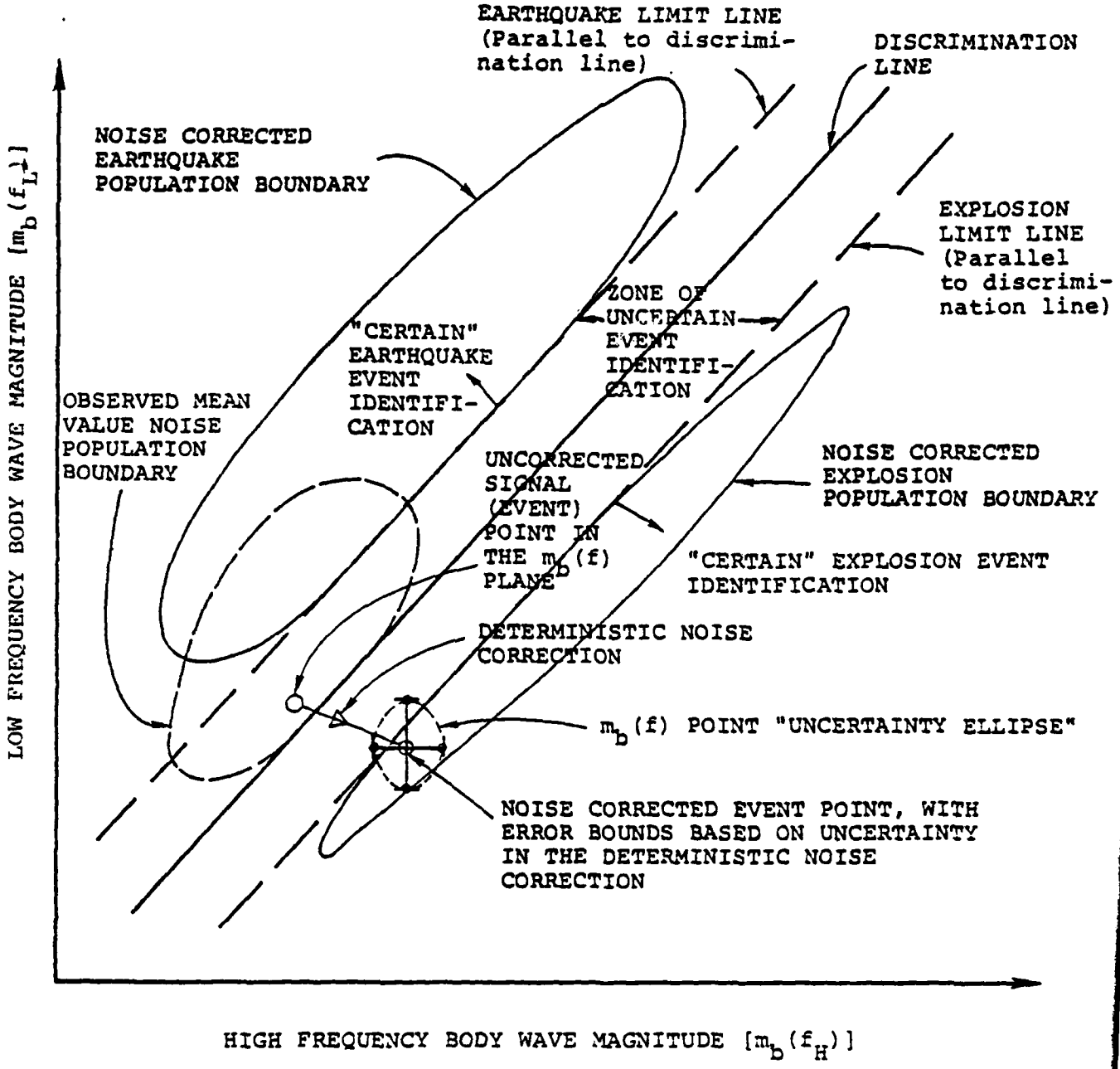

Figure 11b. Typical event distributions in the $m_b(f)$ plane for noise corrected event data. A discrimination line can be defined on the basis of the definition of these populations using known events, or on the basis of theoretical predictions.

III. VFM DISCRIMINATION RESULTS FROM A TEN STATION NETWORK

3.1 VFM RESULTS FROM TELESEISMIC STATIONS

The $m_b(f)$ results obtained from the ten stations included in this phase of the experiment demonstrate that the VFM approach can discriminate between Eurasian earthquakes and explosions recorded at both teleseismic and regional distances. Individual station performance, however, is largely controlled by the attenuation properties of the upper mantle beneath a particular station. For instance, a station overlying high Q upper mantle (as evidenced either by the siting of the station in a shield region and/or a region characterized by large negative P wave travel-time residuals) provides much greater separation of earthquakes and explosions in the $m_b(f)$ plane representation than a station located over a low Q upper mantle. As examples, we emphasize results from two stations for which a variety of regional geophysical information pertaining to the structure of the upper mantle is available. The two stations are Red Lake, Ontario (RKON) and Albuquerque, New Mexico (ANMO).

Figure 12 shows discrimination results obtained from the vertical component seismograms of short-period P waves recorded at RKON. The epicentral distance range of all the Eurasian events to RKON is 53 to 103 degrees. The particular pair of $m_b(f)$ frequencies, 0.6 Hz and 3.25 Hz, yielded the greatest separation of the majority of earthquakes and explosions recorded at this location.

As seen in Figure 12, the VFM technique discriminates very effectively between earthquakes and explosions over the entire magnitude range of these events. Out of a total of 50 shallow earthquakes (open circles), only one event, number 34, plots in the explosion population. This particular earthquake

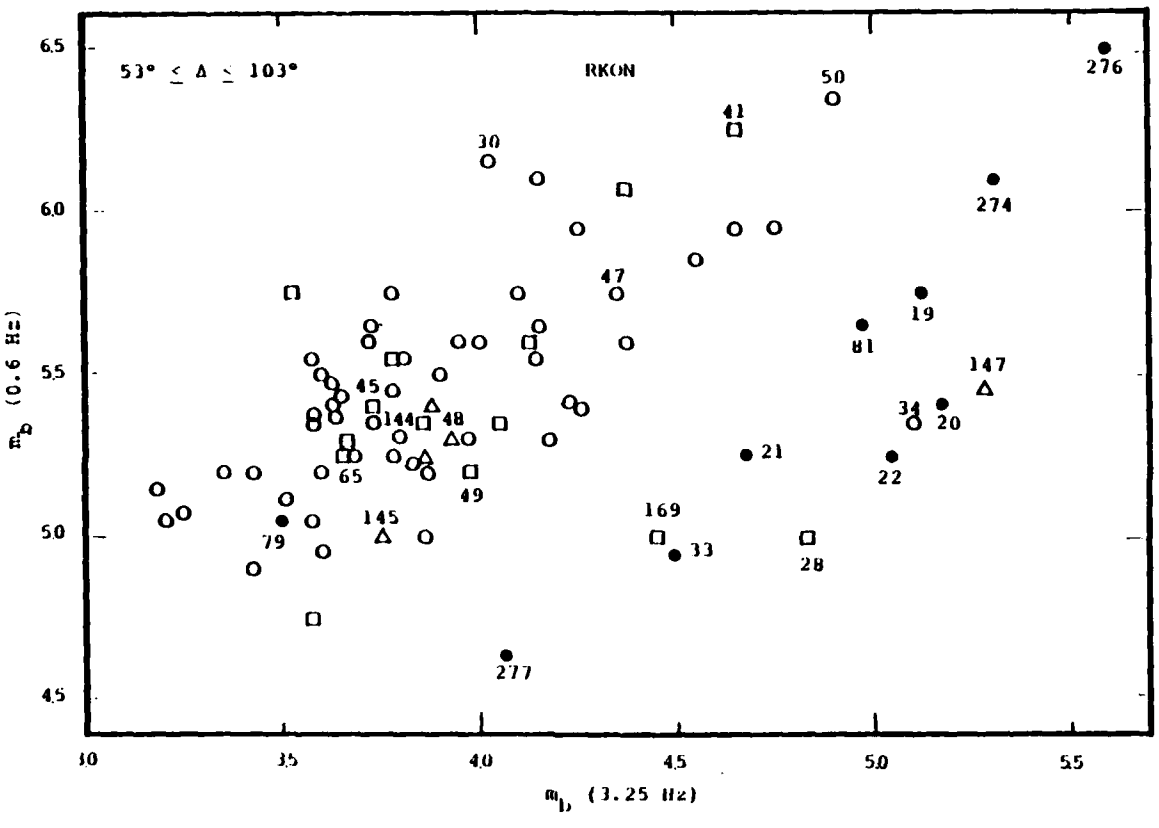

Figure 12. VFM results for the station located at Red Lake, Ontario (RKON). Open circles depict shallow earthquakes ($h \leq 50$ km), open squares intermediate focal depths ($50 < h < 250$ km), open triangles deep events ($h \geq 250$ km) and closed circles presumed explosions.

is one of several aftershocks following a large, m_b = 5.7, Tibetan earthquake (Event Number 30). The remaining three earthquakes that fail to discriminate at RKON are all relatively deep focus events. The focal depths reported in the Preliminary Determination of Epicenters, Monthly Listings, published by the U. S. Geological Survey (USGS) are as follows: Event 28, 157 km; Event 147, 479 km; Event 169, 118 km. As noted in previous studies (Savino and Archambeau, 1974; Savino, et al., 1975), the majority of events that fail to discriminate using the VFM technique are deep. We point out, however, that while these three deep earthquakes plot in the explosion population in Figure 12, 16 other deep events, including two with reported depths in excess of 500 km, plot well within the shallow earthquake population.

Other than Event number 79, a small presumed explosion in eastern Kazakhstan, the remaining nine explosions recorded at RKON are well separated from the earthquakes in Figure 12. It is particularly interesting to note that while there are only ten explosions recorded at this station, these ten events originate in four separate Eurasian source regions. These include Novaya Zemlya, Lake Baikal, eastern Kazakhstan and north of the Caspian Sea.

As for the attenuation properties of the upper mantle beneath RKON we note that this station is located on the Canadian Shield in a region characterized by relatively low heat flow and large negative travel-time residuals (Masso, et al., 1978). The negative travel-time residuals for teleseismic events imply relatively high velocities in the deep crust and upper mantle beneath RKON. These geophysical data sets, together with results from several other studies (e.g., Brune and Dorman, 1963), suggest that the upper mantle in this region is relatively high Q (low attenuation). In a later section of this report, we attempt to demonstrate how the

interplay of a high Q upper mantle and the prevailing spectrum of background earth noise determine the performance of the VFM discriminant at a particular station.

VFM discrimination results similar to those obtained for RKON were found for two other stations: Kabul, Afghanistan (KAAO) and Charters Towers, Australia (CTAO). The results for CTAO are shown in Figure 13.

While the number of available event recordings from CTAO (Figure 13) is rather small, the general separation of shallow earthquakes and presumed explosions is quite striking, more than 0.5 m_b units for either a fixed low or high frequency $m_b(f)$ level. The only earthquake that plots in with the presumed explosions is an event with intermediate focal depth (Event 169). The presumed explosion, Event number 21, plotting in with the shallow earthquake population is anomalous at several other stations and is addressed in more detail in Savino, et al. (1980).

In contrast to an RKON-type station, we have the VFM discrimination results for ANMO (Figure 14). This station is located in the Basin and Range Province of the western United States and is in a region characterized by large positive travel-time residuals and high heat flow (Masso, et al., 1978). Numerous geophysical studies performed in this region (Thompson and Burke, 1974) indicate the existence of an extensive low Q-low velocity zone in the upper mantle. In terms of discrimination, an $m_b(f)$ plot obtained for the Eurasian events recorded at ANMO can best be described as a shotgun pattern over most of the event magnitude range, with significant overlap of explosions and earthquakes of all focal depths.

A detailed comparison of the VFM results for ANMO (Figure 14) with those for RKON (Figure 12) reveals some interesting features. For instance, note in Figure 14 that the high frequency $m_b(f)$ estimates at ANMO do not exceed a value of

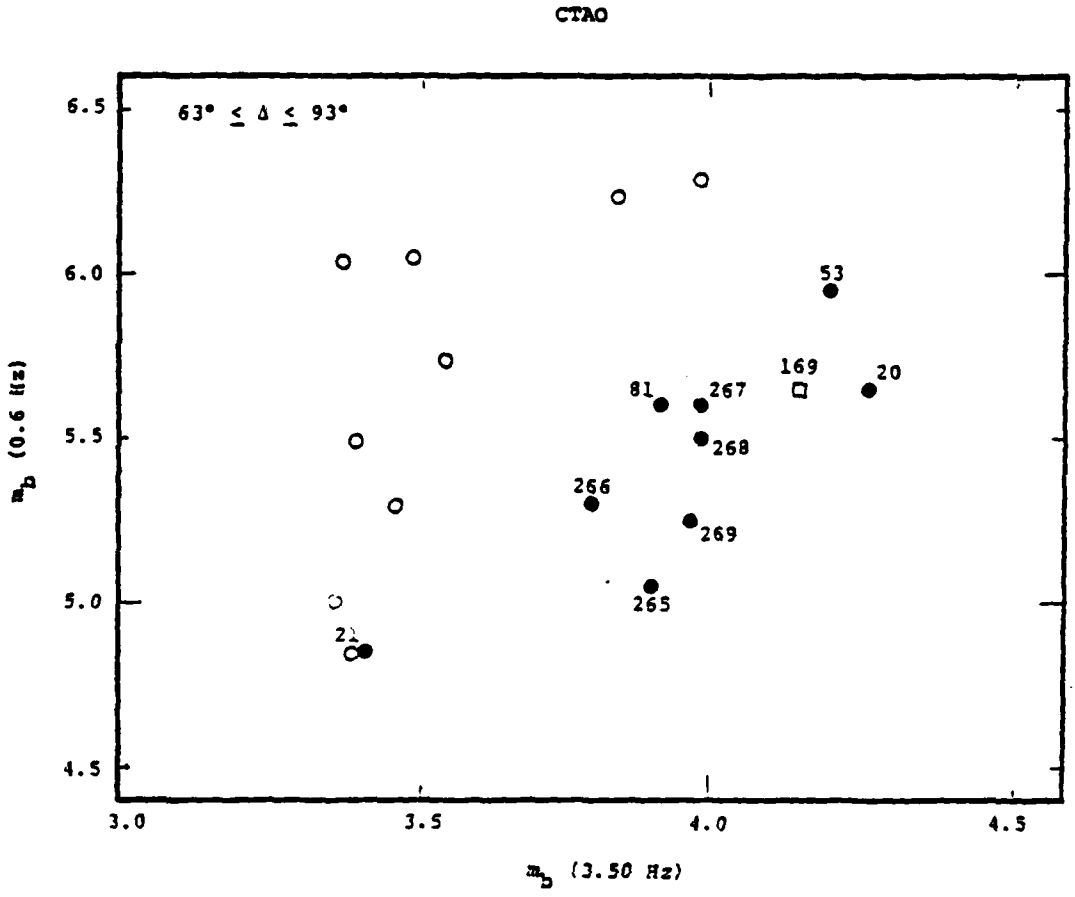

Figure 13. VFM results for the station located at Charters Towers, Australia (CTAO). Legend for symbols same as in Figure 12.

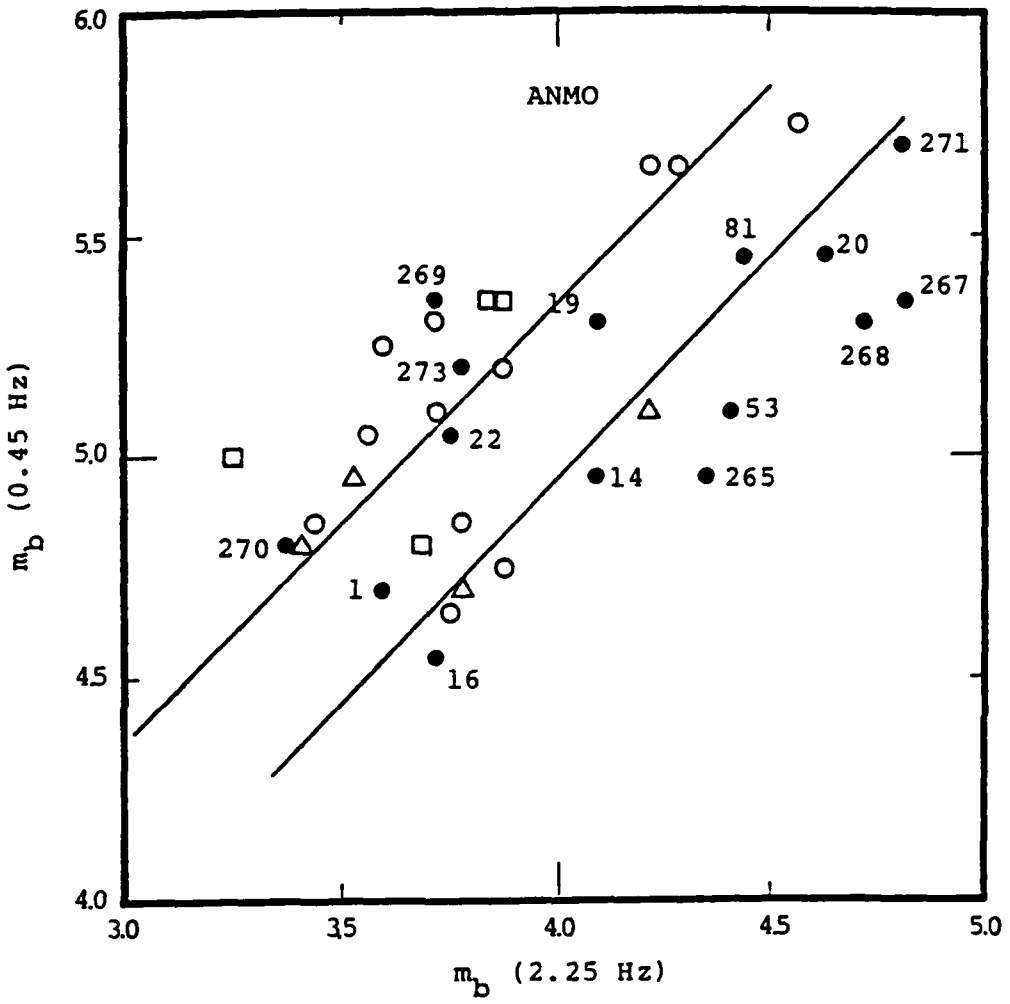

Figure 14. VFM results for the station located at Albuquerque, New Mexico (ANMO). Legend for symbols same as in Figure 12.

about 4.8. This is for a frequency of 2.25 Hz. At RKON (Figure 12), however, the high frequency $m_b(f)$ estimates, now at 3.25 Hz, attain values as high as 5.2. In more detail, consider the four explosions (Events 19, 20, 22 and 81) which are recorded at both stations. The high frequency $m_b(f)$ estimates for these events are between 0.5 and 1.3 units higher at RKON than at ANMO. The low frequency estimates, on the other hand, differ by only 0.2 to 0.3 magnitude units. The fact that two of these explosions (Events 20 and 81) are located in eastern Kazakhstan, one (Event 19) at Novaya Zemlya and the fourth (Event 22) north of the Caspian Sea argues against a systematic source region effect being responsible for differences in the high frequency spectral levels observed at these two stations. In addition, the overlap in the ranges of epicentral distances of the common events in Figures 12 and 14, 54 to 79 degrees at RKON and 71 to 95 degrees to ANMO, argues against possible variations in the lower mantle, where the rays bottom, as the cause of the observed spectral differences. Given the observations, the most likely explanation is that the known differences in high frequency attenuation beneath these two recording sites are responsible for the relative positions of the Eurasian events in the $m_b(f)$ planes shown in Figures 12 and 14.

Other stations which behave like ANMO, and in some cases are known to be situated in regions characterized by large positive travel-time residuals, are the following: Mashhad, Iran (MAIO); Chiang Mai, Thailand (CHTO); Taipei, Taiwan (TATO); and Zongo Valley, Bolivia (ZOBO). Figure 15 shows VFM results from three stations in the ANMO category. These stations are TATO (Figure 15a), CHTO (Figure 15b) and ZOBO (Figure 15c). While the number of events available for analysis at TATO and ZOBO is fairly small, in general, the dominant feature of these three station $m_b(f)$ plots is the lack of separation of the earthquake and explosion populations.

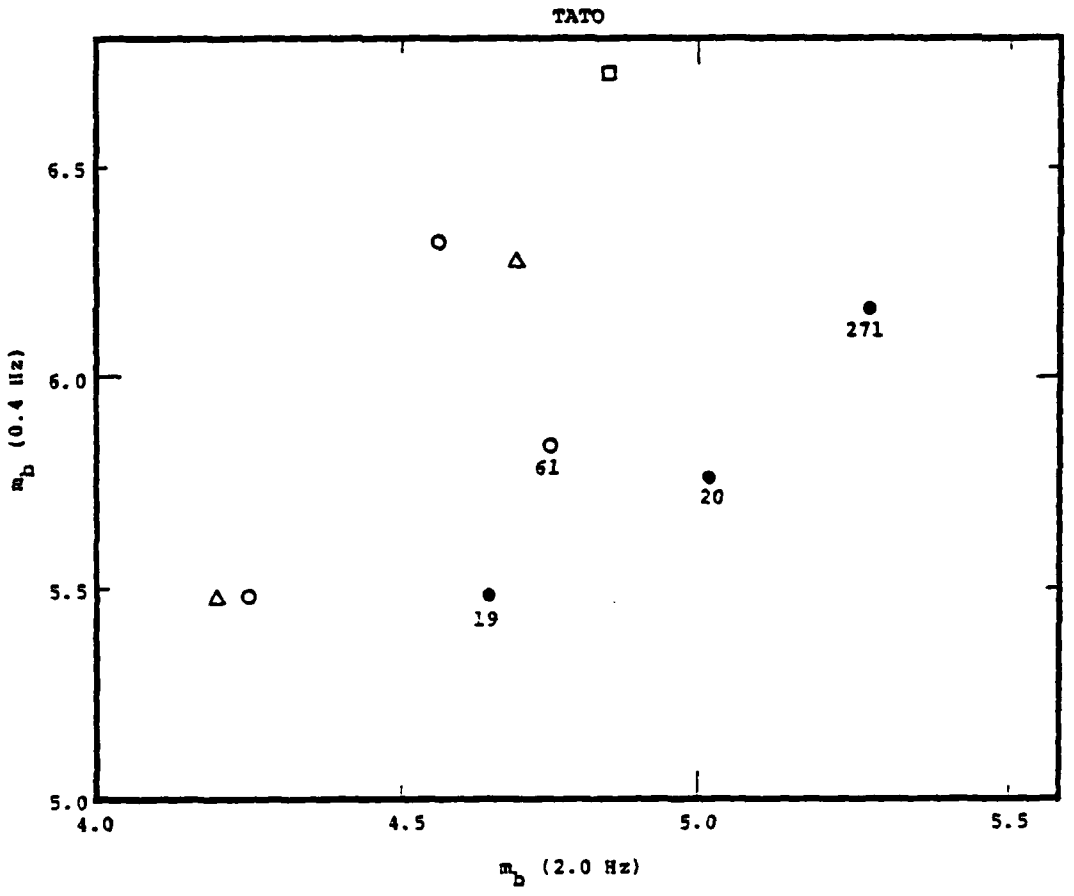

Figure 15a. VFM results for all events recorded at the station in Taipei, Taiwan (TATO). Legend for symbols same as in Figure 12.

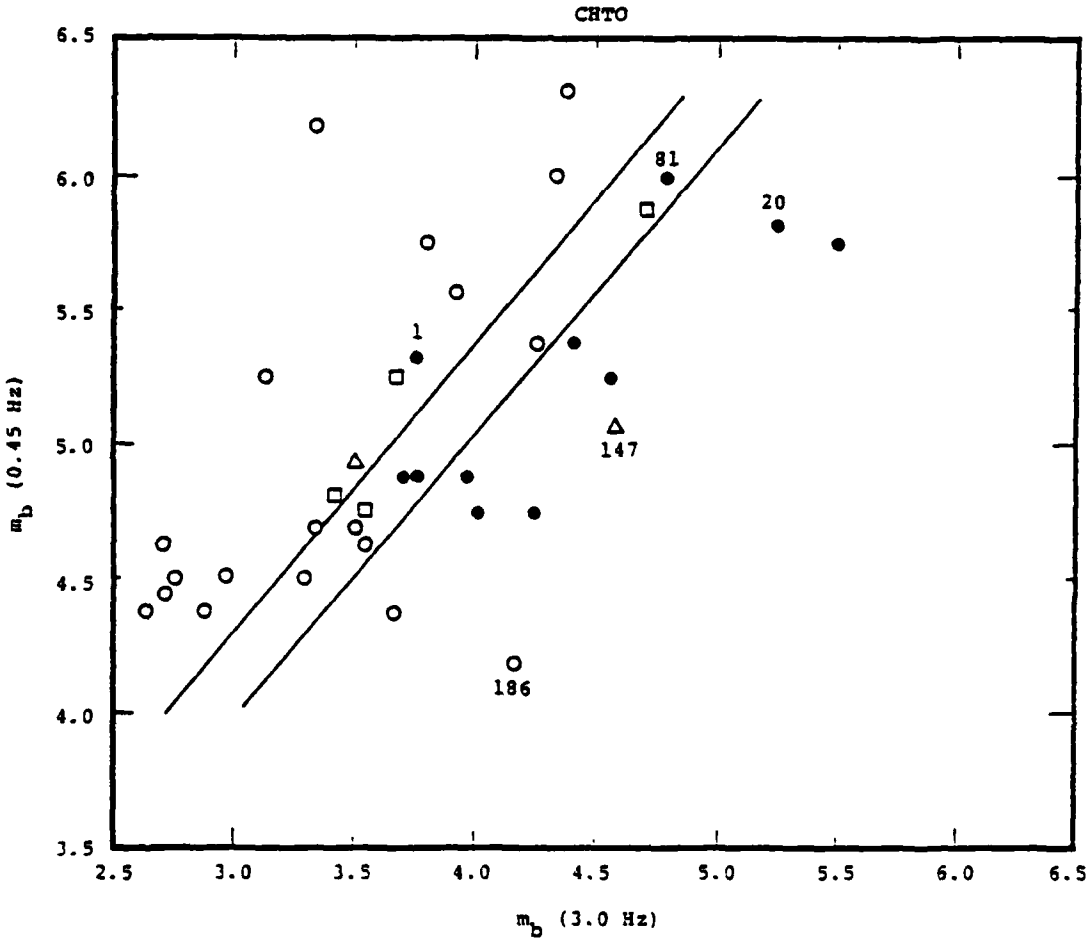

Figure 15b. VFM results for the station located at Chiang Mai, Thailand (CHTO). Legend for symbols same as in Figure 12.

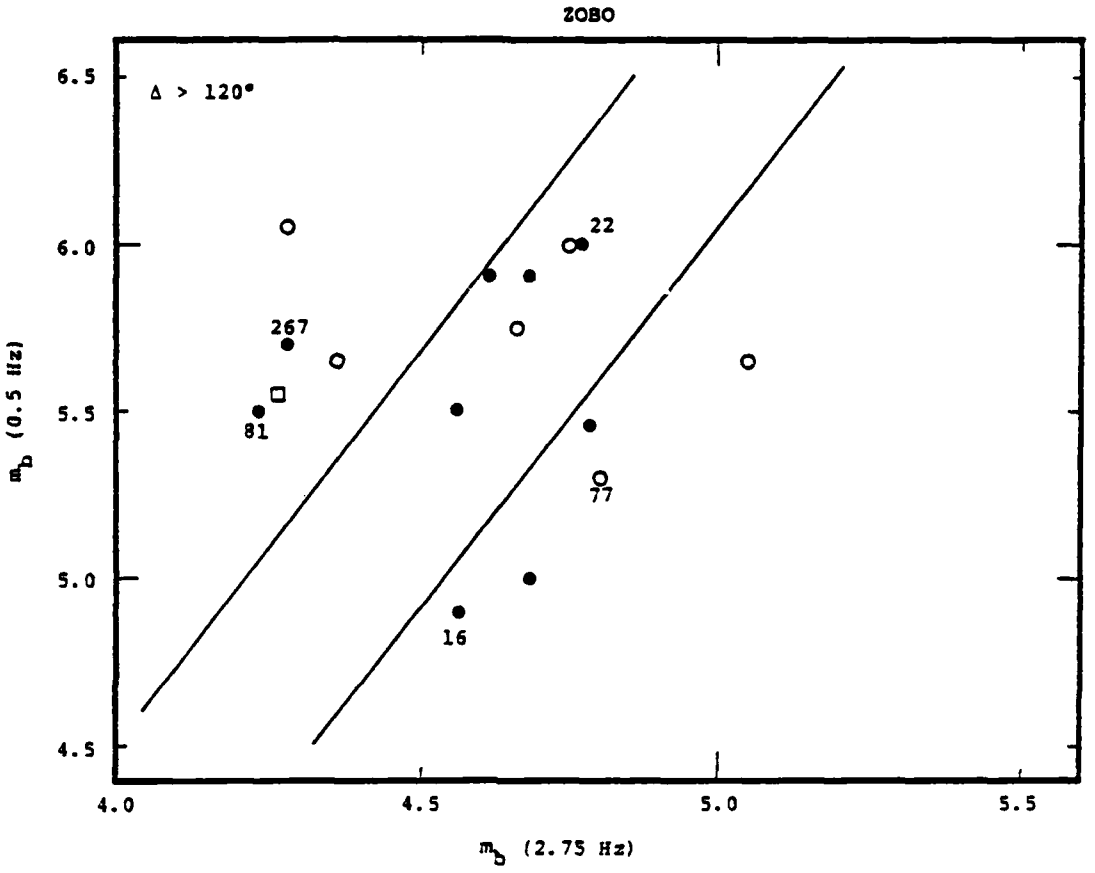

Figure 15c. VFM results for the station located at Zongo Valley, Bolivia (ZOBO). Legend for symbols same as in Figure 12.

The remaining stations at teleseismic distances from the Eurasian events are Houlton, Maine (HNME) and the center subarray at LASA (LAO). HNME is located in the Appalachian Highlands and LAO in the Great Plains Geologic Province. These two regions are characterized by essentially average values of heat flow, P_n velocities and crustal thicknesses as compared to either the Canadian Shield (RKON) or Basin and Range (ANMO) Provinces. As seen in Figures 16a and 16b, the VFM discrimination results for HNME and LAO are intermediate to those for RKON and ANMO.

3.2 VFM RESULTS FROM STATIONS AT REGIONAL AND TELESEISMIC DISTANCES

In the following, we summarize the most important results obtained from three stations that recorded events at both regional and teleseismic distances. These stations are KAAO, ILPA and MAIO.

Figure 17 shows the locations of 18 shallow earthquakes (open circles) and ten presumed explosions (closed circles) relative to the Seismic Research Observatory (SRO) station, KAAO. The epicentral distance range of these events to KAAO is 15 to 23 degrees, with the nine presumed explosions in eastern Kazakhstan at approximately 17 degrees. The VFM results for these 28 events are given in Figure 18a. As can be seen, the presumed explosions clearly separate from the shallow earthquakes over the entire magnitude range. In particular, the VFM technique successfully discriminates Events 80, 162, 163 and 272, all of which are close to explosion test sites. The implication here is that differences in the propagation path are minimized and we are seeing differences in explosion and earthquake source spectra.

A very important point to note about the $m_b(f)$ estimates in Figure 18a is the value of the filter center frequency used

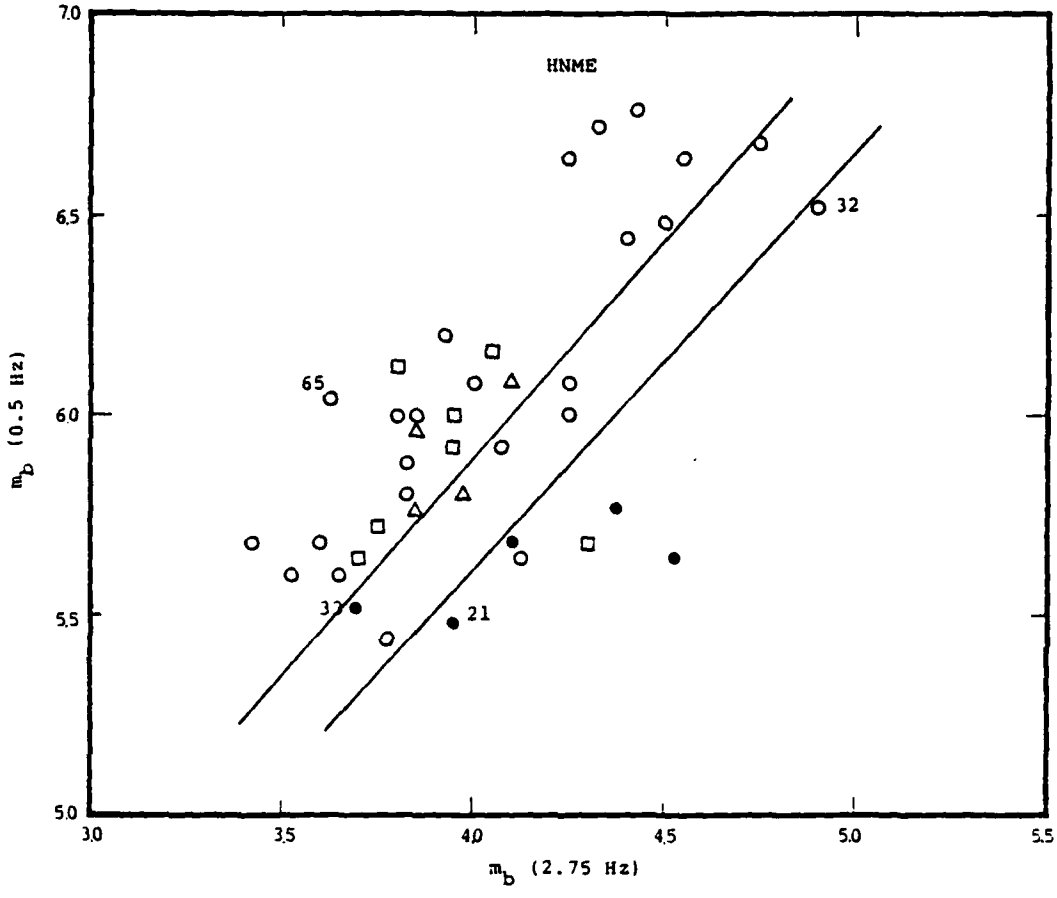

Figure 16a. VFM results for the station located at Houlton, Maine (HNME). Legend for symbols same as in Figure 12. We suspect that the digital gain factors supplied by the SDAC for the eight shallow earthquakes with m_b (0.5 Hz) values of 6.5 and greater are incorrect – too high, in fact. Incorrect gain factors, however, only move event points along diagonals in the $m_b(f)$ plane and do not impair separation of event populations.

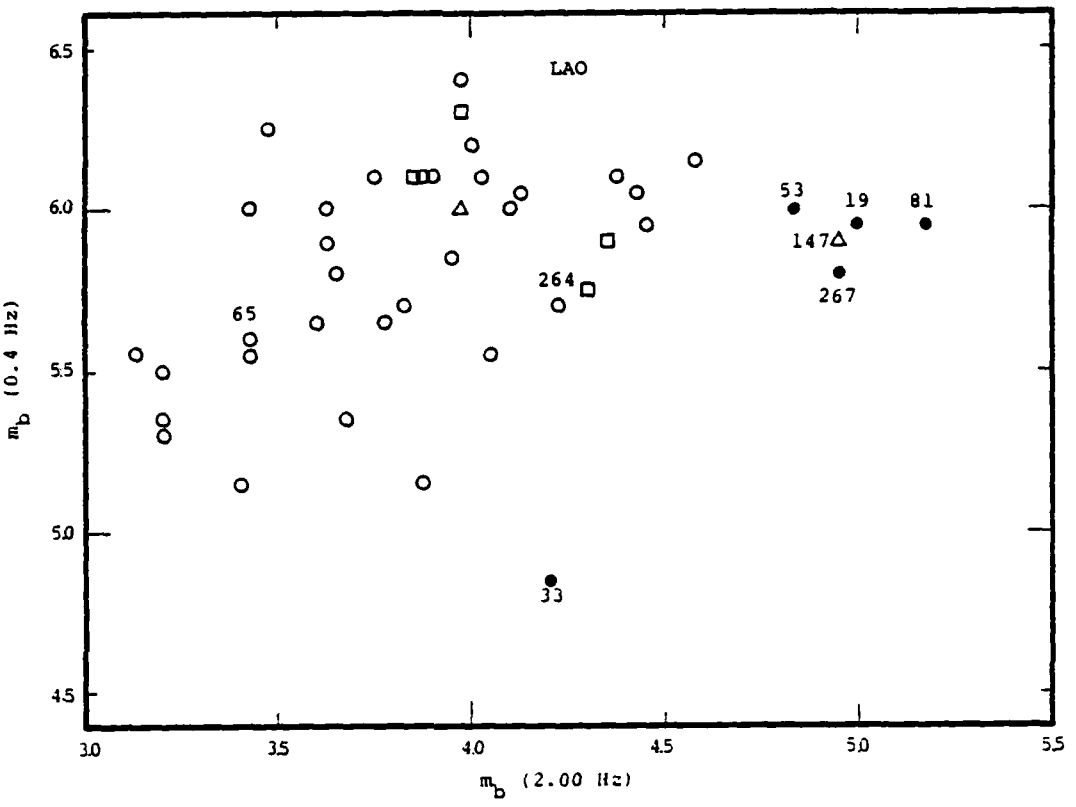

Figure 16b. VFM results for the center subarray at LASA (LAO). Legend for symbols same as in Figure 12.

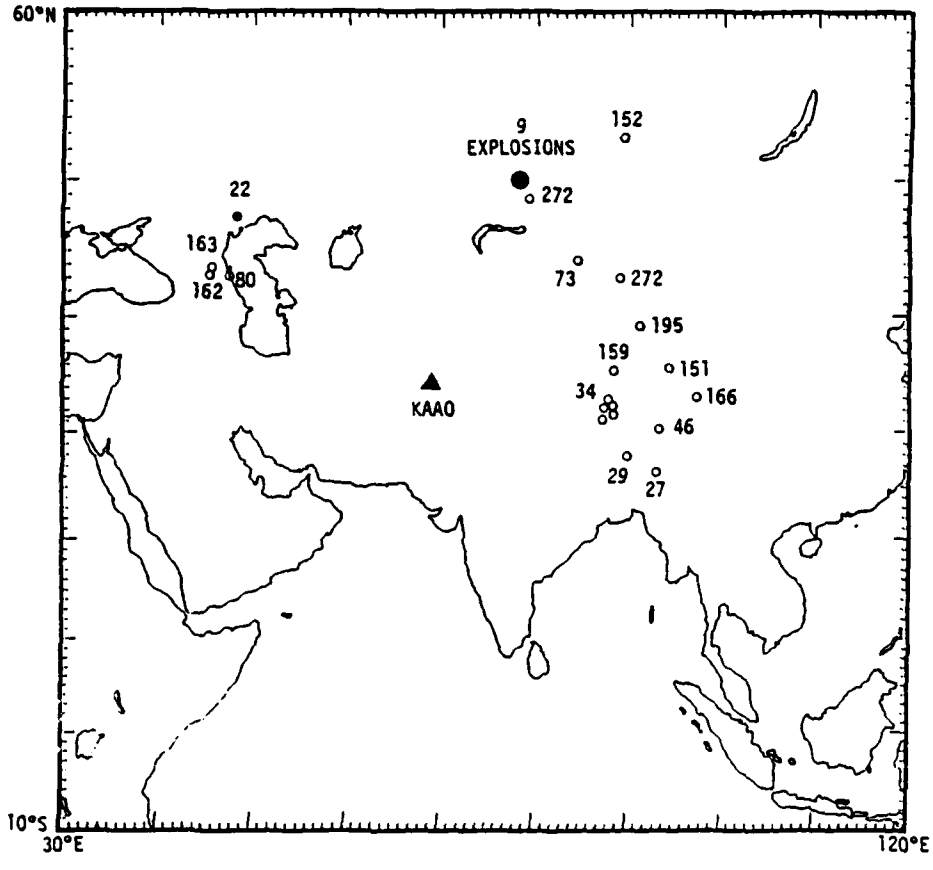

Figure 17. Map of Eurasian earthquakes (open circles) and presumed explosions (closed circles) located between 15 and 23 degrees from the SRO station at Kabul, Afghanistan (KAAO).

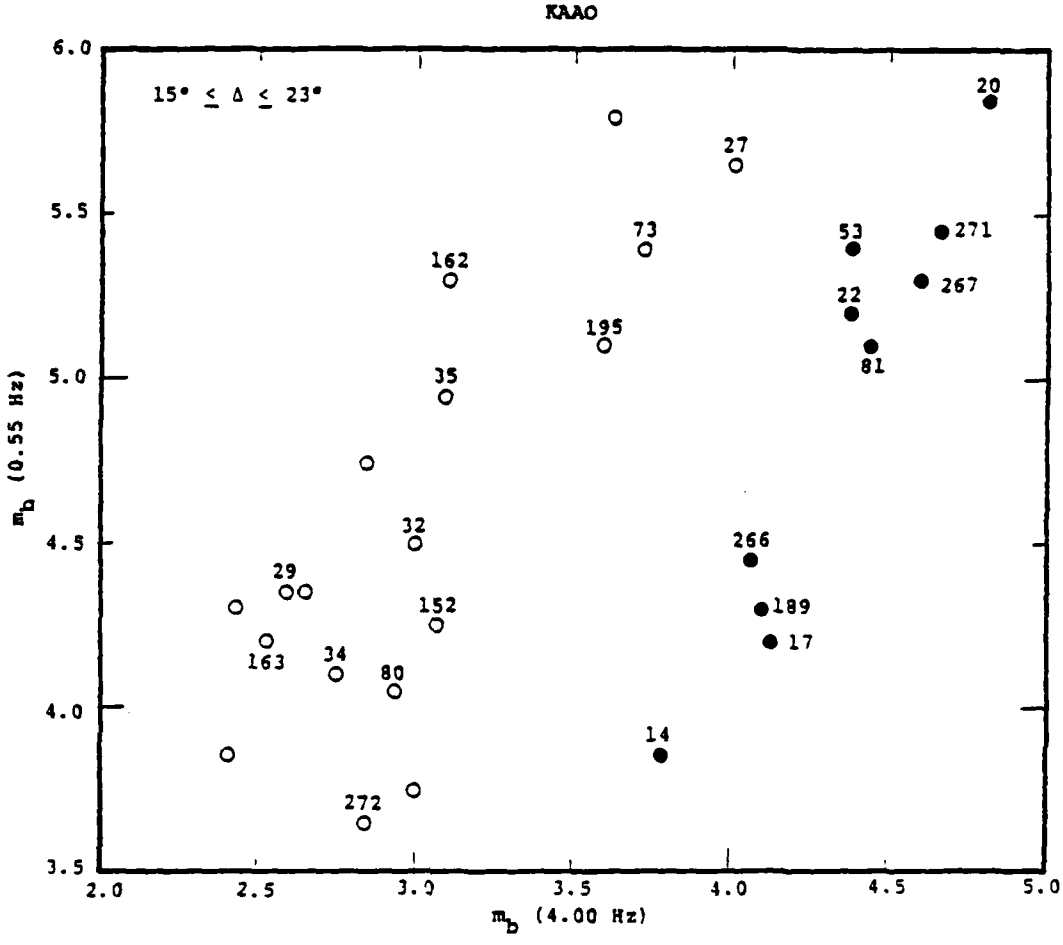

Figure 18a. VFM discrimination results for Kabul, Afghanistan (KAAO) for the earthquakes (open circles) and presumed explosions (closed circles) mapped in Figure 17. These events are located between 15° and 23° from KAAO. Note the separation between Event 272 and the nearby nine presumed explosions at eastern Kazakhstan.

for the high frequency estimates (i.e., 4.0 Hz). This is quite high compared to previous results (Savino, et al., 1979) and is probably a result of propagation over a fairly high Q path in the topmost mantle considering the far regional distance range of the events. The results in Figure 18b support this interpretation. In this figure, we give $m_b(f)$ results for events at teleseismic distances from KAAO. The particular pair of high and low frequencies (2.75 and 0.4 Hz, respectively) in this figure gave the best discrimination results. Most of the events in Figure 18b that fail to discriminate can be explained in terms of either large focal depth (the open triangles and squares) or anomalous attenuation in the upper mantle near the source region of two of the presumed explosions, 21 and 16 (Savino, et al., 1980). The point we want to note here is that the frequency corresponding to the high frequency $m_b(f)$ estimate is lower in the case of events at teleseismic distances than at far regional distances.

A similar dependence of the frequency value of the high frequency $m_b(f)$ estimates on event distances is shown in Figures 19a and 19b. The events in question occurred throughout the same general region shown in the map in Figure 17. The recording station in this case is the Iranian Long Period Array (ILPA). In Figure 19a we see an interesting separation of (1) earthquakes and the only presumed explosion recorded in this distance range at ILPA, and (2) earthquakes at distances of 6.9 to 9.2 degrees from earthquakes at distances between 12.5 and 19 degrees. The presumed explosion, Event number 22, is approximately 12.5 degrees from ILPA. The VFM results in Figure 19a are primarily based on P_g for the regional events included within the solid line and mantle P waves for all the other events. While the presumed explosion separates extremely well from events at equal or greater distances, the separation between it and the six earthquakes at closer distances is much less. This is most likely due to the more efficient high frequency P_g propagation in the case of the earthquakes.

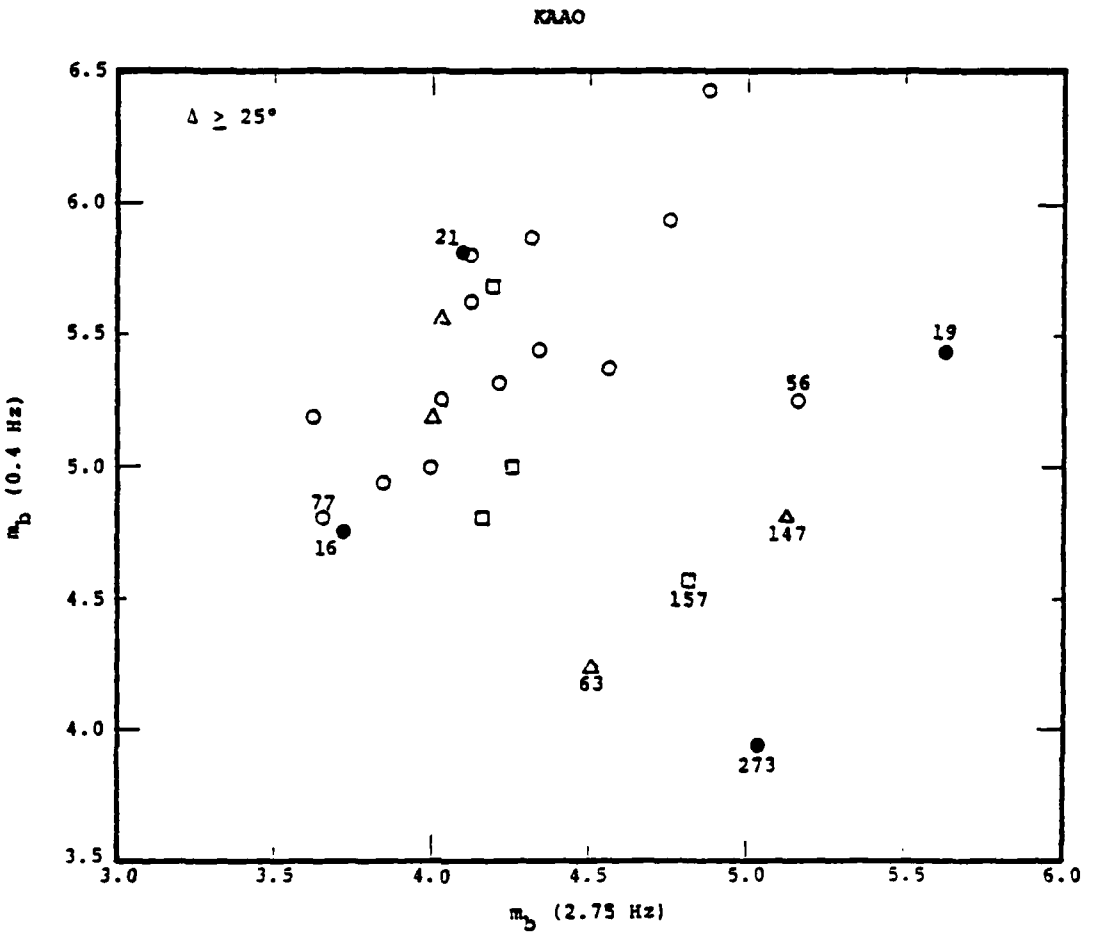

Figure 18b. VFM results for teleseismic events recorded at KAAO. The open squares denote earthquakes with focal depths between 50 and 250 km. The open triangles denote earthquakes deeper than 250 km.

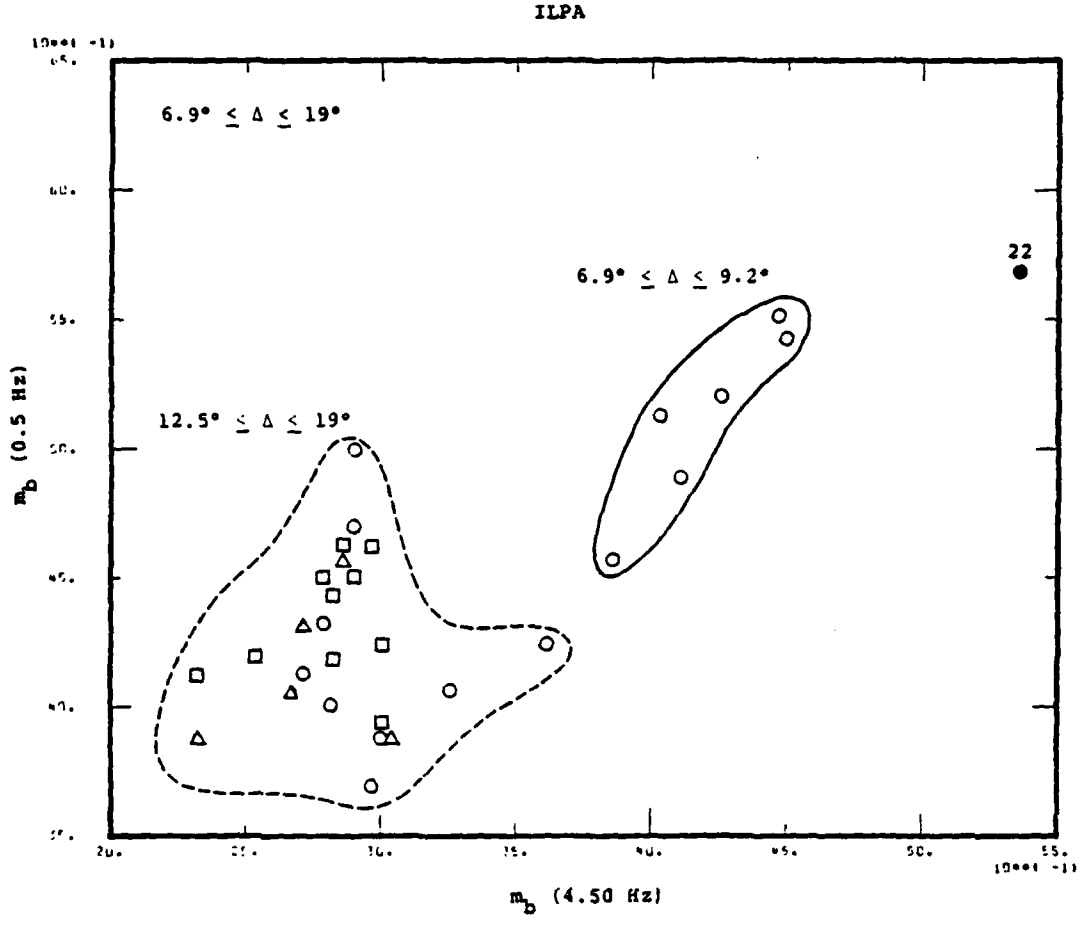

Figure 19a. VFM results for regional events recorded at ILPA. The dashed and solid curves group events in the two distance ranges. The epicentral distance of the presumed explosion, Event 22, to ILPA is 12.5 degrees. See Figures 12 and 18b for definitions of symbols.

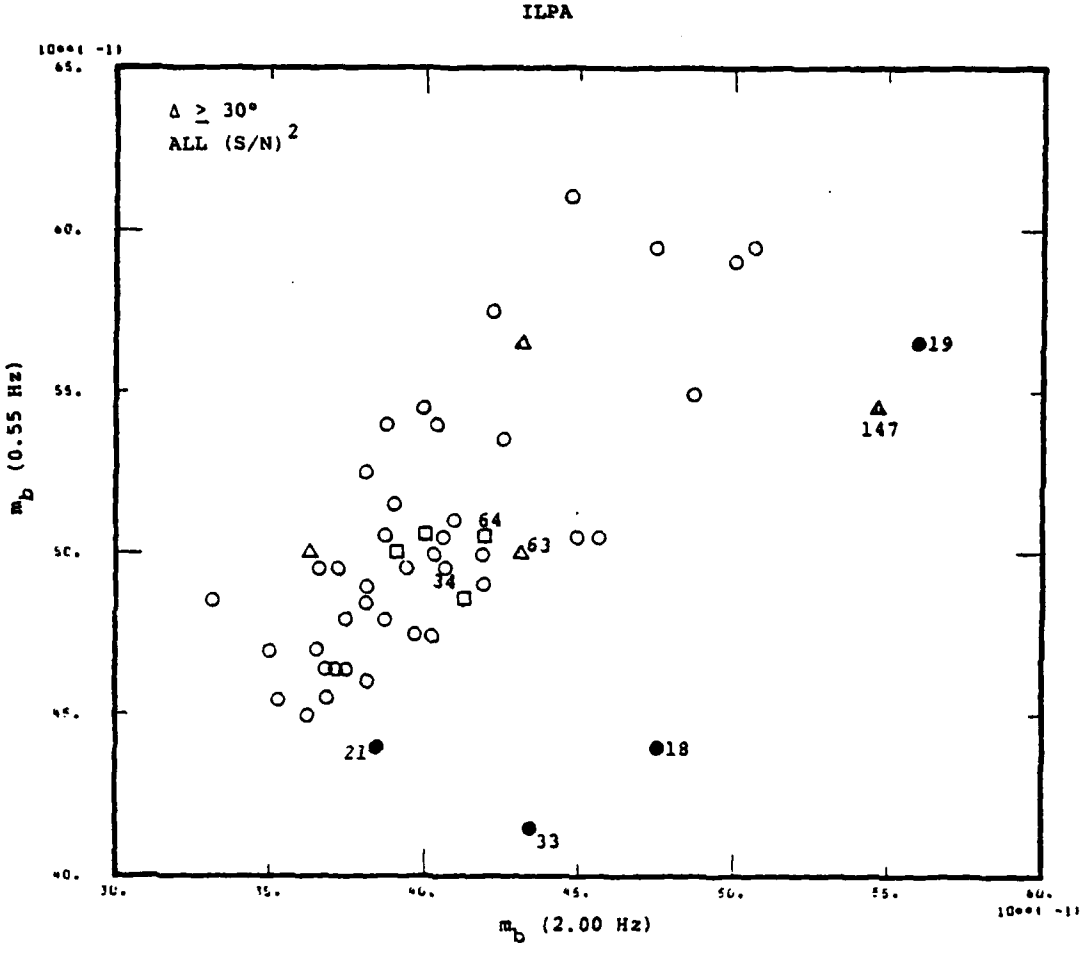

Figure 19b. VFM results for teleseismic events recorded at ILPA. See Figures 12 and 18b for definitions of symbols.

Figure 19b shows VFM discrimination results for events at telseismic distances ($\Delta \geq 30°$) from ILPA. As we saw for KAAO, going from regional to teleseismic distances results in a reduction in the frequency of the high frequency $m_b(f)$ estimates that provide optimal discrimination.

In Figure 20a we give the VFM results for the SRO station located in Mashhad, Iran (MAIO) for most of the events mapped in Figure 17. The first point to be noted is that while the distance range to MAIO (i.e., $18.7° \leq \Delta \leq 28.7°$) is comparable to KAAO ($15° \leq \Delta \leq 23°$, Figure 18a), the highest frequencies reliably observed at MAIO are only 2.25 Hz. Secondly, it is immediately obvious that the degree of separation of event populations at MAIO is significantly less than the separation seen at KAAO.

For events at teleseismic distances from MAIO we have the results plotted in Figure 20b. The epicentral distances of all the events are greater than 30 degrees. As mentioned previously, MAIO behaves like ANMO in terms of VFM type discrimination, yielding essentially no separation of earthquake and explosion populations.

Differences in the performance of the VFM discrimination technique at KAAO, ILPA and MAIO are primarily attributed to differences in attenuation in the upper mantle beneath these stations. Support for this statement comes from a study (Masso, et al., 1978) of teleseismic P-wave residuals determined for a global network of seismograph stations, including several stations located within the region being considered here. Figure 21 is a map of P-wave residuals determined from bulletins of the International Seismological Center (ISC) for stations (solid triangles) in this region. Each residual value plotted in this figure is based on a minimum of 100 globally distributed events. What we observe is that stations in the vicinity of KAAO, including the KAAO location itself, are

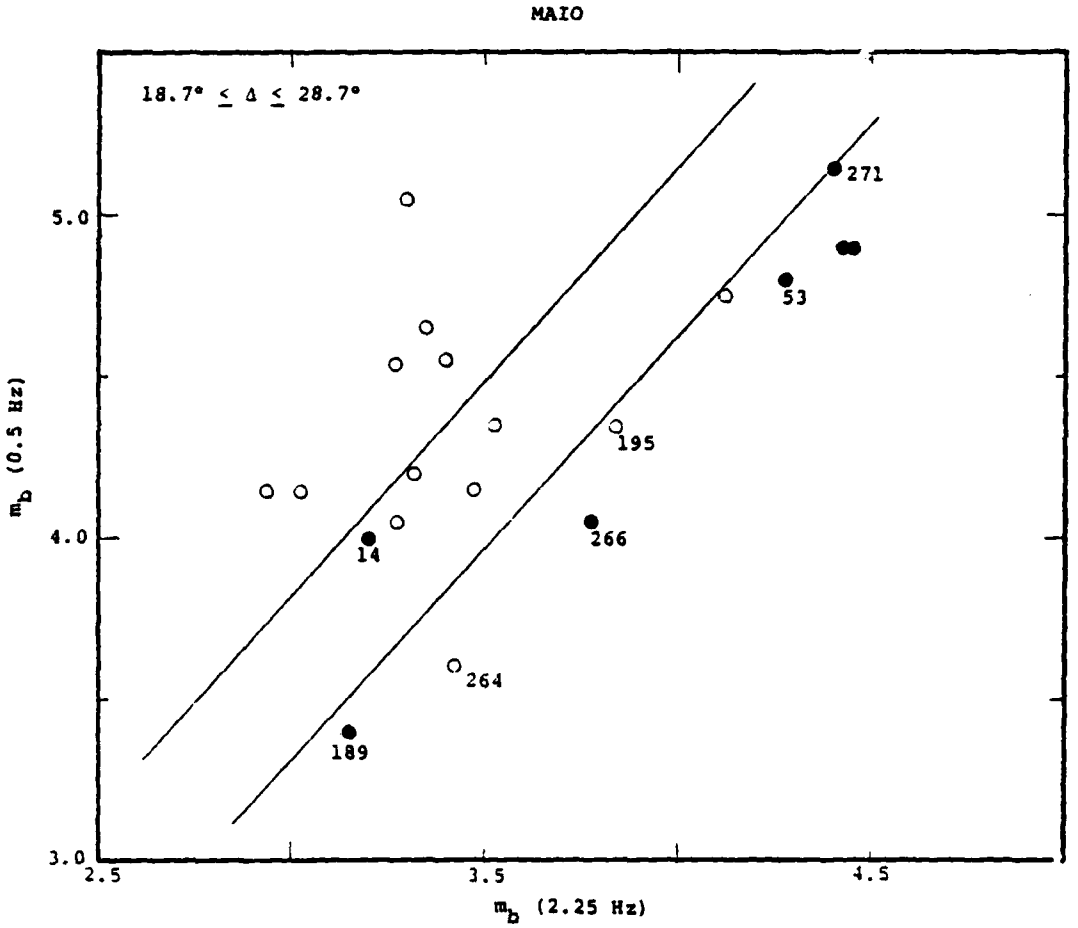

Figure 20a. VFM results for the station at Mashhad, Iran (MAIO) for events in the distance range 18.7° ≤ Δ ≤ 28.7°. The open circles are earthquakes, the closed circles presumed explosions.

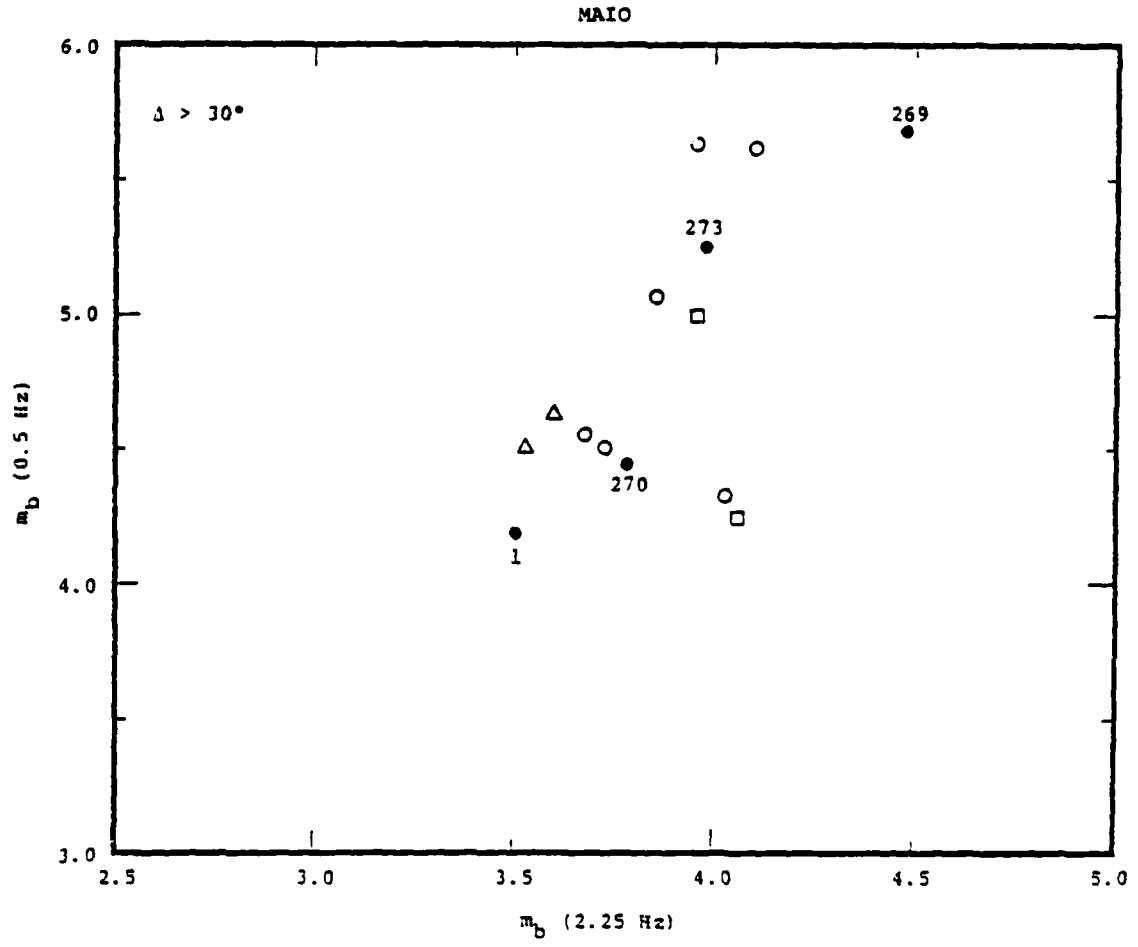

Figure 20b. VFM results for teleseismic events recorded at MAIO.

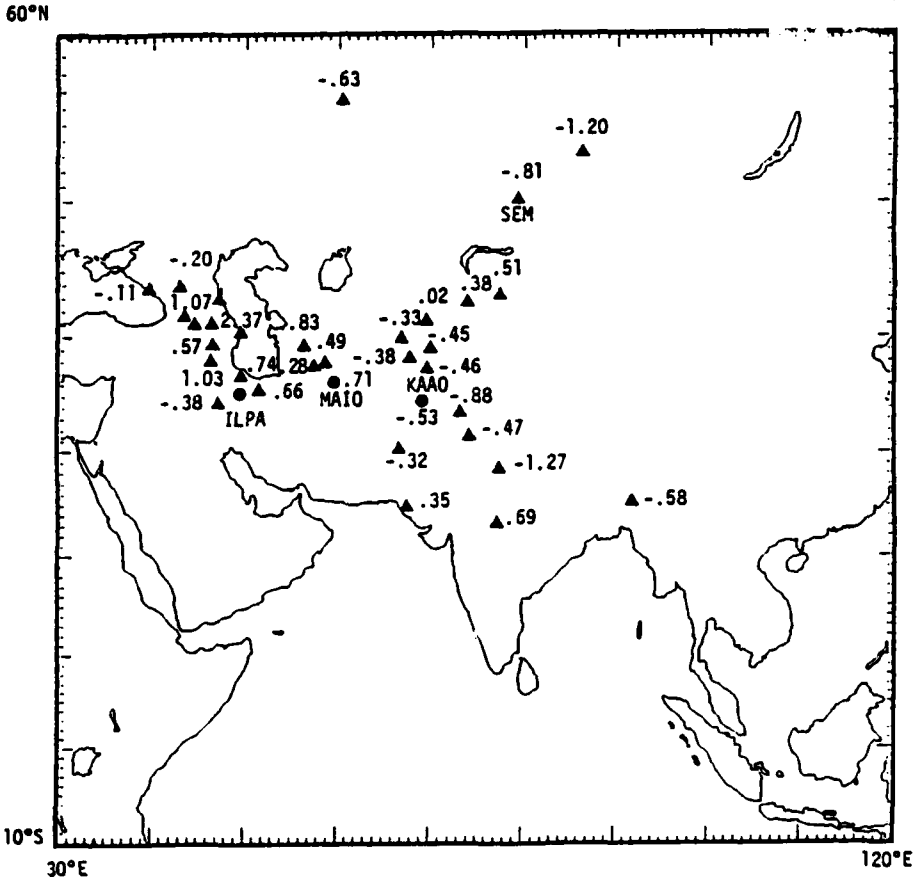

Figure 21. Teleseismic P-wave residuals based on data from the bulletins of the ISC for seismograph stations (closed triangles) in the region of, and including, MAIO, KAAO and ILPA. These latter three stations are denoted by the closed circles.

characterized by large negative residuals. MAIO and nearby stations, on the other hand, exhibit large positive residuals. While we lack information from ILPA, we note that this station is surrounded by stations to the north with relatively large positive residuals and one station to the southwest with a negative residual. Based on similar measurements for stations in other parts of the world, a regional distribution of large negative P-wave residuals (i.e., near KAAO) is attributed to a relatively fast, low-attenuating upper mantle whereas large positive residuals (e.g., near MAIO) are usually associated with a slow, highly attenuating upper mantle.

IV. DISCUSSION AND CONCLUSIONS

In the previous sections of this report we introduced arguments to explain various characteristics of the VFM discriminant observed at the different stations included in this experiment. In particular, we suggested that the combined effects of background earth noise and anelastic attenuation play an important role in determining the performance of the VFM technique at the individual stations. In the following we will develop these arguments in more detail.

4.1 INFLUENCE OF PATH AND SOURCE EFFECTS ON VFM DISCRIMINATION

The way in which we view anelastic attenuation in the upper mantle and background earth noise at a particular recording location contributing to VFM discrimination is as follows. Anelastic attenuation beneath a given station affects P waves from both earthquakes and explosions at teleseismic distances in the same way, basically imposing an exponentially shaped low pass filter on the incoming signals. Both event populations, when viewed in an $m_b(f)$ plane, are supposedly shifted by the same amount with the largest changes being in the high frequency $m_b(f)$ values (i.e., recall the behavior of explosions recorded at RKON relative to ANMO, in Figures 12 and 14, respectively, in Section III). However, because of the presence of a station noise background that is largely unaffected by the upper mantle, the event populations cannot freely shift through the noise population in the $m_b(f)$ plane (Savino, et al., 1979). Thus, earthquakes (which occupy a region in the $m_b(f)$ plane close to, and even overlapping in the case of small magnitude events, the noise population) will approach and eventually totally merge with the noise population as the station upper mantle Q becomes lower and lower. When the earthquake $m_b(f)$ estimates are within or very close to the noise population they

can no longer move in the $m_b(f)$ plane and so will not shift any more even if the station Q is further reduced.

The explosion population, as a function of lower and lower mantle Q, will also appear to move toward the noise population in the same way as the earthquakes, but because they occupy a region with larger high frequency $m_b(f)$ values than those for earthquakes (for whatever reason), they will continue to shift toward the earthquake population with lowering station Q, even then the earthquakes are no longer able to shift. In this case, when the earthquake population reaches the "noise stop" then the explosions will begin to converge on the earthquakes with a resultant reduction in the "discrimination gap" seen at high Q stations. Thus, for stations in very low mantle Q zones and/or with high noise levels, one would expect to see converging or overlapping event populations in the $m_b(f)$ plane. This appears, in fact, to be the case when $m_b(f)$ discrimination at high Q mantle stations (RKON, KAAO) is compared to $m_b(f)$ discrimination at stations over low Q mantle zones (ANMO, MAIO). Also, especially for event populations defined by small numbers of events, this would cause variations in the position and slope of the discrimination lines separating earthquakes and explosions at stations over different mantle Q structures. Since high frequencies are used, this variation is quite large.

The sensitivity of the VFM technique to variations in the propagation path raises another possibility concerning the reasons (source versus path effects) for its overall applicability. For instance, it might be argued that the compressional wave radiation spectra from earthquakes and explosions are not different in any significant way. Rather, the reason for the discrimination observed in Section III is that the Eurasian explosions are shallow events, so there is low frequency cancellation due to pP interference. In addition, since they occur in regions that are aseismic and, in several cases

tectonically stable with shield-like upper mantle structures, the paths in the source region are "high Q paths." On the other hand, all the earthquakes are reasonably deep with little or no pP low frequency cancellation and occur in tectonically active zones within which "low Q mantle" paths can be expected. Thus, the differences in the observed spectral content, as manifested by the $m_b(f)$ discrimination data for the Eurasian events, are due to differences in both low frequency pP cancellation and attenuation between events in different tectonic regions. In this case, the high frequencies from the earthquakes would be expected to be more strongly reduced by attenuation due to their occurrence in low Q mantle regions. While this argument could explain the overall separation of earthquakes and explosions obtained at the high Q stations (e.g., RKON, KAAO, CTAO), when we consider the results in more detail we find that this argument encounters several difficulties.

In order to address these difficulties we repeat the VFM discrimination results for KAAO and RKON in Figure 22. Two tests that we can perform, given the discrimination results from this experiments, for distinguishing between source differences or propagation path (Q) differences as the underlying reason for $m_b(f)$ discrimination are (1) to compare $m_b(f)$ results for collocated earthquakes and explosions and (2) examine the $m_b(f)$ behavior of earthquakes for which the entire propagation paths are presumably high Q – certain shallow trench events and deep earthquakes recorded at Class I stations.

With respect to the first test, we refer the reader to Figure 17. In that figure we mapped the locations of 18 shallow earthquakes in the regional distance range from KAAO. Of particular interest is Event 272, a shallow earthquake, located within 150 km of the eastern Kazakhstan test site. As seen in Figure 22a, $m_b(f)$ estimates for Event 272 plot within the population of earthquakes recorded at KAAO, with a difference

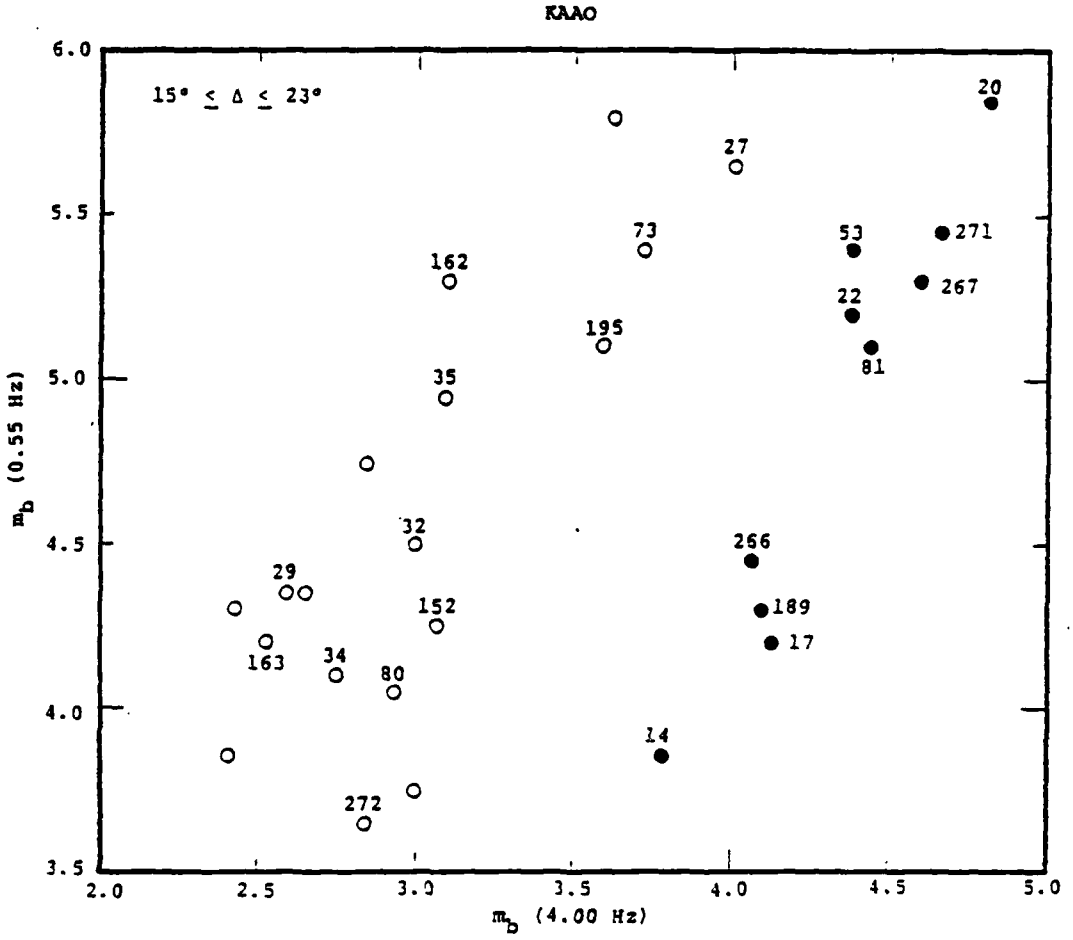

Figure 22a. VFM discrimination results for Kabul, Afghanistan (KAAO) for the earthquakes (open circles) and presumed explosions (closed circles) mapped in Figure 17. These events are located between 15° and 23° from KAAO. Note the separation between Event 272 and the nearby nine presumed explosions at eastern Kazakhstan.

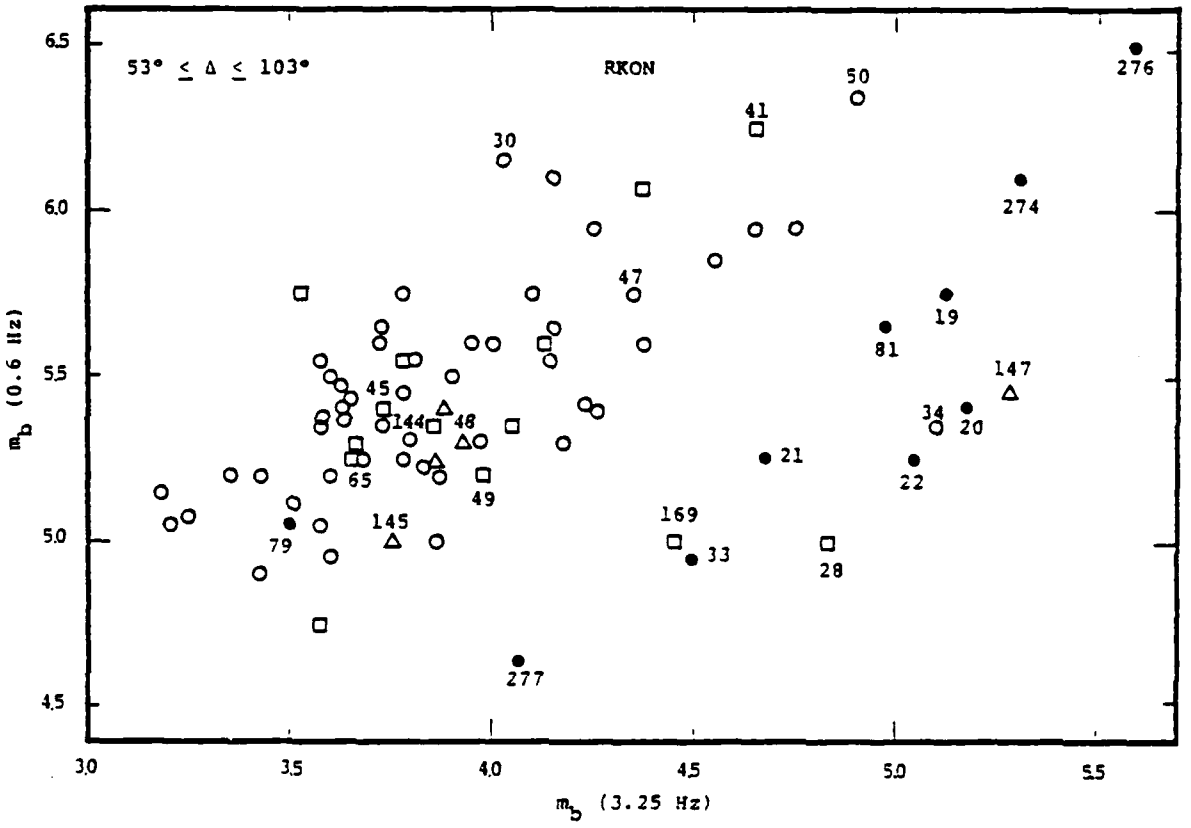

Figure 22b. VFM results for the station located at Red Lake, Ontario (RKON). This figure is similar to Figure 12 except that several additional earthquakes in the Japan-Kuril arcs and Hindu Kush regions have been identified.

of at least one m_b unit in the high frequency magnitude estimates for this event compared to those for presumed explosions at eastern Kazakhstan. Similar comments apply to the three shallow earthquakes west of the Caspian Sea (Events 80, 162, 163) compared to the presumed explosion in that region (Event 22), although these events are not nearly as close as Event 272 is to the nine presumed explosions at eastern Kazakhstan. The conclusion we draw from this comparison is that, with differences in propagation paths minimized, the reason the earthquakes and presumed explosions separate in the $m_b(f)$ plane (Figure 22a) is the enriched high frequency source spectra of the presumed explosions relative to the earthquakes.

For the second test, we select earthquakes and recording stations for which the entire paths to the stations are most likely high Q paths. Event-station combinations that most likely satisfy this criterion are (1) shallow trench earthquakes with receiving stations on the oceanic side of the events and (2) deep earthquakes (i.e., below low Q zones) recorded at stations sited on shields. Given these experimental conditions, if the earthquake and explosion source spectra are really not much different, then all the explosions should appear in the earthquake populations.

The $m_b(f)$ results from all the Class I stations for events along the Japan-Kuril-Kamchatka arcs and in the Hindu Kush region argue strongly for differences in source spectra – see Tables A.1 and A.2 in Appendix A of the report by Savino, et al. (1980) for Events 47, 48, 49, 50, 62, 63, 64, 69, 143, 144, 145, 147, 165 and 169. As an example, we repeat $m_b(f)$ results for the Class I station RKON in Figure 22b. Several additional shallow and deep events occurring along the island arc systems and in the Hindu Kush region are identified on this figure. First we note that the only shallow earthquake that appears explosion-like at this station is Event 34, an aftershock of a large Tibetan earthquake (Event 30). None of the shallow

trench earthquakes (e.g., Events 47 and 50) plots in the explosion population. The second point is that out of a total of 19 deep events analyzed at this station, only three appear explosion-like. The fact that the locations of these three events (147 and 169 in the Kuril Islands, 28 in the Hindu Kush) are common to the 16 events that appear earthquake-like, argues against systematic path effects being responsible for discrimination. Rather, based on the multistation results for all these events (Savino, et al., 1980), the preferred explanation is that the source spectra for the earthquakes and explosions are different and the occasional explosion-like behavior of certain earthquakes at individual stations can be attributed to azimuthal variations in source radiation patterns.

4.2 CONCLUSIONS

The principal conclusions resulting from the discrimination experiment are the following:

- VFM discrimination can be achieved to $m_b \sim 4$ at Class I regional stations.
- VFM discrimination based on both regional and teleseismic stations is approximately 95 percent effective for all the events in this experiment.
- Stations can be classified as to VFM discrimination effectiveness/reliability using P-wave travel-time residual data and other information pertaining to the attenuation properties of the upper mantle beneath a site.
- The VFM technique is an effective discriminant principally because of the enriched high frequency source spectra of explosions relative to earthquakes with the same spectral level near two seconds period.

V. REFERENCES

Archambeau, C. B., D. G. Harkrider and D. V. Helmberger (1974), "Studies of Multiple Seismic Events," California Institute of Technology, Final Contract Report (Draft) prepared for the U. S. Arms Control and Disarmament Agency.

Brune, J. N. and J. Dorman (1963), "Seismic Waves and Earth Structure in the Canadian Shield," BSSA, 53, pp. 167-209.

Gutenberg, B. and C. F. Richter (1956), "Magnitude and Energy of Earthquakes," Ann. Geofis., 9.

Masso, J. F., J. M. Savino and T. C. Bache (1978), "Station Transfer Functions, Analysis of P-Wave Residuals and Summary of Current Research," Systems, Science and Software Quarterly Technical Report, SSS-R-78-3559, January.

Masso, J. F., C. B. Archambeau and J. M. Savino (1979), "Implementation, Testing and Specification of a Seismic Event Detection and Discrimination System," Systems, Science and Software Final Report (Draft) submitted to the U. S. Arms Control and Disarmament Agency, SSS-R-79-3963, March.

Rodi, W. L., J. M. Savino, T. G. Barker, S. M. Day and T. C. Bache (1978), "Analysis of Explosion Generated Surface Waves in Africa, Results from the Discrimination Experiment and Summary of Current Research, "Systems, Science and Software Quarterly Technical Report SSS-R-78-3653 submitted to the Advanced Research Projects Agency, April 1978.

Savino, J. M. and C. B. Archambeau (1974), "Discrimination of Earthquakes from Single and Multiple Explosions Using Spectrally Defined Event Magnitudes," Trans. Amer. Geophys. Union, EOS (Abstract), 56, pp. 1148.

Savino, J. M., T. C. Bache, J. T. Cherry, K. G. Hamilton, D. G. Lambert and J. F. Masso (1975), "Application of Advanced Methods for Identification and Detection of Nuclear Explosions from the Asian Continent," Systems, Science and Software Semi-Annual Technical Report, SSS-R-76-2792, December.

V. REFERENCES (continued)

Savino, J. M., J. F. Masso and C. B. Archambeau (1979), "Discrimination Results from the Priority 1 Stations (U)," Systems, Science and Software Interim Report submitted to the Advanced Research Projects Agency, SSS-CR-79-4026, May. (S)

Savino, J. M., C. B. Archambeau and J. F. Masso (1980), "VFM Discrimination Results for Eurasian Events Using the Priority 1 and Priority 2 Stations (U)," Systems, Science and Software Technical Report (Draft) SSS-CR-80-4570, July.

Thompson, G. A. and D. B. Burke (1974), "Regional Geophysics of the Basin and Range Province," Annual Review of Earth and Planetary Sciences, pp. 213-238.

APPENDIX A

TABULATION OF DISCRIMINATION PARAMETERS

This appendix presents a complete summary of the fixed-frequency discrimination data base for the ten stations included in this experiment: CHTO, CTAO, KAAO, MAIO, TATO, ZOBO, LAO, ILPA, RKON and HNME. Included in the tabulation for each station are only those individual events which satisfy the distance range criteria defined below after excluding certain seismograms judged to be erroneous. The individual seismograms were first processed by MARS, with the primary signal detection and noise information generated for each of 40 narrow-band filters being saved. All of these output for approximately 513 seismograms were merged to create a common Multi-Frequency Discrimination Data Base of over 2.9 megabytes. A special purpose S^3 Seismic Data Management System (SDMS) was designed to operate as a MARS post-processor. The SDMS was applied to this common data base for all ten stations first to select all of the events processed for a given station and to generate a new single-station multi-frequency data base of more modest size; a set of single-station data bases was thereby created for more efficient post-processing. Subsequent applications of the SDMS were then performed in order (1) to exclude erroneous seismogram determined by prior runs; (2) to apply minimum S/N and distance range criteria; (3) to apply the VFM discrimination algorithm and finally (4) to select an appropriate set of discrimination parameters suitable for each individual station. Once these station-dependent discrimination parameters were determined, the SDMS was used to create a series of output files containing the final discrimination results for each station.

These output files for the set of stations listed above were then merged to create the Fixed-Frequency Discrimination Data Base for the stations listed above. The station tabulations given here summarize these results. The tabulation column headings are described below.

EVENT - Event number.

DISTANCE - Epicentral distance in degrees.

FREQ - The fixed high and low discrimination frequencies f_H and f_L (Hz).

Signal Information

MB(F) - The magnitude estimate at the discrimination frequencies given by the relation,

$$MB(F) = \log_{10} [A(F) \cdot F] + b,$$

where A(F) is the fitted value of the noise corrected amplitude at the discrimination frequency, F = f_H or f_L, and b is distance correction.

MB(+), MB(-) - Uncertainty in the magnitude estimate as given by the relation,

$$MB(\pm) = \log_{10} [(A(F) \pm \Delta A_N(F)) \cdot F] + b - MB(F).$$

Noise Information

AMP - The fitted value for the noise amplitude at the fixed high (f_H) or low (f_L) frequency. These fitted values are computed from the least squares polynomial, of degree two which best approximates the unweighted set of log $\bar{A}_N(f_K)$ values over the frequency set $\{f_L\}$ or $\{f_H\}$, where $\bar{A}_N(f_K)$ is the mean noise amplitude at frequency f_K.

MB - The magnitude estimate corresponding to the fitted value of the noise amplitude at the fixed high or low frequency.

(S/N)**2 - The simple mean signal-to-noise power $[A_g^*(f_k)/\bar{A}_N(f_k)]^2$ averaged over the high $\{f_H\}$ or low $\{f_L\}$ frequency bands.

Signal Arrival Information

TG - The noise weighted mean signal group arrival time (seconds) estimated for the high or low frequency bands measured with respect to the event origin time;

$$\bar{t}_g = \sum_{k=1}^{m} w_k \, t_g(f_k) \Big/ \sum_{k=1}^{m} w_k \, ,$$

where $t_g(f_k)$ is the identified signal group arrival time for frequency f_k, w_k is the weight factor, and the summation is over the high or low frequency bands.

TGBAR - Mean group arrival time $\bar{\bar{t}}_g$ measured from the event origin.

TSIGMA - Mean deviation in $\bar{\bar{t}}_g$; t_σ^+ (first line), t_σ^- (second line).

NOISE WINDOW - Length in seconds of the noise window used in the calculation of mean noise amplitudes.

NFFT - The number of frequency samples used in the discrete Fourier transform.

****** SUMMARY OF DISCRIMINATION DATA AT STATION RKON

HIGH FREQUENCY AT 3.25 HZ LOW FREQUENCY AT .60 HZ

EVENT	DISTANCE (DEGREES)	FREQ	SIGNAL INFORMATION MB(F)	MB(+)	MB(-)	NOISE INFORMATION MB	AMP	(S/N)**2	SIGNAL ARRIVAL INFORMATION TG	TGBAR	TSIGMA	NOISE WINDOW	NFFT
3	67.9	3.25	3.607	.094	-.121	3.371	7.23-02	4.72+00	685.81	683.34	7.59	50.00	2048
3		.60	5.178	.129	-.184	5.101	2.10+01	2.00+00	686.43	683.34	-5.53	50.00	2048
4	91.6	3.25	4.060	.057	-.065	3.756	1.39-01	2.39+00	751.66	749.34	9.41	50.00	2048
4		.60	5.339	.099	-.128	5.289	2.58+01	1.33+00	748.39	749.34	-9.85	50.00	2048
7	99.8	3.25	4.748	.075	-.091	4.553	4.18-01	2.46+00	824.33	823.55	8.82	50.00	2048
7		.60	5.937	.115	-.158	5.825	4.23+01	2.16+00	825.36	823.55	-7.87	50.00	2048
8	80.0	3.25	3.207	.111	-.149	3.048	6.85-02	2.64+00	716.31	714.57	9.18	50.00	2048
8		.60	5.038	.097	-.125	4.833	2.26+01	2.20+00	717.22	714.57	-6.95	50.00	2048
9	91.6	3.25	4.120	.141	-.211	4.186	3.75-01	2.86+00	763.26	761.06	6.29	50.00	2048
9		.60	5.608	.099	-.128	5.422	3.50+01	2.51+00	761.71	761.06	-5.52	50.00	2048
10	92.2	3.25	3.651	.096	-.124	3.486	7.15-02	2.45+00	794.45	796.98	7.59	45.00	2048
10		.60	5.262	.091	-.115	5.168	1.86+01	2.38+00	797.78	796.98	-9.45	45.00	2048
19	54.2	3.25	5.121	.002	-.002	3.140	6.73-02	5.71+03	569.63	569.46	.29	20.00	2048
19		.60	5.733	.019	-.020	4.787	1.62+01	1.80+04	568.84	569.46	-.38	20.00	2048
20	79.3	3.25	5.167	.001	-.001	3.091	6.44-02	1.78+04	728.14	728.04	.31	45.00	2048
20		.60	5.383	.030	-.032	4.666	1.31+01	8.81+03	727.94	728.04	-.93	45.00	2048
21	71.0	3.25	4.665	.007	-.007	3.219	6.41-02	9.58+02	674.75	674.78	.28	45.00	2048
21		.60	5.249	.067	-.079	4.890	1.63+01	1.17+02	674.61	674.78	-.38	45.00	2048
22	76.4	3.25	5.058	.003	-.003	3.418	1.01-01	8.91+02	713.19	713.14	.36	50.00	2048
22		.60	5.229	.045	-.050	4.728	1.12+01	1.62+02	712.52	713.14	-.20	50.00	2048
23	91.5	3.25	4.378	.148	-.227	4.260	4.44-01	3.35+00	819.23	817.81	10.37	50.00	2048
23		.60	5.597	.091	-.115	5.409	3.40+01	3.10+00	815.75	817.81	-9.65	50.00	2048

24	96.5	3.25	4.662	.136	-.199	4.514	4.49-01	3.76+00	773.46	773.41	3.45	50.00	2048
24		.60	5.939	.075	-.091	5.639	3.24+01	5.36+00	774.38	773.41	-.86	50.00	2048
25	91.4	3.25	3.733	.082	-.101	3.510	7.90-02	3.54+00	806.23	801.70	13.30	50.00	2048
25		.60	5.647	.102	-.134	5.473	3.93+01	2.09+00	809.40	801.70	-9.85	50.00	2048
26	92.8	3.25	3.516	.103	-.136	3.413	5.26-02	1.52+00	779.26	779.97	7.16	50.00	2048
26		.60	5.762	.058	-.067	5.382	2.66+01	2.77+00	776.89	779.97	-10.04	50.00	2048
27	102.8	3.25	4.095	.083	-.102	3.776	6.09-02	6.80+00	846.37	845.21	4.06	45.00	2048
27		.60	5.769	.150	-.232	5.751	3.11+01	1.61+00	843.55	845.21	-3.39	45.00	2048
28	90.7	3.25	4.828	.021	-.022	4.006	2.65-01	3.34+01	731.91	732.82	1.59	45.00	2048
28		.60	5.020	.149	-.229	5.023	1.50+01	2.99+00	731.38	732.82	-3.25	45.00	2048
29	101.4	3.25	3.909	.072	-.087	3.728	7.52-02	2.18+00	804.36	805.92	5.87	50.00	2048
29		.60	5.522	.119	-.164	5.384	1.84+01	2.04+00	805.94	805.92	-5.11	50.00	2048
30	96.8	3.25	4.023	.078	-.094	3.743	7.10-02	9.48+00	817.53	817.08	1.81	50.00	2048
30		.60	6.126	.030	-.033	5.427	1.86+01	3.57+01	817.05	817.08	-1.85	50.00	2048
31	96.9	3.25	3.778	.134	-.194	3.707	6.38-02	2.06+00	780.01	777.82	5.96	40.00	2048
31		.60	5.743	.074	-.090	5.491	2.10+01	2.02+00	776.67	777.82	-4.33	40.00	2048
32	96.8	3.25	3.945	.095	-.122	3.682	6.17-02	4.97+00	805.95	807.25	10.12	20.00	2048
32		.60	5.610	.080	-.099	5.357	1.58+01	2.19+00	812.20	807.25	-9.55	20.00	2048
33	53.8	3.25	4.494	.009	-.009	3.231	8.70-02	3.48+02	566.36	566.43	.34	50.00	2048
33		.60	4.951	.116	-.158	4.891	2.15+01	1.34+02	566.67	566.43	-.23	50.00	2048
34	96.8	3.25	5.095	.028	-.030	4.503	4.09-01	4.67+01	796.51	796.30	1.34	45.00	2048
34		.60	5.370	.168	-.277	5.448	1.95+01	3.07+00	796.20	796.30	-.90	45.00	2048
35	96.9	3.25	4.145	.081	-.100	3.896	9.86-02	2.41+00	801.60	802.72	7.04	45.00	2048
35		.60	5.664	.104	-.137	5.594	2.66+01	1.84+00	798.13	802.72	-12.00	45.00	2048
36	65.9	3.25	3.779	.085	-.105	3.556	1.11-01	3.09+00	666.81	666.40	12.39	45.00	2048
36		.60	5.270	.097	-.124	5.075	1.98+01	2.75+00	665.81	666.40	-11.93	45.00	2048
37	60.3	3.25	3.598	.053	-.061	3.222	7.58-02	8.93+00	602.90	601.64	3.85	50.00	2048

**** INCLUDE LOW SIGNAL-TO-NOISE EVENTS **** DATABASE RHONO2 ****

DATE 090579 PAGE 12

37		.60	4.972	.155	-.244	4.974	2.32+01	1.90+00	603.57	601.64	-2.65	50.00	2048
38	92.0	3.25	3.879	.064	-.075	3.690	1.20-01	3.71+00	800.14	803.09	8.20	25.00	2048
38		.60	5.387	.082	-.102	5.259	2.40+01	2.28+00	798.79	803.09	-11.36	25.00	2048
39	96.8	3.25	3.996	.110	-.147	3.831	8.70-02	1.83+00	794.55	796.13	11.75	40.00	2048
39		.60	5.607	.112	-.150	5.552	2.48+01	1.89+00	800.74	796.13	-12.11	40.00	2048
41	91.3	3.25	4.650	.065	-.077	4.217	4.03-01	5.20+00	773.21	774.25	1.91	50.00	2048
41		.60	6.227	.097	-.125	6.050	1.48+02	3.22+00	775.58	774.25	-2.99	50.00	2048
44	70.0	3.25	3.599	.061	-.071	3.311	7.92-02	3.12+00	747.98	744.95	9.03	40.00	2048
44		.60	5.494	.090	-.114	5.220	3.48+01	3.12+00	749.40	744.95	-5.48	40.00	2048
45	92.1	3.25	3.715	.119	-.165	3.661	1.09-01	1.53+00	751.02	753.96	13.08	50.00	2048
45		.60	5.385	.090	-.114	5.165	1.89+01	2.88+00	759.89	753.96	-8.94	50.00	2048
46	98.7	3.25	4.147	.087	-.108	3.832	6.60-02	2.62+00	816.47	815.38	3.10	40.00	2048
46		.60	6.076	.059	-.068	5.647	2.34+01	3.99+00	815.42	815.38	-2.09	40.00	2048
47	98.7	3.25	4.354	.064	-.075	4.028	1.04-01	4.05+00	630.04	629.06	11.12	50.00	2048
47		.60	5.762	.105	-.138	5.621	2.20+01	4.41+00	630.06	629.06	-6.62	50.00	2048
48	92.1	3.25	3.920	.040	-.043	3.472	7.08-02	7.26+00	792.06	793.24	3.53	45.00	2048
48		.60	5.316	.089	-.113	5.142	1.79+01	2.04+00	793.13	793.24	-8.13	45.00	2048
49	64.0	3.25	3.972	.073	-.088	3.750	1.73-01	1.84+01	630.11	630.37	1.29	45.00	2048
49		.60	5.205	.085	-.106	4.896	1.31+01	1.02+01	629.18	630.37	-2.54	45.00	2048
50	55.4	3.25	4.892	.028	-.030	4.165	7.12-01	9.59+01	583.99	583.39	.75	45.00	2048
50		.60	6.333	.040	-.044	5.804	1.68+02	2.22+02	582.73	583.39	-1.14	45.00	2048
52	70.0	3.25	3.352	.129	-.185	3.373	9.15-02	2.71+00	716.32	717.43	2.08	40.00	2048
52		.60	5.181	.078	-.096	4.962	1.92+01	2.52+00	715.50	717.43	-3.72	40.00	2048
55	64.2	3.25	3.721	.075	-.091	3.513	1.00-01	4.06+00	632.38	630.26	5.72	50.00	2048
55		.60	5.330	.101	-.131	5.189	2.58+01	1.62+00	633.01	630.26	-3.46	50.00	2048
56	67.2	3.25	3.568	.081	-.100	3.360	7.04-02	2.29+00	622.18	624.24	8.97	50.00	2048
56		.60	5.346	.106	-.140	5.209	2.69+01	2.04+00	624.59	624.24	-9.81	50.00	2048

57	63.3	3.25	3.676	.095	-.123	3.511	1.17-01	2.73+00	616.73	617.92	9.00	50.00	2048
57		.60	5.234	.109	-.146	5.102	2.48+01	1.98+00	617.89	617.92	-10.69	50.00	2048
58	59.1	3.25	3.184	.139	-.207	3.202	7.77-02	1.73+00	618.02	618.15	4.45	50.00	2048
58		.60	5.174	.099	-.128	4.949	2.35+01	3.04+00	619.51	618.15	-5.65	50.00	2048
59	89.3	3.25	3.435	.093	-.119	3.405	7.82-02	3.46+00	808.66	805.29	8.04	50.00	2048
59		.60	5.189	.095	-.122	5.012	1.71+01	2.56+00	807.63	805.29	-5.79	50.00	2048
60	67.2	3.25	3.585	.094	-.120	3.441	8.50-02	2.34+00	632.42	634.37	13.29	50.00	2048
60		.60	5.025	.132	-.191	4.977	1.58+01	1.71+00	636.26	634.37	-12.90	50.00	2048
61	87.1	3.25	3.433	.115	-.158	3.316	6.22-02	2.70+00	766.82	763.85	9.20	50.00	2048
61		.60	4.916	.138	-.205	4.968	1.51+01	2.44+00	765.75	763.85	-6.06	50.00	2048
62	66.8	3.25	3.571	.074	-.089	3.294	6.06-02	4.32+00	664.01	664.01	4.45	50.00	2048
62		.60	4.753	.207	-.406	4.948	1.48+01	6.75+00	664.71	664.01	-3.99	50.00	2048
65	71.2	3.25	3.625	.041	-.045	3.188	5.98-02	5.46+00	703.56	703.33	5.55	50.00	2048
65		.60	5.384	.067	-.080	5.057	2.39+01	2.13+00	708.13	703.33	-6.82	50.00	2048
66	89.0	3.25	3.784	.111	-.149	3.625	1.30-01	2.25+00	737.84	735.31	14.40	50.00	2048
66		.60	5.460	.100	-.131	5.278	3.16+01	2.13+00	738.32	735.31	-9.95	50.00	2048
68	97.1	3.25	4.245	.100	-.131	4.070	1.41-01	1.89+00	817.65	816.98	6.88	50.00	2048
68		.60	5.957	.086	-.108	5.734	3.51+01	2.69+00	816.21	816.98	-6.32	50.00	2048
76	91.5	3.25	3.587	.070	-.083	3.344	5.40-02	2.47+00	778.61	771.85	13.09	45.00	2048
76		.60	5.544	.082	-.101	5.296	2.62+01	2.72+00	773.49	771.85	-8.46	45.00	2048
77	65.9	3.25	4.180	.026	-.028	3.427	1.01-01	3.72+01	756.79	756.85	.53	45.00	2048
77		.60	5.313	.078	-.095	5.016	2.13+01	5.39+01	756.72	756.85	-.88	45.00	2048
78	101.4	3.25	3.795	.103	-.135	3.607	5.69-02	2.75+00	821.97	820.85	6.39	50.00	2048
78		.60	5.546	.117	-.160	5.446	2.13+01	2.27+00	819.52	820.85	-5.86	50.00	2048
79	79.9	3.25	3.499	.070	-.084	3.286	9.65-02	2.28+00	711.76	713.11	9.55	50.00	2048
79		.60	5.061	.098	-.128	4.899	2.24+01	3.36+00	716.34	713.11	-7.73	50.00	2048
81	79.4	3.25	4.983	.002	-.002	3.007	5.43-02	4.42+03	728.73	728.73	.40	50.00	2048

41		.60	5.642	.025	-.027	4.853	2.07+01	3.54+03	728.79	728.73	-.25	50.00	2048
143	59.6	3.25	4.559	.006	-.006	3.231	8.30-02	4.88+02	606.71	606.78	1.07	50.00	2048
143		.60	5.852	.016	-.017	4.962	2.42+01	3.76+02	605.61	606.78	-1.62	50.00	2048
144	73.7	3.25	3.846	.050	-.056	3.350	8.68-02	1.38+01	667.81	668.07	1.13	50.00	2048
144		.60	5.329	.077	-.094	5.063	2.43+01	1.20+01	669.07	668.07	-.72	50.00	2048
145	79.7	3.25	3.738	.036	-.039	2.972	5.37-02	6.51+01	672.00	671.83	.27	30.00	2048
145		.60	5.002	.140	-.207	4.963	2.85+01	1.09+02	671.72	671.83	-.48	30.00	2048
146	55.9	3.25	3.674	.070	-.083	3.294	9.60-02	2.65+00	1152.67	1155.50	4.77	50.00	2048
146		.60	5.226	.091	-.115	5.002	2.65+01	1.90+00	1158.54	1155.50	-5.03	50.00	2048

****** SUMMARY OF DISCRIMINATION DATA AT STATION KAAO

HIGH FREQUENCY AT 4.00 HZ LOW FREQUENCY AT .55 HZ

EVENT	DISTANCE (DEGREES)	FREQ	SIGNAL INFORMATION MB(F)	MB(+)	MB(-)	NOISE INFORMATION MB	AMP	(S/N)**2	SIGNAL ARRIVAL INFORMATION TG	TGRAR	ISIGMA	NOISE WINDOW	NFFT
14	16.6	4.00	3.768	.004	-.004	2.292	6.17-02	9.25+02	239.83	239.91	.70	35.00	2048
14		.55	3.847	.031	-.034	3.153	3.26+00	1.07+02	239.40	239.91	-1.00	35.00	2048
17	16.7	4.00	4.116	.008	-.008	2.721	1.66-01	1.21+03	240.73	240.83	.57	25.00	2048
17		.55	4.225	.024	-.026	3.454	6.51+00	3.32+03	240.72	240.83	-.67	25.00	2048
20	17.2	4.00	4.809	.002	-.002	3.000	3.15-01	2.80+04	247.83	248.06	2.29	15.00	2048
20		.55	5.847	.001	-.001	3.655	1.03+01	8.08+04	247.34	248.06	-1.88	15.00	2048
22	20.5	4.00	4.374	.006	-.006	2.970	2.08-01	3.90+02	285.16	284.98	.73	20.00	2048
22		.55	5.201	.013	-.013	3.982	1.56+01	1.72+03	285.68	284.98	-1.54	20.00	2048
27	22.2	4.00	3.999	.003	-.003	2.161	2.18-02	9.08+03	303.77	301.74	-.57	25.00	2048
27		.55	5.634	.002	-.002	3.936	9.44+00	8.54+04	301.20	301.74	-.83	25.00	2048
29	19.0	4.00	2.645	.237	-.564	2.753	1.42-01	4.42+00	260.01	259.92	-.97	20.00	2048
29		.55	4.354	.047	-.053	3.816	1.19+01	1.10+02	259.63	259.92	-.90	20.00	2048
32	16.1	4.00	2.996	.051	-.058	2.679	1.50-01	5.57+00	263.92	264.05	2.18	35.00	2048
32		.55	4.468	.026	-.028	3.653	1.03+01	4.65+02	264.25	264.05	-1.44	35.00	2048
34	16.2	4.00	2.748	.040	-.045	2.245	5.53-02	1.05+02	239.26	236.83	2.77	20.00	2048
34		.55	4.081	.081	-.099	3.834	1.56+01	1.54+02	235.97	236.83	-3.54	20.00	2048
35	16.2	4.00	3.092	.024	-.025	2.115	4.10-02	3.91+02	232.80	234.43	2.50	15.00	2048
35		.55	4.964	.007	-.007	3.692	1.13+01	1.89+04	232.82	234.43	-3.47	15.00	2048
39	16.2	4.00	2.596	.044	-.049	2.109	9.04-02	2.44+01	237.58	238.61	3.29	30.00	2048
39		.55	4.342	.046	-.051	3.732	1.24+01	9.37+01	238.81	238.61	-2.86	30.00	2048
46	40.8	4.00	2.412	.123	-.173	2.301	4.16-02	1.84+00	281.87	282.97	5.46	15.00	1024
46		.55	3.848	.165	-.271	3.831	1.02+01	1.61+00	280.68	282.97	-6.60	15.00	1024
53	16.9	4.00	4.390	.002	-.002	2.732	1.70-01	5.99+03	240.83	243.63	4.21	19.00	2048
53		.55	5.405	.002	-.002	3.520	7.58+00	3.65+04	244.80	243.63	-4.72	19.00	2048
58	15.8	4.00	2.435	.057	-.065	2.053	2.96-02	2.81+01	230.48	229.41	2.37	15.00	2048
58		.55	4.322	.035	-.038	3.777	1.14+01	8.76+01	231.35	229.41	-2.10	15.00	2048
73	15.4	4.00	3.726	.018	-.019	2.659	1.31-01	4.89+02	229.71	230.22	2.74	20.00	2048
73		.55	5.398	.005	-.005	3.782	7.97+00	3.81+03	230.38	230.22	-2.60	20.00	2048
80	14.8	4.00	2.930	.119	-.164	2.799	1.65-01	1.22+00	269.42	269.41	5.25	30.00	2048
80		.55	4.052	.065	-.077	3.486	5.43+00	2.82+01	269.61	269.41	-1.44	30.00	2048
81	17.0	4.00	4.435	.004	-.004	2.724	1.66-01	1.17+04	247.18	248.80	.58	15.00	2048
81		.55	5.120	.001	-.001	3.420	6.02+00	1.18+05	249.17	248.80	-.57	15.00	2048
151	20.9	4.00	2.849	.042	-.046	2.292	3.98-02	6.97+02	288.91	287.74	.99	30.00	2048
151		.55	4.769	.011	-.011	3.557	5.32+00	6.26+03	287.77	287.74	-1.38	30.00	2048

152	23.5	4.00	3.071	.121	-.168	3.029	1.34-01	1.05+01	319.92	320.77	1.21	30.00	2048
152		.55	4.265	.078	-.096	4.074	1.08+01	4.21+01	319.69	320.77	-4.35	30.00	2048
159	15.9	4.00	2.986	.060	-.069	2.897	2.27-01	1.73+00	299.24	298.53	4.62	20.00	2048
159		.55	3.753	.057	-.066	3.535	7.15+00	3.20+01	298.88	298.53	-1.33	20.00	2048
162	20.5	4.00	3.099	.033	-.036	2.610	9.07-02	3.45+02	283.24	282.14	.73	30.00	2048
162		.55	5.323	.003	-.003	3.655	7.32+00	1.59+04	282.04	282.14	-.70	30.00	2048
163	20.4	4.00	2.543	.142	-.212	2.377	5.43-02	2.62+01	286.65	284.83	.59	25.00	2048
163		.55	4.179	.056	-.064	3.717	8.64+00	9.56+02	284.78	284.83	-.53	25.00	2048
166	23.7	4.00	3.624	.050	-.057	2.898	9.91-02	2.46+02	318.93	319.03	.97	12.50	2048
166		.55	5.788	.003	-.003	3.980	8.71+00	7.88+03	319.45	319.03	-.91	12.50	2048
189	16.7	4.00	4.083	.008	-.008	2.620	1.31-01	5.72+02	241.69	242.42	.88	25.00	1024
189		.55	4.290	.022	-.023	3.384	5.54+00	8.39+02	242.71	242.42	-1.31	25.00	1024
195	18.2	4.00	3.586	.036	-.037	2.747	1.68-01	3.62+02	263.16	263.63	.51	30.00	2048
195		.55	5.084	.003	-.003	3.647	7.70+00	1.29+04	263.59	263.63	-1.18	30.00	2048
266	16.8	4.00	4.076	.005	-.005	2.659	1.14-01	9.31+02	239.54	239.46	1.26	25.00	2048
266		.55	4.429	.025	-.027	3.790	1.26+01	7.42+02	238.03	239.46	-1.64	25.00	2048
267	17.1	4.00	4.606	.004	-.004	2.910	2.56-01	1.08+04	243.26	244.33	1.96	35.00	2048
267		.55	5.307	.003	-.003	3.745	1.27+01	1.42+04	245.45	244.33	-1.42	35.00	2048
271	16.8	4.00	4.671	.001	-.001	2.445	8.77-02	2.22+04	253.27	253.30	1.78	30.00	2048
271		.55	5.452	.002	-.002	3.516	7.51+00	3.50+04	252.45	253.30	-1.39	30.00	2048
272	17.7	4.00	.633	.024	-.026	1.914	2.58-02	7.33+02	302.61	302.85	.95	22.00	2048
272		.55	.640	.073	-.187	3.360	5.49+00	9.21+02	303.75	302.85	-.86	22.00	2048

****** SUMMARY OF DISCRIMINATION DATA AT STATION KAAO

HIGH FREQUENCY AT 2.75 HZ LOW FREQUENCY AT .40 HZ

EVENT	DISTANCE (DEGREES)	FREQ	SIGNAL INFORMATION MB(F)	MB(F+)	MB(-)	NOISE INFORMATION NP	AMP	(S/N)**2	SIGNAL ARRIVAL INFORMATION TG	TGRAR	TSIGMA	NOISE WINDOW	NFFT
3	44.5	2.75	4.017	.087	-.109	3.623	3.41-01	2.11+03	508.44	507.50	.66	35.00	2048
3		.40	5.240	.079	-.097	5.142	4.89+01	4.15+01	507.37	507.50	-.89	35.00	2048
16	34.2	2.75	3.705	.058	-.067	3.219	1.20-01	2.01+01	411.08	411.13	.44	25.00	2048
16		.40	4.778	.105	-.140	4.535	1.71+01	5.02+02	411.01	411.13	-.61	25.00	2048
19	39.6	2.75	5.611	.001	-.001	3.635	6.25-01	8.60+03	456.45	456.32	.53	30.00	2048
19		.40	5.652	.036	-.039	4.926	8.40+01	5.60+03	455.91	456.32	-1.15	30.00	2048
21	33.8	2.75	4.083	.052	-.058	3.607	2.93-01	1.14+02	404.05	402.75	.98	35.00	2048
21		.40	5.626	.044	-.048	5.217	8.23+01	3.62+02	401.82	402.75	-1.86	35.00	2048
50	64.6	2.75	4.313	.134	-.195	4.227	6.19-01	2.38+01	635.66	637.34	2.63	20.00	2048
50		.40	5.873	.025	-.027	5.171	3.71+01	6.77+02	634.64	637.34	-5.71	20.00	2048
56	62.4	2.75	5.193	.040	-.044	4.472	1.18+00	1.50+01	763.03	765.38	5.28	10.00	1024
56		.40	5.264	.165	-.270	5.094	3.41+01	1.65+01	769.27	765.38	-3.82	10.00	1024
57	60.6	2.75	4.009	.107	-.142	3.901	4.00-01	5.13+00	597.58	597.19	1.04	15.00	2048
57		.40	4.992	.126	-.183	4.910	2.81+01	1.50+01	597.02	597.19	-.80	15.00	2048
63	57.8	2.75	4.502	.004	-.004	3.216	9.47-02	2.87+02	578.12	577.83	.57	15.00	2048
63		.40	4.267	.434	-.865	5.259	7.19+01	2.13+02	577.16	577.83	-.97	15.00	2048
64	64.1	2.75	4.246	.088	-.110	3.929	3.09-01	3.18+00	627.90	629.54	1.15	20.00	2048
64		.40	4.992	.103	-.136	5.058	2.86+01	6.96+00	628.54	629.54	-4.07	20.00	2048
77	39.0	2.75	3.641	.053	-.060	3.183	2.21-01	9.08+00	446.58	447.03	.70	30.00	2048
77		.40	4.830	.073	-.088	4.593	3.90+01	8.91+02	447.18	447.03	-.72	30.00	2048
143	63.7	2.75	4.755	.018	-.019	3.769	2.29-01	3.36+02	634.13	634.49	1.76	15.00	2048
143		.40	5.943	.017	-.018	5.215	4.39+01	4.11+03	634.34	634.49	-1.22	15.00	2048
144	58.5	2.75	4.161	.022	-.023	3.192	8.96-02	8.81+01	581.52	581.51	.36	25.00	2048
144		.40	4.802	.204	-.397	4.863	2.89+01	4.60+02	581.34	581.51	-.71	25.00	2048
145	48.4	2.75	4.047	.055	-.063	3.563	1.84-01	2.00+01	476.75	475.91	.38	30.00	2048
145		.40	5.532	.057	-.066	5.136	4.72+01	1.16+02	475.64	475.91	-.99	30.00	2048
147	57.4	2.75	5.130	.009	-.009	3.879	4.36-01	3.92+02	544.22	544.28	.44	20.00	2048
147		.40	4.819	.373	-.293	5.002	3.98+01	8.74+02	544.48	544.28	-.41	20.00	2048
154	58.8	2.75	4.011	.059	-.068	3.605	2.32-01	3.02+01	551.68	551.17	.31	30.00	2048
154		.40	5.157	.096	-.123	5.067	4.63+01	1.73+02	550.99	551.17	-.61	30.00	2048
157	62.5	2.75	4.080	.019	-.020	3.882	3.11-01	4.81+01	539.96	539.72	.86	15.00	1024
157		.40	4.572	.376	-1.020	5.086	3.42+01	1.32+01	539.28	539.72	-.53	15.00	1024
164	59.1	2.75	4.565	.016	-.016	3.680	2.76-01	3.74+01	599.09	598.01	.23	20.00	2048
164		.40	5.389	.041	-.145	4.715	2.06+01	2.11+04	598.01	598.01	-.19	20.00	2048

165 165	64.1	2.75 .40	4.131 5.824	.115 .038	-.157 -.092	4.066 5.189	4.24-01 3.86+01	2.15+00 5.42+01	631.32 631.06	631.22 631.22	-.32 -1.56	30.00 30.00	2048 2048
169 169	63.2	2.75 .40	4.187 5.687	.106 .024	-.140 -.026	3.999 4.939	4.36-01 2.61+01	8.57+00 1.65+02	653.56 653.64	654.04 654.04	-.74 -.99	40.00 40.00	2048 2048
171 171	63.4	2.75 .40	3.843 4.938	.065 .209	-.076 -.420	3.507 5.076	1.34-01 3.42+01	8.55+00 6.99+00	626.43 625.40	626.07 626.07	-.63 -1.46	30.00 30.00	2048 2048
178 178	63.7	2.75 .40	4.677 6.456	.005 .010	-.005 -.010	3.229 5.054	6.60-02 3.03+01	1.15+03 2.34+03	630.11 631.49	630.79 630.79	1.31 -1.44	15.00 15.00	2048 2048
180 180	63.6	2.75 .40	3.632 5.195	.138 .111	-.204 -.150	3.649 5.022	1.78-01 2.88+01	1.08+00 8.32+00	645.33 648.33	639.40 639.40	18.15 -7.24	45.00 45.00	2048 2048
182 182	63.8	2.75 .40	4.357 5.408	.066 .077	-.078 -.094	4.015 5.264	3.95-01 4.81+01	8.10+00 1.17+01	641.77 640.94	639.09 639.09	-3.91 -3.19	25.00 25.00	2048 2048
183 183	65.6	2.75 .40	4.208 5.322	.015 .041	-.015 -.116	3.200 4.975	5.76-02 2.36+01	5.04+02 8.34+01	650.07 647.86	648.30 648.30	-5.39 -1.67	35.00 35.00	2048 2048
193 193	64.0	2.75 .40	4.138 5.595	.141 .014	-.209 -.037	4.094 5.002	4.51-01 2.51+01	1.32+00 1.44+01	639.44 636.26	636.97 636.97	-1.69 -4.12	25.00 25.00	2048 2048
273 273	33.1	2.75 .40	5.018 3.932	.001 .408	-.001 -.630	3.047 4.643	8.08-02 2.19+01	3.26+03 5.05+04	404.11 403.59	403.77 403.77	-.68 -.34	30.00 30.00	2048 2048

****** SUMMARY OF DISCRIMINATION DATA AT STATION CTAO

HIGH FREQUENCY AT 3.50 HZ LOW FREQUENCY AT .60 HZ

EVENT	DISTANCE (DEGREES)	FREQ	SIGNAL INFORMATION MB(F)	MB(+)	MB(-)	NOISE INFORMATION MB	AMP	(S/N)**2	SIGNAL ARRIVAL INFORMATION TG	TGBAR	TSIGMA	NOISE WINDOW	NFFT
20	91.6	3.50	4.261	.050	-.056	3.748	1.27-01	2.00+01	791.21	790.40	.51	30.00	1024
20		.60	5.655	.046	-.051	5.195	2.07+01	2.75+02	790.12	790.40	-.96	30.00	1024
21	89.0	3.50	3.913	.069	-.083	3.196	4.49-02	4.18+00	748.35	748.11	.32	50.00	2048
21		.60	4.867	.139	-.205	4.867	1.23+01	2.18+01	748.15	748.11	-.33	50.00	2048
47	69.7	3.50	3.984	.031	-.033	3.355	7.60-02	6.54+02	592.65	592.93	2.73	25.00	2048
47		.60	6.284	.012	-.012	5.227	3.31+01	2.40+03	589.67	592.93	-4.97	25.00	2048
50	77.7	3.50	3.555	.137	-.202	3.624	1.51-01	5.19+01	728.24	729.82	1.86	25.00	2048
50		.60	5.773	.031	-.034	4.959	1.91+01	1.14+02	729.30	729.82	-1.34	25.00	2048
53	91.8	3.50	4.197	.029	-.031	3.571	8.46-02	1.38+02	794.79	794.20	1.24	30.00	2048
53		.60	5.937	.060	-.069	5.659	6.09+01	6.34+01	793.02	794.20	-1.28	30.00	2048
56	66.5	3.50	3.493	.187	-.336	3.642	1.25-01	3.25+00	1015.19	1013.90	1.26	15.00	1024
56		.60	6.030	.042	-.046	5.354	3.77+01	8.61+00	1013.42	1013.90	-1.45	15.00	1024
81	91.5	3.50	3.911	.071	-.084	3.531	7.70-02	2.95+01	790.98	790.81	.59	35.00	2048
81		.60	5.607	.039	-.043	5.105	1.69+01	9.39+01	790.20	790.81	-1.32	35.00	2048
143	73.6	3.50	3.379	.092	-.117	3.201	6.56-02	5.53+01	694.84	695.31	.51	30.00	2048
143		.60	6.072	.011	-.011	4.935	2.08+01	4.81+02	694.91	695.31	-5.38	30.00	2048
164	63.0	3.50	3.461	.095	-.122	3.339	7.85-02	2.05+01	626.92	625.58	.39	25.00	2048
164		.60	5.282	.033	-.036	4.492	6.52+00	3.95+02	625.29	625.58	-.68	25.00	2048
166	70.6	3.50	3.361	.070	-.083	2.991	3.52-02	2.48+01	677.19	678.18	1.84	25.00	2048
166		.60	4.984	.073	-.087	4.594	8.35+00	4.86+01	678.33	678.18	-2.69	25.00	2048
169	76.0	3.50	4.151	.020	-.021	3.272	6.73-02	5.20+02	695.76	695.90	.28	50.00	2048
169		.60	5.643	.022	-.023	4.852	1.49+01	1.23+03	696.08	695.90	-.20	50.00	2048
170	87.6	3.50	3.842	.028	-.029	3.047	2.77-02	7.82+01	773.76	773.18	1.58	25.00	2048
170		.60	6.273	.009	-.009	5.174	2.17+01	3.84+02	772.78	773.18	-2.05	25.00	2048
176	73.7	3.50	3.407	.006	-.007	2.671	1.98-02	6.11+01	707.35	706.59	1.27	5.00	1024
176		.60	5.492	.174	-.174	5.264	4.53+01	2.68+01	706.02	706.59	-1.32	5.00	1024
191	82.1	3.50	3.401	.075	-.091	3.138	4.82-02	3.24+00	766.49	767.27	5.12	20.00	2048
191		.60	4.864	.109	-.146	4.704	1.04+01	2.23+00	770.87	767.27	-5.95	20.00	2048
265	92.1	3.50	3.902	.116	-.159	3.780	1.34-01	8.69+00	796.64	796.45	.41	20.00	2048
265		.60	5.037	.102	-.134	4.863	9.49+00	2.85+02	796.46	796.45	-.60	20.00	2048
266	92.1	3.50	3.195	.051	-.058	3.541	7.70-02	4.15+00	791.07	791.36	1.06	20.00	2048
266		.60	5.281	.089	-.112	5.017	1.35+01	1.79+01	790.53	791.36	-3.19	20.00	2048
267	91.5	3.50	3.985	.087	-.108	4.013	2.34-01	1.36+01	790.13	788.56	.57	13.00	1024
267		.60	5.584	.142	-.213	5.512	4.31+01	6.05+01	788.08	788.56	-1.11	13.00	1024

268	92.1	3.50	3.988	.062	-.073	3.584	8.50-02	5.15+01	789.99	789.41	-.59	30.00	1024
268		.60	5.529	.146	-.222	5.523	4.31+01	2.64+01	789.58	789.41	-.56	30.00	1024
269	85.4	3.50	3.970	.026	-.027	3.211	5.09-02	2.55+02	758.64	758.59	-.32	24.00	2048
269		.60	5.261	.169	-.281	5.218	3.02+01	1.85+02	758.29	758.59	-.31	24.00	2048

**** EXCLUDE LOW SIGNAL-TO-NOISE EVENTS **** DATABASE LAO02 **** DATE 050779 PAGE 7

****** SUMMARY OF DISCRIMINATION DATA AT STATION LAO

HIGH FREQUENCY AT 2.00 HZ LOW FREQUENCY AT .40 HZ

			SIGNAL INFORMATION			NOISE INFORMATION			SIGNAL ARRIVAL INFORMATION				
EVENT	DISTANCE (DEGREES)	FREQ	M(F)	DM(F)	MFR-D	MB	AMP	(S/N)**2	TG	TGPAR	TSIGMA	NOISE WINDOW	NFFT
1 1	136.4	2.00 .40	4.360 6.172	.176 .119	-.038 -.164	3.870 6.305	6.75-02 4.79+01	1.06+01 1.55+00	915.50 914.44	915.14 915.14	2.21 -3.21	54.00 53.00	2049 2048
7 7	103.8	2.00 .40	4.562 6.179	.050 .194	-.056 -.170	4.135 5.904	1.79-01 5.37+01	1.99+01 1.98+00	841.77 841.40	843.08 843.08	2.61 -5.17	46.00 40.00	2048 2048
9 9	46.9	2.00 .40	3.867 6.114	.177 .167	-.040 -.107	3.184 5.846	3.11-02 7.77+01	5.08+00 2.62+00	901.23 899.10	901.41 901.41	9.22 -11.70	46.00 40.00	2048 2048
19 19	59.5	2.00 .40	4.955 5.473	.034 .176	-.026 -.021	3.464 4.117	2.31-01 5.18+01	1.17+03 7.74+03	608.64 608.06	608.22 608.72	.35 -1.15	50.00 50.00	2048 2048
23 23	54.6	2.00 .40	3.956 6.697	.172 .176	-.086 -.095	3.578 5.976	6.65-02 9.07+01	5.16+00 2.66+00	896.12 899.21	896.08 896.08	15.13 -16.12	46.00 46.00	2048 2048
24 24	95.6	2.00 .40	3.672 6.397	.160 .764	-.081 -1.305	3.741 5.828	9.77-02 5.97+01	1.29+01 1.62+01	789.52 790.28	790.00 790.00	1.54 -1.12	20.00 20.00	2048 2048
26 26	67.9	2.00 .40	4.353 5.923	.129 .140	-.131 -.227	3.675 5.977	7.66-02 7.68+01	5.45+00 1.57+00	808.94 808.01	809.36 809.38	5.18 -7.95	46.00 46.00	2048 2048
31 31	66.9	2.00 .40	4.106 6.212	[illegible] .041	-.059 -.172	3.481 5.976	5.69-02 7.32+01	2.15+01 3.64+00	903.52 903.07	903.93 903.93	.72 -3.44	50.00 50.00	2048 2048
32 32	59.9	2.03 .40	3.744 6.676	.171 .051	-.096 -.170	3.503 5.861	6.20-02 7.66+01	3.09+00 2.57+00	864.21 862.67	865.63 865.63	10.66 -12.31	50.00 50.00	2048 2048
33 33	50.2	2.00 .40	4.191 4.632	.106 .164	-.326 -.655	2.856 5.263	5.71-02 6.37+01	6.00+01 4.69+01	664.89 665.29	605.34 605.34	.70 -1.01	50.00 50.00	2048 2048
40 41	101.1	2.00 .40	4.101 5.967	[illegible] .081	-.044 -.110	3.396 5.765	6.09-02 7.64+01	6.62+00 3.67+00	923.45 925.34	921.31 921.31	7.66 -3.40	40.00 40.00	2048 2048
47 47	61.1	2.00 .40	5.479 5.571	.123 .047	-.197 -.405	3.471 5.369	1.55-01 6.26+01	2.34+00 2.93+02	617.15 617.50	612.49 612.49	.25 -.26	44.00 44.00	2048 2048
46 46	57.2	2.00 .40	7.963 6.550	.114 .044	-.152 -.120	3.051 5.561	1.35-01 6.89+01	2.71+00 2.66+00	804.71 791.36	799.82 799.82	17.45 -20.98	46.00 46.00	2048 2048
[illegible]	52.7	2.00 .40	3.867 5.171	.060 .127	[illegible] -.196	4.671 5.173	4.17-02 6.67+01	7.35+01 2.58+03	566.26 566.84	567.19 567.19	1.15 -2.94	56.00 56.00	2048 2048
[illegible]	73.6	2.00 .40	3.519 5.467	[illegible]	-.126 [illegible]	3.261 6.518	5.26-02 6.24+01	5.27+04 6.64+03	756.89 754.73	755.13 755.13	.33 -.69	56.00 56.00	2048 2048
[illegible]	[illegible]	2.00 .40	[illegible]	[illegible]	-.171 -.146	7.197 6.376	1.01-01 6.01+01	7.66+00 2.42+01	725.71 716.44	715.46 715.46	15.58 -17.51	56.00 53.00	2048 2048
[illegible]	4.1	2.00 .40	5.645 5.677	[illegible] .11	-.261 -.147	4.154 [illegible]	5.50-01 6.40+01	2.66+01 3.27+00	617.66 616.09	605.95 605.95	7.10 -6.44	40.00 40.00	2048 2048

**** EXCLUDE LOW SIGNAL-TO-NOISE EVENTS **** DATABASE LAND2 **** DATE 09F779 PAGE 9

175		.40	6.294	.173	-.134	6.170	1.34+02	2.91+00	827.24	827.35	-10.02	50.00	2048
11[illegible]	[illegible].7	2.00	3.159	.161	-.076	[illegible].911	5.13-02	3.47+00	583.06	587.04	.09	50.00	2048
11[illegible]		.40	6.279	.141	-.270	6.294	7.79+01	1.27+02	583.14	583.00	-.26	50.00	2048
115	94.0	2.00	3.446	.152	-.166	3.169	5.86-02	1.98+00	836.86	838.99	10.17	50.00	2048
116		.40	6.416	.156	-.176	5.663	9.06+01	2.30+00	839.83	838.99	-4.35	50.00	2048
1[illegible]1	92.7	2.00	2.429	.199	-.376	3.649	6.27-02	7.41+00	937.45	930.67	12.77	50.00	2048
1[illegible]1		.40	6.960	.141	-.211	5.993	9.14+01	1.87+00	931.73	930.67	-6.71	50.00	2048
1[illegible]	1.4.2	2.00	4.454	.190	-.114	4.227	2.02-01	1.23+01	838.27	838.17	1.89	50.00	2048
1[illegible]		.40	6.926	.156	-.652	6.143	8.33+01	2.55+00	836.56	838.17	-1.58	50.00	2048
267	17.6	2.00	4.961	.106	-.006	3.559	1.61-01	1.53+02	752.04	752.60	1.12	50.00	2049
267		.45	5.786	.044	-.056	5.266	4.64+01	5.71+03	750.84	752.06	-2.45	50.00	2048

**** EXCLUDE LOW SIGNAL-TO-NOISE EVENTS **** DATABASE HNME02 **** DATE 090579

ЗDATA,L 44HNME.
DATAHRI S3-A 73RI-2 09/05/79 14:30:06(1)

1. HNME ****** SUMMARY OF DISCRIMINATION DATA

	EVT	DIST	FREQ	MR(F)	MR(+)	MP(-)	MRN	AMPN	(S/N)**2	TG	TGBAR	TSTEPA
2.												
3.	3	77.6	2.75	3.771	.059	-.069	3.490	1.42-01	2.72+00	715.21	713.39	7.73
4.	3	77.6	.50	5.443	.127	-.180	5.475	7.51+01	2.21+00	714.70	50.00	-1.05
5.	10	90.0	2.75	3.740	.079	-.096	3.546	1.28-01	2.08+00	743.42	749.31	9.93
6.	10	90.0	.50	5.710	.114	-.155	5.563	7.31+01	2.48+00	746.51	45.00	-14.17
7.	19	54.5	2.75	4.532	.014	-.014	3.434	1.56-01	3.27+02	572.04	572.28	.72
8.	19	54.5	.50	5.625	.058	-.067	5.224	5.30+01	3.79+02	571.52	30.00	-.77
9.	20	79.9	2.75	4.856	.003	-.003	3.106	9.05-02	2.30+03	735.36	734.41	1.37
10.	20	79.9	.50	5.480	.066	-.076	5.131	5.27+01	2.22+03	733.05	50.00	-1.23
11.	21	76.6	2.75	3.953	.051	-.058	3.532	1.56-01	1.70+01	711.32	711.10	.61
12.	21	76.8	.50	5.499	.142	-.212	5.428	6.75+01	4.81+00	710.95	45.00	-.74
13.	22	71.1	2.75	4.101	.030	-.032	3.466	1.34-01	2.35+01	683.93	683.75	1.16
14.	22	71.1	.50	5.664	.151	-.234	5.687	1.22+02	4.52+00	682.02	45.00	-2.73
15.	25	94.1	2.75	3.916	.055	-.063	3.573	1.06-01	3.19+00	788.83	786.61	7.28
16.	25	94.1	.50	6.198	.108	-.143	6.056	1.77+02	2.08+00	787.38	50.00	-3.00
17.	27	105.7	2.75	4.742	.052	-.058	4.208	1.17-01	5.02+00	872.66	867.22	17.11
18.	27	105.7	.50	6.664	.112	-.150	6.574	1.50+02	1.59+00	868.46	45.00	-6.37
19.	30	98.7	2.75	4.397	.170	-.284	4.413	2.96-01	1.05+00	825.74	825.48	1.87
20.	30	98.7	.50	6.459	.124	-.174	6.458	1.81+02	4.70+00	824.65	50.00	-1.56
21.	32	98.7	2.75	4.908	.043	-.048	4.323	2.42-01	1.20+01	785.21	765.20	.42
22.	32	98.7	.50	6.533	.169	-.286	6.566	2.33+02	1.63+00	785.46	45.00	-.86
23.	33	54.0	2.75	3.695	.067	-.079	3.331	1.23-01	4.66+00	570.04	570.26	.96
24.	33	54.0	.50	5.536	.131	-.187	5.442	8.76+01	5.89+00	569.18	40.00	-1.96
25.	35	98.7	2.75	4.556	.101	-.132	4.337	2.50-01	2.98+00	829.85	827.97	9.16
26.	35	98.7	.50	6.643	.109	-.145	6.541	2.20+02	2.44+00	827.42	50.00	-9.75
27.	39	98.7	2.75	4.315	.103	-.135	4.132	1.56-01	2.45+00	836.11	836.86	7.73
28.	39	98.7	.50	6.718	.073	-.088	6.398	1.58+02	3.08+00	841.77	50.00	-7.75
29.	41	89.5	2.75	3.946	.082	-.102	3.706	1.85-01	3.01+00	757.12	755.31	6.65
30.	41	89.5	.50	5.989	.105	-.139	5.814	1.30+02	2.37+00	752.63	50.00	-8.12
31.	44	70.0	2.75	3.666	.062	-.073	3.316	9.48-02	2.75+00	720.40	722.26	4.85
32.	44	70.0	.50	6.318	.069	-.082	6.084	3.05+02	2.79+00	722.53	40.00	-5.55
33.	45	90.0	2.75	3.943	.085	-.105	3.683	1.75-01	2.21+00	744.66	747.01	7.94
34.	45	90.0	.50	5.911	.117	-.161	5.861	1.45+02	2.95+00	748.99	50.00	-7.29
35.	49	77.6	2.75	4.299	.053	-.061	3.773	2.71-01	1.19+01	717.23	720.45	7.99
36.	49	77.6	.50	5.668	.106	-.140	5.617	1.04+02	4.76+00	719.72	50.00	-9.13
37.	50	68.9	2.75	4.068	.056	-.064	3.661	1.67-01	1.10+01	674.59	674.64	.92
38.	50	68.9	.50	5.935	.091	-.115	5.691	9.81+01	8.66+00	674.00	45.00	-.56
39.	56	80.9	2.75	3.525	.107	-.142	3.355	1.33-01	1.55+00	718.53	719.32	2.92
40.	56	80.9	.50	5.620	.058	-.068	5.173	4.83+01	5.50+00	717.38	50.00	-5.23
41.	58	72.6	2.75	3.599	.095	-.122	3.476	1.37-01	2.34+00	670.90	675.71	7.23
42.	58	72.6	.50	5.661	.101	-.132	5.581	9.59+01	2.21+00	673.96	50.00	-7.25
43.	59	87.9	2.75	3.857	.095	-.121	3.655	1.33-01	2.34+00	763.16	761.12	8.95
44.	59	87.9	.50	6.015	.086	-.107	5.826	1.09+02	2.49+00	760.23	50.00	-9.51
45.	60	80.7	2.75	3.431	.098	-.122	3.315	1.27-01	2.30+00	728.23	728.75	8.68
46.	60	80.7	.50	5.686	.077	-.094	5.397	6.46+01	2.53+00	725.05	50.00	-16.01
47.	61	83.6	2.75	3.835	.077	-.093	3.517	1.19-01	2.62+00	744.70	743.50	5.65
48.	61	83.6	.50	5.891	.094	-.120	5.667	9.30+01	2.66+00	738.72	50.00	-6.77
49.	62	80.3	2.75	3.703	.056	-.065	3.318	1.41-01	4.52+00	731.37	734.26	6.47
50.	62	80.3	.50	5.628	.087	-.108	5.341	8.16+01	2.98+00	732.33	50.00	-8.08
51.	63	83.9	2.75	3.963	.110	-.147	3.839	2.51-01	7.09+00	733.49	733.57	1.15
52.	63	83.9	.50	5.793	.097	-.126	5.599	7.94+01	3.17+00	733.14	40.00	-2.61
53.	65	77.4	2.75	3.613	.091	-.115	3.461	1.32-01	2.59+00	722.28	720.69	9.07
54.	65	77.4	.50	6.031	.075	-.091	5.812	1.63+02	3.08+00	722.87	50.00	-8.85
55.	66	87.8	2.75	4.008	.088	-.111	3.648	1.34-01	4.47+00	759.34	758.81	5.03
56.	66	87.8	.50	6.093	.095	-.122	5.957	1.51+02	2.12+00	757.81	50.00	-4.50
57.	68	98.8	2.75	4.497	.088	-.110	4.279	2.19-01	2.18+00	780.01	779.53	10.85
58.	68	98.8	.50	6.492	.080	-.099	6.247	1.12+02	2.37+00	779.53	50.00	-7.93
59.	73	86.7	2.75	4.122	.047	-.053	3.635	1.68-01	7.01+00	768.04	767.77	3.10
60.	73	86.7	.50	5.625	.175	-.298	5.811	1.39+02	3.46+00	770.12	50.00	-3.55
61.	76	89.4	2.75	3.791	.074	-.089	3.592	1.42-01	2.47+00	752.04	754.82	11.21
62.	76	89.4	.50	6.011	.152	-.236	6.023	2.11+02	2.38+00	757.95	50.00	-11.27
63.	81	80.1	2.75	4.365	.013	-.013	3.297	1.40-01	1.13+02	734.81	733.92	.37
64.	81	80.1	.50	5.756	.072	-.087	5.449	1.10+02	6.97+02	733.79	50.00	-.67
65.	143	73.2	2.75	4.956	.007	-.007	3.562	1.75-01	4.76+02	692.09	692.15	.41
66.	143	73.2	.50	5.675	.125	-.176	5.930	2.24+02	8.06+01	692.10	50.00	-.40

END DATA.

****** SUMMARY OF DISCRIMINATION DATA AT STATION ILPA

HIGH FREQUENCY AT 2.00 HZ LOW FREQUENCY AT .55 HZ

			SIGNAL INFORMATION			NOISE INFORMATION			SIGNAL ARRIVAL INFORMATION				
EVENT	DISTANCE (DEGREES)	FREQ	MB(F)	MB(+)	MB(-)	MB	AMP	(S/N)**2	TG	TGBAR	TSIGMA	NOISE WINDOW	NFFT
3	56.2	2.00	3.809	.135	-.197	3.748	4.44-01	1.53+00	579.60	581.33	3.22	50.00	2048
3		.55	4.839	.111	-.149	4.775	1.53+01	1.02+01	582.08	581.33	-2.88	50.00	2048
6	45.2	2.00	4.017	.074	-.089	3.733	5.15-01	2.45+00	511.07	509.49	6.49	40.00	2048
6		.55	4.748	.050	-.057	4.259	6.30+00	6.38+00	506.39	509.49	-7.33	40.00	2048
18	41.1	2.00	4.765	.037	-.041	4.437	4.33+00	3.49+00	474.05	476.89	8.41	50.00	2048
18		.55	4.399	.133	-.193	4.326	1.22+01	3.98+00	468.88	476.89	-13.77	50.00	2048
19	38.1	2.00	5.595	.002	-.002	3.629	6.88-01	6.84+02	445.24	445.13	.52	50.00	2048
19		.55	5.651	.005	-.005	4.239	1.02+01	2.06+03	444.66	445.13	-.70	50.00	2048
21	47.7	2.00	3.851	.054	-.062	3.245	2.78-01	4.72+00	483.11	483.81	3.25	50.00	2048
21		.55	4.394	.106	-.141	4.251	1.02+01	3.76+00	482.73	483.81	-5.65	50.00	2048
24	31.6	2.00	3.959	.091	-.116	3.796	6.23-01	4.63+00	420.78	416.04	13.60	50.00	2048
24		.55	4.737	.102	-.134	4.680	1.73+01	1.30+00	418.08	416.04	-4.98	50.00	2048
25	32.2	2.00	3.797	.110	-.148	3.541	3.46-01	1.65+00	383.00	386.08	2.16	50.00	2048
25		.55	4.924	.129	-.184	4.975	3.43+01	4.79+00	385.09	386.08	-7.46	50.00	2048
27	37.2	2.00	4.569	.010	-.010	3.419	4.15-01	2.31+01	432.81	432.27	-.53	50.00	2048
27		.55	5.026	.072	-.086	4.894	4.50+01	8.70+00	431.51	432.27	-.76	50.00	2048
29	34.1	2.00	3.614	.132	-.191	3.631	4.26-01	6.36+00	434.09	429.89	9.95	50.00	2048
29		.55	4.497	.104	-.148	4.367	8.44+00	1.93+00	429.28	429.89	-6.71	50.00	2048
30	31.2	2.00	4.359	.012	-.012	3.752	5.63-01	8.21+00	388.49	389.32	1.66	50.00	2048
30		.55	5.972	.005	-.005	4.478	1.09+01	1.84+03	389.35	389.32	-1.55	50.00	2048
31	31.3	2.00	3.541	.206	-.408	3.708	5.09-01	2.53+00	394.74	396.93	6.82	50.00	2048
31		.55	4.556	.175	-.296	4.655	1.64+01	3.22+00	398.98	396.93	-6.42	50.00	2048
32	31.3	2.00	3.723	.110	-.148	3.673	4.70-01	2.18+00	414.70	414.50	3.22	50.00	2048
32		.55	4.665	.093	-.118	4.486	1.11+01	4.83+00	415.16	414.50	-3.03	50.00	2048
33	38.3	2.00	4.359	.021	-.022	3.520	5.61-01	5.56+00	443.46	444.05	.66	50.00	2048
33		.55	4.162	.143	-.215	4.166	9.02+00	2.74+01	443.88	444.05	-.86	50.00	2048
34	31.2	2.00	4.193	.077	-.094	3.847	7.01-01	2.51+00	375.45	373.22	10.20	50.00	2048
34		.55	4.910	.087	-.109	4.783	2.20+01	1.54+00	376.32	373.22	-7.98	50.00	2048
35	31.2	2.00	3.720	.122	-.170	3.690	4.89-01	1.22+00	388.53	389.57	2.27	50.00	2048
35		.55	4.935	.116	-.158	4.887	2.80+01	2.29+01	389.59	389.57	-5.06	50.00	2048
37	41.3	2.00	3.671	.179	-.310	3.875	4.41-01	2.77+00	621.45	620.59	8.67	50.00	2048
37		.55	4.912	.120	-.166	4.921	1.78+01	2.33+00	617.43	620.59	-11.23	50.00	2048
39	31.3	2.00	4.039	.106	-.141	3.867	7.35-01	5.06+00	387.06	389.49	6.32	50.00	2048
39		.55	5.004	.066	-.078	4.654	1.64+01	2.82+00	385.98	389.49	-8.79	50.00	2048

46 46	35.9	2.00 .55	3.751 4.664	.103 .063	-.135 -.074	3.503 4.284	3.90-01 8.59+00	2.22+00 3.16+00	413.72 414.61	414.81 414.81	-15.67 -11.23	50.00 50.00	2048 2048
47 47	72.5	2.00 .55	3.694 4.562	.031 .161	-.033 -.258	3.005 4.642	6.37-02 1.00+01	6.48+00 2.55+00	690.67 680.86	691.07 691.07	-4.21 -2.16	50.00 50.00	2048 2048
50 50	72.6	2.00 .55	4.470 6.099	.075 .008	-.090 -.008	4.098 4.806	7.88-01 1.46+01	2.93+00 5.16+02	698.81 698.07	698.05 698.05	-.63 -.60	50.00 50.00	2048 2048
55 55	72.9	2.00 .55	3.603 5.236	.104 .067	-.137 -.079	3.656 5.001	2.45-01 2.29+01	2.29+00 2.69+00	693.52 698.53	694.74 694.74	-6.57 -8.85	50.00 50.00	2048 2048
56 56	73.1	2.00 .55	4.012 5.455	.081 .072	-.100 -.086	3.770 5.221	3.29-01 3.69+01	1.28+00 5.70+00	702.26 696.69	702.77 702.77	-7.45 -9.28	50.00 50.00	2048 2048
57 57	70.2	2.00 .55	4.498 5.037	.032 .154	-.034 -.241	3.813 5.078	4.09-01 2.74+01	2.97+00 1.26+01	666.03 666.02	666.18 666.18	-1.02 -1.38	40.00 40.00	2048 2048
58 58	72.5	2.00 .55	4.043 5.418	.096 .130	-.123 -.186	3.838 5.431	4.33-01 6.18+01	2.73+00 1.78+00	702.76 704.01	703.55 703.55	-5.77 -8.24	50.00 50.00	2048 2048
63 63	69.1	2.00 .55	4.299 4.998	.048 .175	-.054 -.158	3.783 4.926	3.10-01 3.57+01	3.86+00 3.93+01	652.49 652.63	652.73 652.73	-.39 -.91	50.00 50.00	2048 2048
64 64	72.3	2.00 .55	4.174 5.047	.082 .094	-.102 -.090	3.911 4.735	5.13-01 1.24+01	2.43+00 3.98+00	686.25 681.91	682.93 682.93	-7.20 -8.04	50.00 50.00	2048 2048
68 68	33.8	2.00 .55	3.739 4.785	.101 .084	-.131 -.104	3.578 4.607	3.25-01 1.54+01	1.97+00 2.37+00	341.84 340.61	340.74 340.74	10.58 -8.55	50.00 50.00	2048 2048
77 77	52.4	2.00 .55	2.708 5.287	.495 .028	1.294 -.030	3.063 4.605	1.15-01 1.46+01	6.84+00 2.77+03	558.87 560.32	560.32 560.32	-.13 -.46	50.00 50.00	2048 2048
78 78	34.1	2.00 .55	3.643 4.772	.098 .116	-.127 -.160	3.497 4.665	3.13-01 1.68+01	1.59+00 2.08+00	432.03 426.60	427.93 427.93	9.88 -8.65	50.00 50.00	2048 2048
143 143	72.7	2.00 .55	5.051 5.947	.014 .008	-.014 -.008	3.950 4.605	5.62-01 9.21+00	1.38+01 2.47+02	705.86 696.61	699.74 699.74	8.22 -7.15	50.00 50.00	2048 2048
144 144	69.8	2.00 .55	4.140 4.828	.091 .115	-.116 -.157	3.799 4.728	3.78-01 1.17+01	1.57+00 8.45+00	655.82 658.24	657.12 657.12	-1.19 -4.11	50.00 50.00	2048 2048
145 145	61.0	2.00 .55	3.631 4.999	.202 .076	-.369 -.093	3.609 4.745	2.56-01 1.27+01	1.78+00 1.84+01	563.64 564.07	563.30 563.30	-.57 -.82	50.00 50.00	2048 2048
146 146	72.3	2.00 .55	3.869 5.030	.088 .103	-.111 -.136	3.753 4.906	3.57-01 1.85+01	1.96+00 1.82+00	661.69 661.39	661.63 661.63	-9.97 -7.44	50.00 50.00	2048 2048
147 147	68.1	2.00 .55	5.457 5.446	.007 .049	-.007 -.075	4.025 4.997	5.29-01 1.81+01	7.45+01 4.39+02	615.42 615.31	615.44 615.44	-.26 -.25	50.00 50.00	2048 2048
154 154	68.9	2.00 .55	4.318 5.635	.057 .068	-.066 -.081	3.878 5.419	3.77-01 4.77+01	3.12+00 3.55+01	617.79 617.27	617.59 617.59	-.53 -1.82	50.00 50.00	2048 2048
156 156	72.2	2.00 .55	4.243 5.372	.079 .062	-.091 -.072	3.999 5.008	6.28-01 2.80+01	1.77+00 3.09+00	659.24 662.06	659.50 659.50	8.87 -6.48	50.00 50.00	2048 2048
157	72.0	2.00	4.015	.070	-.083	3.647	2.93-01	2.80+00	678.81	682.06	7.40	50.00	2048

157		.55	5.069	.116	-.160	4.944	2.01+01	2.04+00	679.52	682.06	-10.98	50.00	2048
159	30.6	2.00	4.053	.051	-.058	3.642	4.79-01	1.76+00	382.18	381.24	2.21	50.00	2048
159		.55	5.065	.152	-.237	5.145	5.56+01	2.13+00	380.30	381.24	-5.03	50.00	2048
160	62.2	2.00	4.216	.083	-.103	3.990	5.12-01	2.16+00	523.22	526.70	7.13	50.00	2048
160		.55	5.757	.056	-.065	5.406	4.85+01	3.54+00	520.43	526.70	-15.81	50.00	2048
164	70.7	2.00	4.991	.009	-.009	3.632	2.69-01	3.61+01	677.22	676.03	.57	50.00	2048
164		.55	5.906	.027	-.028	5.246	4.04+01	6.54+02	675.82	676.03	-.97	50.00	2048
165	73.3	2.00	4.101	.092	-.117	3.963	6.20-01	2.20+00	707.51	706.72	7.90	50.00	2048
165		.55	5.077	.091	-.116	5.052	2.76+01	2.77+00	709.58	706.72	-6.13	50.00	2048
169	71.7	2.00	3.920	.134	-.194	3.733	3.41-01	2.47+00	691.46	694.50	7.24	50.00	2048
169		.55	5.001	.056	-.065	4.640	1.00+01	1.67+01	691.20	694.50	-8.23	50.00	2048
171	72.8	2.00	3.878	.111	-.150	3.712	3.24-01	2.14+00	683.24	685.46	7.66	50.00	2048
171		.55	4.792	.131	-.188	4.609	1.17+01	2.59+00	685.78	685.46	-10.23	50.00	2048
176	70.6	2.00	3.912	.106	-.141	3.695	3.12-01	2.73+00	758.07	758.57	3.68	50.00	2048
176		.55	5.166	.092	-.118	4.930	1.95+01	2.15+00	759.85	758.57	-4.46	50.00	2048
178	77.7	2.00	4.885	.013	-.019	3.886	4.84-01	7.78+00	704.96	705.11	1.21	50.00	2048
178		.55	5.501	.028	-.029	4.751	1.29+01	1.46+02	704.87	705.11	-2.22	50.00	2048
180	72.6	2.00	3.934	.091	-.116	3.662	2.89-01	3.00+00	705.33	705.16	5.63	50.00	2048
180		.55	4.948	.077	-.094	4.695	1.13+01	2.57+00	705.19	705.16	-4.46	50.00	2048
182	72.7	2.00	3.877	.114	-.155	3.719	3.30-01	2.00+00	704.39	703.56	8.51	50.00	2048
182		.55	5.392	.071	-.085	5.085	2.78+01	3.42+00	704.18	703.56	-8.63	50.00	2048
183	74.3	2.00	4.075	.063	-.079	3.648	3.52-01	1.30+01	713.11	711.62	7.36	50.00	2048
183		.55	4.962	.135	-.196	4.952	2.58+01	1.71+00	712.20	711.62	-3.57	50.00	2048
186	72.2	2.00	4.181	.072	-.087	3.866	4.63-01	4.09+00	686.01	689.19	7.05	50.00	2048
186		.55	4.990	.174	-.294	5.191	3.55+01	2.08+00	688.67	689.19	-7.61	50.00	2048
187	37.6	2.00	3.806	.126	-.178	3.695	4.94-01	2.10+00	396.57	401.33	9.33	50.00	2048
187		.55	5.236	.094	-.121	5.009	3.71+01	1.94+00	398.72	401.33	-16.01	50.00	2048
192	34.1	2.00	3.676	.061	-.072	3.241	1.74-01	2.41+00	409.88	409.02	6.99	50.00	2048
192		.55	4.613	.091	-.116	4.498	1.14+01	7.89+00	410.54	409.02	-3.14	50.00	2048
193	72.4	2.00	3.823	.094	-.129	3.635	2.72-01	3.67+00	705.30	709.59	7.73	50.00	2048
193		.55	4.578	.162	-.260	4.643	1.10+01	2.63+00	714.60	709.59	-8.76	50.00	2048
194	71.9	2.00	3.321	.136	-.204	3.326	1.33-01	2.13+00	674.20	671.96	9.18	50.00	2048
194		.55	4.848	.085	-.106	4.611	9.34+00	1.74+00	673.58	671.96	-8.83	50.00	2048
195	32.2	2.00	3.500	.150	-.209	3.565	3.67-01	1.24+00	400.78	400.33	2.35	50.00	2048
195		.55	4.723	.078	-.378	4.344	8.01+00	1.58+01	398.95	400.33	-3.48	50.00	2048

**** EXCLUDE LOW SIGNAL-TO-NOISE EVENTS **** DATABASE ILPAD2 **** DATE 090579 PAGE 23

****** SUMMARY OF DISCRIMINATION DATA AT STATION ILFA

HIGH FREQUENCY AT 2.00 HZ LOW FREQUENCY AT .55 HZ

			SIGNAL INFORMATION			NOISE INFORMATION			SIGNAL ARRIVAL INFORMATION				
EVENT	DISTANCE (DEGREES)	FREQ	MB(F)	MB(+)	MB(-)	MB	AMP	(S/N)**2	TG	TGBAR	TSIGMA	NOISE WINDOW	NFFT
4	14.7	2.00	3.484	.082	-.101	3.256	3.68-01	3.10+00	165.69	165.18	2.98	50.00	2048
4		.55	4.511	.075	-.090	4.166	1.09+01	2.50+00	165.64	165.18	-2.45	50.00	2048
7	26.4	2.00	4.261	.017	-.019	3.258	3.29-01	1.19+01	342.24	343.53	1.84	40.00	2048
7		.55	4.455	.062	-.072	4.040	7.23+00	1.11+02	341.59	343.53	-4.47	40.00	2048
9	15.0	2.00	3.756	.056	-.065	3.359	5.73-01	1.97+00	229.71	228.20	6.29	40.00	2048
9		.55	4.126	.123	-.173	4.006	9.24+00	5.14+00	223.90	228.20	-9.53	40.00	2048
20	25.2	2.00	4.950	.005	-.005	3.527	5.57-01	6.70+01	352.31	352.66	.78	50.00	2048
20		.55	5.845	.007	-.007	4.623	2.53+01	6.97+03	352.77	352.66	-.78	50.00	2048
23	17.1	2.00	2.334	.427	.867	2.948	5.59-01	1.93+01	311.91	312.81	1.19	50.00	2048
23		.55	3.969	.105	-.139	3.912	1.87+01	1.58+00	312.05	312.81	-3.78	50.00	2048
28	19.0	2.00	3.136	.060	-.069	2.906	4.03-01	2.27+00	275.76	277.49	5.74	50.00	2048
28		.55	3.629	.130	-.187	3.842	1.26+01	7.52+00	278.00	277.49	-3.34	50.00	2048
38	16.5	2.00	2.921	.079	-.096	2.604	2.53-01	2.68+00	254.44	252.42	6.12	50.00	2048
38		.55	3.766	.080	-.098	3.578	8.66+00	2.15+00	246.23	252.42	-6.96	50.00	2048
41	17.3	2.00	3.221	.031	-.034	2.549	2.23-01	2.20+01	242.07	241.61	.87	50.00	2048
41		.55	3.953	.065	-.106	3.693	1.13+01	6.99+01	240.74	241.61	-.92	50.00	2048
45	16.7	2.00	3.692	.030	-.032	2.953	5.65-01	5.11+00	236.41	237.41	1.94	50.00	2048
45		.55	4.431	.026	-.028	3.668	1.07+01	4.88+01	235.69	237.41	-4.25	50.00	2048
48	16.7	2.00	3.549	.053	-.060	2.950	5.62-01	7.59+00	223.70	224.31	1.27	50.00	2048
48		.55	4.274	.191	-.348	4.455	6.53+01	5.79+00	224.95	224.31	-1.81	50.00	2048
59	18.5	2.00	3.364	.046	-.051	2.816	3.67-01	2.74+00	278.08	280.50	5.98	50.00	2048
59		.55	3.911	.074	-.089	3.704	1.03+01	1.72+01	283.13	280.50	-5.98	50.00	2048
66	18.9	2.00	2.989	.142	-.211	2.886	3.95-01	1.32+01	294.81	293.63	3.46	50.00	2048
66		.55	4.064	.049	-.055	3.850	1.32+01	2.70+00	291.73	293.63	-2.38	50.00	2048
67	17.1	2.00	3.223	.053	-.060	2.885	4.83-01	1.73+00	237.49	237.42	1.17	50.00	2048
67		.55	4.077	.050	-.056	3.591	8.93+00	5.38+01	237.27	237.42	-1.24	50.00	2048
69	16.6	2.00	2.993	.075	-.090	2.595	2.48-01	3.86+00	224.47	223.67	3.02	50.00	2048
69		.55	3.917	.103	-.136	3.700	1.15+01	2.14+00	222.16	223.67	-2.97	50.00	2048
69	16.6	2.00	2.993	.075	-.090	2.595	2.48-01	3.86+00	224.47	223.67	3.02	50.00	2048
69		.55	3.917	.103	-.136	3.700	1.15+01	2.14+00	222.16	223.67	-2.97	50.00	2048
69	16.6	2.00	2.993	.075	-.090	2.595	2.48-01	3.86+00	224.47	223.67	3.02	50.00	2048
69		.55	3.917	.103	-.136	3.700	1.15+01	2.14+00	222.16	223.67	-2.97	50.00	2048
72	16.7	2.00	3.221	.073	-.088	2.964	5.80-01	5.23+00	237.25	240.55	5.05	50.00	2048
72		.55	4.416	.026	-.028	3.665	1.06+01	4.45+01	240.90	240.55	-4.41	50.00	2048

**** EXCLUDE LOW SIGNAL-TO-NOISE EVENTS **** DATABASE ELPA02 **** DATE 090579 PAGE 24

73	27.2	2.00	3.894	.082	-.101	3.558	5.46-01	1.78+00	373.34	374.29	2.49	50.00	2048
73		.55	4.784	.051	-.058	4.252	9.81+00	2.38+01	373.97	374.29	-3.57	50.00	2048
74	19.8	2.00	2.498	.111	-.150	2.770	2.94-01	3.26+00	280.77	279.81	6.19	50.00	2048
74		.55	3.762	.155	-.230	3.824	1.21+01	3.04+00	280.81	279.81	-5.54	50.00	2048
75	26.5	2.00	3.531	.163	-.264	3.568	6.56-01	2.87+00	344.83	343.58	7.64	50.00	2048
75		.55	4.490	.085	-.106	4.254	1.16+01	5.36+00	340.10	343.58	-7.02	50.00	2048
81	25.2	2.00	5.140	.003	-.003	3.288	3.22-01	3.38+01	351.51	352.15	1.58	50.00	2048
81		.55	5.116	.022	-.023	4.320	1.26+01	4.00+03	352.74	352.15	-.77	50.00	2048
163	17.6	2.00	3.468	.067	-.079	3.247	1.11+00	1.81+00	235.69	236.64	3.06	50.00	2048
163		.55	4.648	.043	-.074	4.376	5.44+01	4.21+00	235.13	236.64	-5.00	50.00	2048
161	16.6	2.00	3.186	.961	-.071	2.775	3.34-01	2.80+00	239.39	240.01	3.70	50.00	2048
161		.55	4.110	.088	-.110	4.008	2.33+01	2.71+00	241.28	240.01	-2.84	50.00	2048
170	21.5	2.00	3.921	.023	-.025	3.200	5.61-01	8.58+00	309.00	310.54	2.62	50.00	2048
170		.55	5.517	.004	-.004	3.976	1.09+01	3.37+03	310.22	310.54	-3.19	50.00	2048
172	21.8	2.00	3.222	.083	-.103	2.872	2.46-01	1.92+00	311.12	311.23	5.75	50.00	2048
172		.55	4.233	.068	-.080	3.851	8.13+00	1.22+01	313.47	311.23	-3.02	50.00	2048
175	15.4	2.00	4.600	.016	-.017	2.971	3.39-01	1.60+01	234.38	236.21	2.67	50.00	2048
175		.55	4.905	.034	-.037	4.277	2.49+01	5.03+01	236.89	236.21	-2.22	50.00	2048
179	14.6	2.00	4.277	.015	-.015	3.210	3.08-01	1.12+01	222.69	221.69	2.19	50.00	2048
179		.55	4.537	.071	-.085	4.249	1.23+01	5.51+01	218.92	221.69	-3.53	50.00	2048
188	15.9	2.00	3.077	.089	-.111	2.771	3.39-01	2.33+00	234.72	233.59	4.36	50.00	2048
188		.55	4.163	.111	-.150	4.054	2.36+01	2.80+00	229.18	233.59	-6.21	50.00	2048
190	17.4	2.00	3.322	.086	-.098	2.986	6.09-01	1.87+00	240.72	240.87	.38	50.00	2048
190		.55	4.119	.047	-.053	3.676	1.09+01	5.65+01	240.84	240.87	-.94	50.00	2048
191	24.8	2.00	3.053	.053	-.060	2.970	5.12-02	6.19+00	329.18	327.22	4.51	50.00	2048
191		.55	4.353	.096	-.123	4.150	8.90+00	6.53+00	329.85	327.22	-5.16	50.00	2048

****** SUMMARY OF DISCRIMINATION DATA AT STATION ILPA

HIGH FREQUENCY AT 4.50 HZ LOW FREQUENCY AT .50 HZ

EVENT	DISTANCE (DEGREES)	FREQ	SIGNAL INFORMATION MB(F)	MB(+)	MB(-)	NOISE INFORMATION MB	AMP	(S/N)**2	SIGNAL ARRIVAL INFORMATION TG	TGBAR	TSIGMA	NOISE WINDOW	NFFT
22	12.5	4.50	5.369	.034	-.084	3.767	1.16-03	1.70+03	197.66	193.56	2.13	50.00	2048
22		.50	5.669	.073	-.048	5.417	4.66+01	3.28+02	195.69	193.56	-5.47	50.00	2048
60	8.1	4.50	4.849	.093	-.118	3.758	1.21-01	1.15+01	133.68	134.48	-1.70	50.00	2048
60		.50	5.137	.103	-.136	5.027	2.03+01	1.27+01	135.70	134.48	-4.21	50.00	2048
162	8.9	4.50	4.476	.048	-.059	4.097	1.89-01	1.66+02	159.55	161.25	-1.48	50.00	2048
162		.50	5.479	.103	-.135	5.511	4.29+01	6.93+02	161.20	161.25	-1.42	50.00	2048
163	9.2	4.50	4.483	.059	-.069	4.051	1.51-01	3.28+01	160.89	161.80	-2.32	50.00	2048
163		.50	5.433	.171	-.286	5.560	4.39+01	5.26+01	161.66	161.80	-1.53	50.00	2048
167	7.5	4.50	3.840	.087	-.109	3.675	1.32-01	2.15+01	128.63	130.27	-1.78	50.00	2048
167		.50	4.561	.308	-.462	5.037	2.74+01	4.32+02	130.36	130.27	-5.08	50.00	2048
168	8.1	4.50	4.239	.069	-.082	3.893	1.62-01	7.99+01	136.35	136.77	-1.97	50.00	2048
168		.50	5.203	.089	-.112	5.119	2.51+01	1.49+02	137.13	136.77	-2.52	50.00	2048
177	6.9	4.50	4.094	.660	-.070	3.869	2.73-01	2.32+03	118.98	119.01	-3.61	50.00	2048
177		.50	4.883	.368	-.041	4.787	2.03+01	5.34+02	121.44	119.01	-2.75	50.00	2048

****** SUMMARY OF DISCRIMINATION DATA AT STATION MAIO

HIGH FREQUENCY AT 2.25 HZ LOW FREQUENCY AT .50 HZ

			SIGNAL INFORMATION			NOISE INFORMATION			SIGNAL ARRIVAL INFORMATION				
EVENT	DISTANCE (DEGREES)	FREQ	MB(F)	MB(+)	MB(-)	MB	AMP	(S/N)**2	TG	TGBAR	TSIGMA	NOISE WINDOW	NFFT
1	37.3	2.25	3.998	.105	-.139	3.295	2.77-01	3.81+00	437.65	436.47	.34	20.00	2048
1		.50	4.209	.072	-.086	3.872	4.71+00	1.19+03	436.46	436.47	-.26	20.00	2048
3	50.7	2.25	4.036	.059	-.069	3.739	4.86-01	3.67+00	538.76	540.57	2.96	35.00	2048
3		.50	4.313	.088	-.130	4.061	4.59+00	1.47+01	540.59	540.57	-2.89	35.00	2048
27	30.2	2.25	3.673	.035	-.038	3.123	1.41-01	4.25+01	371.23	370.53	.25	25.00	2048
27		.50	4.564	.059	-.068	4.328	6.44+00	7.41+02	370.33	370.53	-.39	25.00	2048
50	67.9	2.25	4.090	.129	-.184	4.069	5.21-01	1.24+00	670.04	668.78	.67	25.00	2048
50		.50	5.695	.007	-.007	4.304	4.02+00	3.82+02	668.70	668.78	-.41	25.00	2048
63	61.0	2.25	3.532	.076	-.092	3.296	9.86-02	2.55+00	613.92	613.66	.57	25.00	2048
63		.50	4.524	.100	-.130	4.451	7.12+00	1.22+02	613.76	613.66	-.33	25.00	2048
77	45.5	2.25	3.945	.026	-.028	3.158	1.14-01	8.66+00	501.34	500.53	.27	30.00	2048
77		.50	5.011	.026	-.028	4.273	6.66+00	8.45+03	500.53	500.53	-.36	30.00	2048
144	63.7	2.25	4.038	.082	-.101	3.696	2.36-01	2.62+00	616.59	616.70	2.28	20.00	1024
144		.50	4.252	.203	-.395	4.441	5.91+00	1.41+01	616.96	616.70	-.63	20.00	1024
145	54.4	2.25	3.611	.082	-.102	3.506	2.26-01	3.16+00	518.36	519.68	1.62	18.00	2048
145		.50	4.629	.060	-.069	4.246	5.59+00	1.22+01	518.18	519.68	-4.95	18.00	2048
164	64.5	2.25	3.941	.695	-.122	3.988	4.33-01	1.66+00	635.69	636.14	.38	25.00	2048
164		.50	5.656	.007	-.007	4.388	4.88+00	1.60+03	636.14	636.14	-.31	25.00	2048
166	51.3	2.25	3.720	.100	-.129	3.529	3.00-01	2.01+00	398.11	398.01	6.71	40.00	2048
166		.50	4.523	.075	-.090	4.261	7.27+00	4.63+01	393.17	398.01	-7.67	40.00	2048
178	67.6	2.25	3.896	.159	-.253	3.709	2.25-01	1.26+00	682.92	682.99	2.63	15.00	2048
178		.50	5.059	.062	-.073	4.638	8.68+00	2.35+01	682.43	682.99	-3.78	15.00	2048
269	47.4	2.25	4.463	.121	-.022	3.608	2.27-01	1.96+01	520.89	522.20	1.33	38.00	2048
269		.50	5.710	.006	-.006	4.401	6.34+00	4.41+03	522.22	522.20	-.63	38.00	2048
270	42.4	2.25	3.780	.037	-.041	3.280	2.68-01	1.91+01	479.68	478.83	.70	23.00	2048
270		.50	4.419	.047	-.065	3.981	6.05+00	5.20+02	478.78	478.83	-.61	23.00	2048
273	33.5	2.25	3.967	.108	-.143	3.640	3.87-01	3.89+00	408.56	408.09	.59	10.00	2048
273		.50	5.227	.012	-.013	4.239	6.91+00	1.55+02	408.03	408.09	-.67	10.00	2048

****** SUMMARY OF DISCRIMINATION DATA AT STATION MAID

HIGH FREQUENCY AT 2.25 HZ LOW FREQUENCY AT .50 HZ

EVENT	DISTANCE (DEGREES)	FREQ	SIGNAL INFORMATION MB(F)	MB(+)	MB(-)	NOISE INFORMATION MP	AMP	(S/N)**2	SIGNAL ARRIVAL INFORMATION TG	TGBAR	TSIGMA	NOISE WINDOW	NFFT
14	19.1	2.25	4.205	.060	-.070	2.842	3.09-01	1.35+01	273.35	272.00	3.26	20.00	2048
14		.50	3.999	.030	-.032	3.280	3.81+00	2.77+02	272.92	272.00	-1.42	20.00	2048
29	29.5	2.25	3.696	.071	-.084	3.366	9.11-01	9.30+00	268.51	269.05	4.06	15.00	1024
29		.50	3.991	.075	-.091	3.793	4.95+00	1.87+00	270.24	269.05	-3.99	15.00	1024
31	29.1	2.25	3.392	.111	-.149	3.307	9.31-01	1.73+00	328.06	329.47	1.35	20.00	2048
31		.50	4.545	.122	-.171	4.405	2.43+01	1.51+01	329.39	329.47	-1.33	20.00	2048
32	29.1	2.25	3.280	.105	-.139	3.209	3.44-01	1.24+00	350.93	351.11	1.46	25.00	2048
32		.50	4.531	.031	-.033	3.792	5.93+00	1.69+02	350.96	351.11	-1.37	25.00	2048
34	29.0	2.25	3.266	.072	-.087	3.098	2.79-01	1.48+00	324.25	324.08	2.86	19.00	2048
34		.50	4.073	.078	-.094	3.894	7.86+00	5.14+01	321.92	324.08	-4.40	19.00	2048
35	29.0	2.25	3.311	.080	-.098	3.141	3.08-01	2.08+00	320.33	319.74	1.58	30.00	2048
35		.50	5.038	.008	-.009	3.828	8.74+00	1.36+03	319.73	319.74	-1.31	30.00	2048
39	29.1	2.25	2.950	.075	-.091	2.814	1.38-01	3.09+00	318.72	318.69	.68	25.00	2048
39		.50	4.159	.026	-.028	3.490	2.96+00	2.59+02	318.68	318.69	-.68	25.00	2048
46	28.7	2.25	3.514	.079	-.097	3.292	2.19-01	2.06+00	347.63	347.21	3.33	15.00	1024
46		.50	4.328	.021	-.022	3.684	2.43+00	1.73+01	347.99	347.21	-3.18	15.00	1024
53	19.4	2.25	4.430	.005	-.005	3.027	4.73-01	3.86+02	278.57	277.41	.50	20.00	2048
53		.50	4.893	.003	-.003	3.343	4.41+00	7.64+04	277.38	277.41	-.61	20.00	2048
68	23.6	2.25	3.016	.064	-.075	2.835	1.52-01	1.98+00	324.78	324.71	6.55	15.00	2048
68		.50	4.144	.052	-.059	3.795	6.25+00	8.15+01	327.91	324.71	-5.90	15.00	2048
73	20.6	2.25	4.118	.012	-.013	2.965	3.57-01	1.65+02	281.15	281.47	1.90	15.00	2048
73		.50	4.739	.005	-.005	3.225	2.92+00	5.30+03	282.17	281.47	-1.82	15.00	2048
151	28.3	2.25	3.350	.099	-.128	3.301	2.23-01	1.81+00	357.98	357.16	.51	33.00	2048
151		.50	4.645	.029	-.031	4.012	5.17+00	2.43+02	357.12	357.16	-.68	33.00	2048
152	26.9	2.25	3.329	.100	-.130	3.199	2.27-01	1.65+00	350.31	349.74	1.86	25.00	2048
152		.50	4.200	.085	-.106	3.698	5.12+00	2.76+01	348.33	349.74	-2.98	25.00	2048
184	21.9	2.25	3.471	.108	-.144	3.214	4.70-01	3.03+00	298.98	298.96	.59	15.00	2048
184		.50	4.140	.036	-.039	3.672	6.07+00	2.24+02	298.96	298.96	-.55	15.00	2048
189	19.2	2.25	3.155	.078	-.096	3.113	5.76-01	2.42+00	297.73	296.93	.74	12.50	2048
189		.50	3.396	.192	-.252	3.536	6.87+00	5.56+02	296.94	296.93	-.20	12.50	2048
195	25.1	2.25	3.862	.072	-.086	3.596	5.66-01	1.96+00	335.29	337.34	1.68	20.00	2048
195		.50	4.372	.041	-.053	3.729	3.47+00	4.24+02	335.74	337.34	-10.13	20.00	2048
214	18.7	2.25	3.433	.045	-.050	2.868	3.51-01	9.17+00	312.98	313.22	.70	50.00	2048
214		.50	3.615	.053	-.061	3.417	5.60+00	3.21+03	313.26	313.22	-.45	50.00	2048

**** INCLUDE LOW SIGNAL-TO-NOISE EVENTS **** DATABASE MA1002 ****

266 268	19.2	2.25 .50	3.778 4.047	.020 .045	-.021 -.050	3.029 3.534	9.70-01 6.84+00	3.33+01 8.96+02	273.36 272.68	272.31 272.71	-1.37 -1.19	15.00 15.00	2048 2048
267 267	19.7	2.25 .50	4.456 4.893	.008 .009	-.008 -.009	3.160 3.438	6.93-01 5.48+00	2.16+02 7.47+04	276.20 276.30	276.28 276.28	-.96 -.95	20.00 20.00	2048 2048
268 268	19.2	2.25 .50	4.279 4.805	.005 .013	-.005 -.013	2.860 3.776	3.22-01 1.19+01	3.69+02 2.61+03	266.61 272.08	269.25 269.25	-3.12 -2.84	25.00 25.00	2048 2048
271 271	19.2	2.25 .50	4.395 5.127	.005 .001	-.005 -.001	3.158 3.493	6.39-01 5.55+00	9.52+02 1.33+05	281.55 281.77	282.27 282.27	-1.02 -1.80	35.00 35.00	2048 2048

****** SUMMARY OF DISCRIMINATION DATA AT STATION TATO

HIGH FREQUENCY AT 2.00 HZ LOW FREQUENCY AT .40 HZ

EVENT	DISTANCE (DEGREES)	FREQ	SIGNAL INFORMATION MB(F)	MB(+)	MB(-)	NOISE INFORMATION MB	AMP	(S/N)**2	SIGNAL ARRIVAL INFORMATION TG	TGBAR	TSIGMA	NOISE WINDOW	NFFT
9	45.9	2.00	4.845	.107	-.141	4.810	5.23+00	2.18+00	456.33	457.21	4.33	17.50	1024
9		.40	6.725	.093	-.102	6.477	1.22+03	7.28+00	456.12	457.21	-2.01	17.50	1024
19	59.7	2.00	4.657	.218	-.459	4.840	5.49+00	2.28+00	606.45	607.75	1.64	20.00	1024
19		.40	5.476	.112	-.151	5.444	1.10+02	1.09+01	607.41	607.75	-1.34	20.00	1024
20	41.2	2.00	5.013	.032	-.035	4.211	2.57+00	5.45+00	469.97	471.21	2.01	20.00	2048
20		.40	5.741	.182	-.319	5.956	7.15+02	5.38+00	469.07	471.21	-5.26	20.00	2048
48	44.2	2.00	4.701	.104	-.137	4.484	4.39+00	2.39+00	382.86	383.19	3.75	15.00	1024
48		.40	6.288	.093	-.119	6.359	1.65+03	3.59+00	379.37	383.19	-5.35	15.00	1024
57	36.0	2.00	4.566	.105	-.139	4.299	2.50+00	1.77+00	788.41	790.41	3.64	20.00	1024
57		.40	6.304	.019	-.020	5.769	3.69+02	6.15+00	789.64	790.41	-4.47	20.00	1024
61	50.4	2.00	4.755	.141	-.210	4.781	6.02+00	2.09+00	366.29	366.51	3.10	20.00	1024
61		.40	5.840	.179	-.309	5.851	3.54+02	3.26+00	364.41	366.51	-4.32	20.00	1024
69	44.3	2.00	4.196	.072	-.087	4.007	1.40+00	3.33+00	562.38	560.61	3.07	10.00	1024
69		.40	5.460	.114	-.195	5.483	2.09+02	5.00+00	560.08	560.61	-2.67	10.00	1024
166	22.5	2.00	4.252	.102	-.134	4.234	4.82+00	1.50+00	304.63	306.16	3.28	15.00	1024
166		.40	5.469	.107	-.143	5.238	2.43+02	1.77+01	306.30	306.16	-3.05	15.00	1024
271	41.8	2.00	5.278	.020	-.021	4.449	4.44+00	1.05+01	477.22	477.42	.64	35.00	2048
271		.40	6.160	.095	-.122	6.081	9.52+02	2.16+01	477.39	477.42	-1.64	35.00	2048

****** SUMMARY OF DISCRIMINATION DATA AT STATION CHTO

HIGH FREQUENCY AT 3.00 HZ LOW FREQUENCY AT .45 HZ

			SIGNAL INFORMATION			NOISE INFORMATION			SIGNAL ARRIVAL INFORMATION				
EVENT	DISTANCE (DEGREES)	FREQ	M_b(F)	MR(*)	MP(-)	NR	AMP	(S/N)**2	TG	TGBAR	TSIGMA	NOISE WINDOW	NFFT
1	51.0	3.00	3.759	.026	-.027	3.127	8.92-02	3.61+01	545.92	545.62	.20	12.50	2048
1		.45	5.299	.048	-.054	5.017	4.61+01	1.09+03	545.60	545.62	-.35	12.50	2048
6	9.7	3.00	4.360	.060	-.070	3.979	1.55+00	9.87+00	150.43	149.59	1.99	45.00	2048
6		.45	6.295	.007	-.007	5.066	1.27+02	2.56+02	149.55	149.59	-1.47	45.00	2048
9	31.5	3.00	3.857	.100	-.131	3.680	3.19-01	2.27+00	405.37	404.59	6.76	50.00	2048
9		.45	4.832	.088	-.110	4.655	2.01+01	2.13+00	401.26	404.59	-11.73	50.00	2048
14	35.1	3.00	3.969	.037	-.041	3.483	2.09-01	1.40+01	418.77	418.07	.69	25.00	1024
14		.45	4.886	.097	-.125	4.742	2.51+01	8.75+01	417.51	418.07	-1.34	25.00	1024
18	45.4	3.00	3.733	.033	-.036	2.919	5.09-02	1.33+02	500.30	500.02	.22	5.00	1024
18		.45	4.906	.193	-.357	4.858	2.92+01	4.38+02	499.88	500.02	-.65	5.00	1024
19	59.9	3.00	4.425	.022	-.023	3.718	2.76-01	5.00+01	609.93	609.76	.25	30.00	2048
19		.45	5.409	.031	-.033	4.797	2.21+01	1.51+03	609.70	609.76	-.27	30.00	2048
20	35.0	3.00	5.236	.002	-.002	3.611	2.71-01	1.26+04	417.16	416.90	.48	20.00	2048
20		.45	5.782	.024	-.025	5.090	5.45+01	1.98+04	416.65	416.90	-.48	20.00	2048
27	9.3	3.00	4.276	.122	-.171	4.247	3.47-01	1.18+00	277.13	274.03	7.40	50.00	2048
27		.45	5.677	.081	-.100	5.413	3.38+01	7.99+00	278.66	274.03	-5.39	50.00	2048
30	16.7	3.00	3.331	.030	-.032	2.848	2.96-01	2.72+02	247.85	248.89	1.98	10.00	2048
30		.45	6.219	.001	-.001	3.899	2.22+01	6.31+04	247.21	248.89	-3.09	10.00	2048
31	16.6	3.00	2.974	.060	-.069	2.906	3.38-01	2.55+00	191.41	191.63	.78	20.00	2048
31		.45	4.471	.055	-.063	4.093	3.47+01	8.27+01	191.50	191.63	-1.30	20.00	2048
32	16.6	3.00	2.782	.069	-.083	2.682	2.02-01	2.69+00	273.82	273.44	1.46	20.00	2048
32		.45	4.504	.036	-.040	3.815	1.83+01	1.42+02	273.34	273.44	-2.14	20.00	2048
34	16.8	3.00	2.623	.066	-.078	2.579	1.59-01	6.95+00	238.30	238.61	.66	20.00	2048
34		.45	4.355	.018	-.019	3.805	1.79+01	3.05+02	238.62	238.61	-1.34	20.00	2048
35	16.7	3.00	2.714	.033	-.036	2.326	8.88-02	1.42+02	248.54	249.53	2.41	18.00	2048
35		.45	4.649	.027	-.029	3.823	1.66+01	1.66+03	250.79	249.53	-1.17	18.00	2048
39	16.7	3.00	2.721	.066	-.078	2.567	1.55-01	6.24+00	241.13	240.44	.69	25.00	2048
39		.45	4.455	.053	-.061	3.924	2.35+01	4.75+02	240.42	240.44	-.33	25.00	2048
47	54.3	3.00	3.933	.011	-.011	3.001	5.30-02	1.87+02	624.10	623.98	.56	25.00	2048
47		.45	5.558	.016	-.017	4.673	1.68+01	4.58+03	623.63	623.98	-.99	25.00	2048
49	59.5	3.00	4.711	.002	-.002	3.107	6.76-02	1.48+03	565.37	564.75	.26	10.00	2048
49		.45	5.880	.008	-.008	4.980	1.06+01	2.72+04	564.65	564.75	-.63	10.00	2048
68	16.8	3.00	2.872	.083	-.102	2.650	1.87-01	3.42+00	249.35	247.84	5.37	15.00	2048
68		.45	4.358	.049	-.056	4.083	3.38+01	5.21+01	243.70	247.84	-8.56	15.00	2048

**** EXCLUDE LOW SIGNAL-TO-NOISE EVENTS **** DATABASE CHTOD2 **** DATE 090579 PAGE 8

77	28.4	3.00	3.122	.178	-.306	3.182	1.84-01	1.05+01	334.76	335.48	.47	30.00	2048
77		.45	5.230	.021	-.022	4.358	1.84+01	8.29+02	335.59	335.48	-.70	30.00	2048
81	34.9	3.00	4.791	.015	-.016	3.635	2.87-01	5.27+02	416.69	416.72	-.29	30.00	2048
81		.45	5.978	.010	-.011	4.817	2.91+01	3.12+04	416.67	416.72	-.34	30.00	2048
143	57.7	3.00	4.327	.014	-.020	3.633	2.27-01	5.05+02	593.12	593.43	.49	12.50	2048
143		.45	5.678	.015	-.016	4.833	2.40+01	1.55+03	593.40	593.43	-1.02	12.50	2048
144	47.1	3.00	3.677	.076	-.084	3.446	1.18-01	5.56+01	498.87	498.88	.16	32.00	1024
144		.45	5.247	.091	-.115	4.980	2.67+01	7.86+02	498.89	498.88	-.16	32.00	1024
145	35.8	3.00	3.486	.027	-.028	2.977	7.58-02	6.11+01	376.40	376.12	.28	20.00	2048
145		.45	4.928	.064	-.074	4.665	2.46+01	8.63+02	376.12	376.12	-.35	20.00	2048
147	48.9	3.00	4.599	.008	-.008	3.501	1.46-01	3.44+02	491.15	491.16	.34	20.00	1024
147		.45	5.093	.086	-.108	4.855	2.20+01	4.29+02	491.20	491.16	-.25	20.00	1024
157	55.5	3.00	3.935	.050	-.057	3.242	9.23-02	8.84+00	565.40	565.33	.92	35.00	2048
157		.45	4.788	.078	-.095	4.533	1.20+01	1.65+02	565.36	565.33	-.57	35.00	2048
170	26.0	3.00	3.800	.103	-.135	3.582	3.20-01	1.65+01	388.77	389.98	2.07	30.00	2048
170		.45	5.725	.008	-.008	4.507	3.79+01	1.36+04	390.33	389.98	-1.00	30.00	2048
171	56.2	3.00	3.679	.017	-.018	2.924	4.44-02	2.88+02	579.03	579.26	.30	35.00	2048
171		.45	4.357	.206	-.407	4.572	1.31+01	3.42+02	579.60	579.26	-.74	35.00	2048
178	57.8	3.00	4.264	.012	-.012	3.286	1.02-01	1.61+02	591.35	591.70	.73	20.00	2048
178		.45	5.402	.018	-.019	4.618	1.46+01	1.45+04	591.70	591.70	-.42	20.00	2048
179	31.7	3.00	3.557	.646	-.651	3.138	9.14-02	1.62+01	406.96	407.35	6.26	30.00	2048
179		.45	4.745	.097	-.126	4.603	1.78+01	1.85+02	410.28	407.35	-4.58	30.00	2048
180	57.6	3.00	3.529	.052	-.160	3.233	9.03-02	5.48+00	595.28	595.62	.88	15.00	1024
180		.45	4.612	.121	-.168	4.576	1.33+01	3.41+01	595.94	595.62	-.59	15.00	1024
182	57.9	3.00	3.296	.125	-.177	3.277	1.00-01	1.33+00	590.48	590.65	.60	35.00	2048
182		.45	4.492	.122	-.170	4.488	1.08+01	1.96+02	590.65	590.65	-.64	35.00	2048
183	60.0	3.00	3.487	.030	-.032	3.135	7.21-02	1.35+01	606.08	606.54	2.95	25.00	2048
183		.45	4.658	.114	-.156	4.568	1.30+01	3.60+01	608.24	606.54	-3.95	25.00	2048
186	55.7	3.00	4.159	.063	-.074	3.925	4.45-01	3.19+00	578.16	578.54	.31	35.00	2048
186		.45	4.178	.199	-.377	4.782	2.13+01	1.76+02	578.55	578.54	-.26	35.00	2048
195	21.4	3.00	3.348	.089	-.113	3.224	4.04-01	5.13+00	299.99	299.26	.40	40.00	2048
195		.45	4.686	.023	-.024	3.903	1.29+01	1.66+03	299.26	299.26	-.34	40.00	2048
266	35.3	3.00	4.019	.123	-.133	3.825	4.76-01	1.66+01	418.09	417.87	.44	20.00	1024
266		.45	4.755	.084	-.104	4.319	9.90+00	1.12+02	417.83	417.87	-.86	20.00	1024
269	44.5	3.00	3.719	.660	-.670	3.267	6.71-02	9.20+02	523.11	523.29	.45	22.00	2048
269		.45	4.894	.204	-.349	5.037	3.42+01	7.54+02	523.32	523.29	-.38	22.00	2048
270	48.0	3.00	4.246	.011	-.011	3.319	8.79-02	2.39+02	519.42	519.14	.26	37.00	2048
270		.45	4.755	.206	-.383	4.910	2.61+01	4.64+02	519.01	519.14	-.40	37.00	2048
271	35.3	3.00	5.441	.002	-.002	3.721	3.75-01	8.86+03	422.28	422.12	.34	18.00	2048
271		.45	5.745	.013	-.014	4.683	2.29+01	2.58+04	421.94	422.12	-.23	18.00	2048
273	47.9	3.00	4.549	.011	-.011	3.493	1.30-01	2.10+02	525.23	524.91	1.13	15.00	2048
273		.45	5.342	.066	-.078	4.687	2.16+01	2.55+03	523.82	524.91	-.55	15.00	2048

**** EXCLUDE LOW SIGNAL-TO-NOISE EVENTS **** DATABASE 20B002 **** DATE 090579 PAGE 7

****** SUMMARY OF DISCRIMINATION DATA AT STATION 20B0

HIGH FREQUENCY AT 2.75 HZ LOW FREQUENCY AT .50 HZ

EVENT	DISTANCE (DEGREES)	FREQ	SIGNAL INFORMATION MB(F)	MB(+)	MB(-)	NOISE INFORMATION MP	AMP	(S/N)**2	SIGNAL ARRIVAL INFORMATION TG	TGRAR	ISIGMA	NOISE WINDOW	NFFT
14	145.4	2.75	4.561	.048	-.055	4.182	1.10-01	9.81+01	1181.69	1182.31	.60	17.50	2048
16		.50	4.918	.296	-1.603	5.266	7.40+00	3.54+03	1182.25	1182.31	-.41	17.50	2048
20	137.1	2.75	4.684	.073	-.087	4.443	2.01-01	3.24+00	1173.13	1171.76	-2.54	25.00	2048
20		.50	4.989	.154	-.241	5.217	6.57+00	4.46+01	1172.01	1171.76	-1.23	25.00	2048
22	119.5	2.75	4.772	.076	-.092	4.405	1.84-01	3.75+00	1186.01	1184.69	-2.40	50.00	2048
22		.50	5.987	.092	-.117	5.882	3.04+01	2.62+00	1183.15	1184.69	-2.35	50.00	2048
47	131.7	2.75	4.985	.052	-.059	4.463	2.11-01	9.95+00	1445.77	1444.05	3.30	30.00	2048
47		.50	6.589	.008	-.008	5.349	8.91+00	2.52+03	1444.93	1444.05	-.93	30.00	2048
77	156.3	2.75	4.794	.039	-.037	4.111	9.36-02	1.04+01	1259.62	1260.74	4.20	15.00	2048
77		.50	5.317	.177	-.305	5.326	8.46+00	2.85+00	1260.62	1260.74	-6.49	15.00	2048
81	137.2	2.75	4.242	.113	-.154	4.046	8.06-02	4.19+01	1169.71	1170.70	1.60	35.00	2048
81		.50	5.511	.090	-.114	5.312	8.18+00	9.27+01	1172.17	1170.70	-1.87	35.00	2048
143	127.7	2.75	4.752	.038	-.042	3.971	6.79-02	7.98+01	1149.62	1148.60	-1.26	12.50	2048
143		.50	5.979	.059	-.068	5.291	9.79+00	7.84+01	1147.65	1148.60	-1.44	12.50	2048
174	140.0	2.75	4.372	.064	-.075	3.955	6.54-02	6.26+00	1174.73	1172.82	-3.83	10.00	2048
174		.50	5.663	.075	-.090	5.381	9.60+00	3.98+01	1170.53	1172.82	-3.88	10.00	2048
169	126.2	2.75	4.275	.052	-.059	3.891	5.65-02	8.50+00	1131.74	1131.39	-.75	25.00	2048
169		.50	5.560	.086	-.107	5.297	7.90+00	2.51+01	1130.69	1131.39	-1.65	25.00	2048
170	141.9	2.75	4.283	.076	-.092	4.051	8.16-02	6.57+00	1181.94	1180.54	-2.08	15.00	2048
170		.50	6.074	.027	-.029	5.278	7.56+00	2.63+02	1180.23	1180.54	-1.41	15.00	2048
173	142.2	2.75	5.043	.018	-.019	4.101	9.16-02	9.94+01	1235.83	1236.14	-2.59	30.00	2048
173		.50	5.666	.064	-.075	5.271	7.45+00	2.13+01	1236.02	1236.14	-3.04	30.00	2048
178	127.7	2.75	4.674	.039	-.043	4.077	8.66-02	8.37+00	1146.01	1144.93	-.56	25.00	2048
178		.50	5.760	.077	-.094	5.465	1.16+01	6.24+01	1144.56	1144.93	-2.01	25.00	2048
265	136.7	2.75	4.573	.020	-.024	3.854	5.19-02	8.43+01	1170.96	1171.33	-.76	25.00	2048
265		.50	5.478	.101	-.132	5.315	8.23+00	2.24+01	1172.73	1171.33	-1.78	25.00	2048
267	137.2	2.75	4.290	.114	-.136	4.027	7.72-02	1.27+01	1166.78	1168.81	2.63	15.00	2048
267		.50	5.695	.113	-.153	5.474	1.19+01	1.20+02	1169.86	1168.81	-1.15	15.00	2048
269	131.5	2.75	4.616	.051	-.057	4.138	9.63-02	1.01+01	1157.35	1157.64	-.93	22.00	2048
269		.50	5.890	.045	-.050	5.578	1.34+01	6.33+01	1157.95	1157.64	-1.19	22.00	2048
270	130.3	2.75	4.783	.069	-.055	4.178	9.31-02	1.34+01	1152.96	1153.14	.57	20.00	2048
270		.50	5.936	.078	-.096	5.415	1.04+01	6.24+01	1153.91	1153.14	-.62	20.00	2048
271	136.7	2.75	4.677	.018	-.019	3.948	6.98-02	7.93+01	1175.57	1175.86	-.56	25.00	2048
271		.50	5.896	.057	-.066	5.448	1.12+01	4.71+01	1176.30	1175.86	-1.86	25.00	2048